THE PROCEEDINGS OF
THE PHYSICAL SOCIETY

Section A

VOL. 63, PART 6 1 June 1950 No. 366 A

The Schumann–Runge O_2 Emission Bands in the Region 3100 A.–2500 A.

BY M. W. FEAST
Imperial College, London *

MS. received 19*th October* 1949

ABSTRACT. Rotational and vibrational analyses of the emission Schumann–Runge O_2 bands in the region 3100 A. to 2500 A. are presented. Tables of wavenumbers are given for the (1, 12), (0, 11), (1, 11), (0, 10), (1, 10), (1, 9), (2, 9), (1, 8), (2, 8), (2, 7) bands. The origins of the bands, the rotational differences, and constants for the levels $v''=7$ to 11 are given. Three bands, found in a high voltage arc in oxygen between platinum electrodes, are attributed to PtO.

§ 1. INTRODUCTION

In a previous paper (Feast 1949) an investigation of the Schumann–Runge O_2 bands as emitted by a high voltage arc in oxygen was reported. The pressure dependence of the bands was discussed and an explanation for this was suggested. It was concluded that there is no predissociation in the upper state of the system. During this work it was found possible to extend the system throughout the quartz ultra-violet region of the spectrum and to identify 17 new bands (see Feast 1948 and also the plate given in Feast 1949). The present paper gives details of the rotational and vibrational analyses of those of the new bands which lie in the region 3100 A. to 2500 A. (except the (2, 10) and the (0, 9) bands). Above 3100 A. only one new band (the (2, 22) band) has been found and no measurements of this band have yet been made. Although four new bands have been found at wavelengths shorter than 2500 A. no exact measurement of them has yet been attempted. Mr. W. R. S. Garton and the author have recently obtained absorption spectra from oxygen at high temperatures in this region of the spectrum and it has therefore been decided to defer any further measurements of the emission spectra until the absorption work has been completed.

Since the Schumann–Runge bands have been identified in the solar spectrum (Babcock 1945) and since rocket experiments are enabling this spectrum to be extended further and further into the ultra-violet it appears important that measurements of the Schumann–Runge bands in the region covered by the present investigation should be available.

---

* Now with the National Research Council, Ottawa, Canada.

§2. ANALYSIS

The analysis of the Schumann–Runge bands by Lochte-Holtgreven and Dieke (1929) extended over the region 3100 A. to 4200 A. Tentative analyses of some of the bands at wavelengths shorter than 3100 A. have been published (Millon and Herman 1944, Lal 1948); both these analyses appear however to be in error (see Feast 1948, 1949). No other work appears to have been published on the analysis of the emission spectrum. Lochte-Holtgreven and Dieke gave data on the vibrational and rotational constants for $v'=0,1,2$ and $v''=12$ to 21. Analysis of the absorption bands by Curry and Herzberg (1934) and Knauss and Ballard (1935) has provided data on the constants for the levels $v'=0$ to 15 and $v''=0$ and 1.

Previous work has shown that the bands are emitted by the transition ${}^3\Sigma_u^- \rightarrow {}^3\Sigma_g^-$ and thus each band has six branches (three R and three P). Furthermore, since the nuclear spin of oxygen is zero all the even K value lines are missing. On the dispersion used here the spin triplets are not resolved and hence each band appears simply as consisting of a single P and R branch. The spectrograms used for the present work were taken on a Hilger E.1 spectrograph which has a dispersion of about 56 cm^{-1}/mm. at 3100 A. and about 42 cm^{-1}/mm. at 2475 A. The region 3100 A. to 2475 A. was measured accurately against iron arc lines, the wavelengths of the latter being taken from Burns' Iron Arc Tables (1913).

Table 1 gives the wave-numbers and quantum numbers K for the bands analysed; they are: (1, 12)—part only of the band since too many blended lines occur in this region of the spectrum for a complete analysis to be made—(0, 11), (1, 11), (0, 10), (1, 10), (1, 9), (2, 9), (1, 8), (2, 8), (2, 7). There are too many blended lines in the region of the (2, 10) and the (0, 9) bands for a detailed analysis to be made. The intensities of the lines are given on a visual scale of 0 to 10 and some notes (on blends etc.) are included. The measurements should be accurate to about 0·2 cm^{-1}.

Since the triplet splitting is not resolved the band may be treated as a ${}^1\Sigma \rightarrow {}^1\Sigma$ transition for the present analysis. The formulae for the rotational term differences in the upper and lower states are then (using standard spectroscopic nomenclature) as follows:

$$\mathrm{R}(K)-\mathrm{P}(K)=F'(K+1)-F'(K-1)=\Delta_2F'(K)=(4K+2)[B'+2D'(K^2+K+1)]$$

and

$$\begin{aligned}\mathrm{R}(K-1)-\mathrm{P}(K+1)&=F''(K+1)-F''(K-1)\\&=\Delta_2F''(K)=(4K+2)[B''+2D''(K^2+K+1)].\end{aligned}$$

The last parts of these equations involving the constants B and D are only valid if higher terms than $DK^2(K+1)^2$ in the power series for F'' and F' are negligible as they probably are in the present case. In Table 2 the differences $\Delta_2F''(K)$ for the levels $v''=7$ to 11 are given. The values are the means of the differences obtained from the various bands with a common lower vibrational level. The agreement of common differences from different bands showed that the measurements were within the expected accuracy (0·2 cm^{-1}).

The values of B'' were obtained graphically by plotting $\Delta_2F''(K)/(4K+2)$ against K and extrapolating to $K=0$ (see above equation). The values of B'' are given in Table 3. They are plotted on the graph, on which the values of Lochte-Holtgreven and Dieke (1929) for $v''=12$ to 21 and Curry and Herzberg (1934) for $v''=0$ and 1 are also shown. It will be seen that they fit quite accurately to the straight line and so may be expressed in the form $B_v'' = B_e'' - \alpha(v + \frac{1}{2})$. The slope of the present line gives $\alpha = 0{\cdot}0157\ \mathrm{cm}^{-1}$ whereas Curry and Herzberg (1934) gave $\alpha = 0{\cdot}0158\ \mathrm{cm}^{-1}$ the difference being within the error of the experiments. The value of B_e'' obtained from the experiments is $1{\cdot}447\ \mathrm{cm}^{-1}$. The constant D'' varies little with v'' and is usually taken as equal to D_e'' where $D_e'' = -4(B_e'')^3/\omega_e^2$. The value $D_e'' = 4{\cdot}88 \times 10^{-6}\ \mathrm{cm}^{-1}$ has been given previously by Curry and Herzberg (1934). Curry and Herzberg give the following formula to represent the band origins (ν_0) of the system,

$$\nu_0 = 49357{\cdot}55 + (698{\cdot}86v' - 10{\cdot}708v'^2 - 0{\cdot}194v'^3) - (1568{\cdot}33v'' - 11{\cdot}993v''^2 + 0{\cdot}0517v''^3 - 0{\cdot}00143v''^4).$$

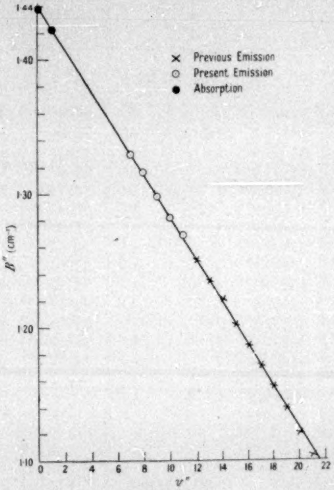

Values of Bv'' found by various observers.

The values of ν_0 for a band may be calculated from the wave-number ν of any line of the band by the formula

$$\nu = \nu_0 + (B' + B'')M + (B' - B'' + D' - D'')M^2 + 2(D' + D'')M^3 + (D' - D'')M^4,$$

where $M = K + 1$ for the R branch and $M = -K$ for the P branch. In the present case the values for the origins were calculated in this way and it was found that if M is less than about 15 the terms in D' and D'' become unimportant, and hence

$$\nu_0 = \nu - (B' + B'')M - (B' - B'')M^2.$$

The result of this calculation is shown in Table 4 together with the values calculated according to the Curry–Herzberg formula. The latter values seem to be consistently slightly higher than the measured values. However this is probably within the accuracy of the formula since the term in v''^4 has a value of about 10 to 20 cm⁻¹ and further terms would be necessary to give the highest accuracy.

Table 1. Wave-numbers and Analysis

Part of (1, 12) band

K	P branch (*ν*)	*I*	R branch (*ν*)	*I*	*K*	P branch (*ν*)	*I*	R branch (*ν*)	*I*
9	32837·9	1			23	32606·4	7 †	32681·3	5
11	32814·0 ?	8 b			25	32559·6	7	32640·2	6 b
13	32789·1	2	32832·1	3 dr	27	32508·5	6	32593·6	3
15	32759·9	5	32809·5	4	29	32440·7	7 d	32540·1	2
17	32727·4	0	32782·0	8 b	31			32480·5	8 b
19	32690·4	6	32752·4	5	33			32396·3	4
21	32650·4	4	32718·7	4					

(0, 11) band

K	P branch (*ν*)	*I*	R branch (*ν*)	*I*	*K*	P branch (*ν*)	*I*	R branch (*ν*)	*I*
1			33515·7	5 b	31	33009·6	8	33111·1	7
3	33498·2	1	33509·9	4 b	33	32947·8	8 b	33055·5	7
5	33486·7	3 b	33504·9	2 b	35	32882·6	8 b	32996·5	8
7	33471·6	5	33496·3	4	37	32814·0	8 b	32933·8	8
9	33453·3	5	33483·9	7 b	39	32740·8	8	32866·9	7
11	33430·7	6	33468·2	5	41	32664·5	7	32796·9	8
13	33405·0	6	33449·0	6	43	32584·9	8	32723·0	6
15	33375·6	6	33425·8	6	45	32501·2	6	32645·7	6
17	33342·3	7	33399·3	6	47	32413·9	4	32564·7	5
19	33305·3	7	33368·9	6	49	32324·2	7 d	32480·5	8 b
21	33265·2	7	33335·1	7	51	32224·6	6 do	32392·0	5
23	33220·9	7 b	33297·5	7	53	32128·8	6 b	32300·4	6 d
25	33173·6	7 . .	33256·4	7	55	32024·7	0	32200·9	8 b
27	33122·6	7	33211·4	7	57			32095·8	1
29	33067·6	7	33162·9	8 b	59			31991·8	2

(1, 11) band

K	P branch (*ν*)	*I*	R branch (*ν*)	*I*	*K*	P branch (*ν*)	*I*	R branch (*ν*)	*I*
3	34185·8	0			37	33483·9	7 b	33601·2	6
5	34173·4	3			39	33408·3	5	33532·3	6
7	34158·7	5	34183·0	3	41	33329·0	5	33460·0	7 do
9	34140·4	6	34169·7	7	43	33247·8	3	33383·0	7 d
11	34118·2	7 b	34154·3	6	45	43162·9	8 b	33303·1	4
13	34090·9	6	34133·7	6	47	33072·1	6	33220·9	7 b
15	34060·5	5	34110·4	6	49	32979·4	3	33132·3	5 dv
17	34026·4	7	34082·4	7	51	32882·6	8 b	33042·1	2
19	33988·7	7	34051·2	6	53	32782·0	8 b	32947·8	8 b
21	33947·8	6	34015·7	7	55	32676·8	5	32848·3	4
23	33902·5	6	33977·1	7	57			32746·8	4 do
25	33853·1	6	33934·8	6	59	32474·9	6	32640·2	6 b
27	33800·9	7	33888·1	6	61			32530·7	4 d
29	33745·0	6	33838·4	6	63	32215·1	0	32415·7	4
31	33684·9	6	33784·6	6	65			32297·9	4
33	33621·2	6	33727·7	6 b	67			32181·8	9 b
35	33554·3	6 do	33666·0	7					

Table 1 (*cont.*)

(0, 10) band

K	P branch (ν)	*I*	R branch (ν)	*I*	*K*	P branch (ν)	*I*	R branch (ν)	*I*
3	34824·8	3			27	34438·0	7	34526·6	7
5	34813·7	1	34834·6	6	29	34381·3	6	34476·3	8
7	34797·6	5	34822·9	6 b	31	34321·4	7	34422·1	8 b
9	34778·5	5	34809·6	6	33	34257·5	7	34364·3	8
11	34755·7	6	34793·3	5	35	34190·1	6	34303·5	7
13	34728·9	6	34772·9	6	37	34118·2	7 b	34238·3	7 do
15	34698·6	6	34749·0	7	39	34043·7	6	34169·7	7 b
17	34664·6	7	34721·2	7	41	33964·7	7 do	34097·3	7 do
19	34626·6	6	34689·5	7	43			34020·8	8 b
21	34585·1	7	34654·4	7	45			33940·6	6 do
23	34540·3	7	34616·1	7	47			33856·5	6 d
25	34490·4	8	34572·8	7					

(1, 10) band

K	P branch (ν)	*I*	R branch (ν)	*I*	*K*	P branch (ν)	*I*	R branch (ν)	*I*
5	35500·7	4	35519·0	7 b	39	34710·9	8	34836·3	6
7	35484·7	4	35508·8	7 b	41	34629·4	6	34759·6	7 dv
9	35465·3	5	35495·2	7 b	43	34545·1	7	34681·1	7
11	35441·6	5	35478·0	7	45	34456·3	8 do	34598·5	8 b
13	35414·6	5	35457·9	6	47	34364·3	8 b	34511·1	8
15	35383·6	6	35433·5	7 b	49	34267·2	5	34422·1	8 b
17	35348·5	6	35404·3	7	51		Vis	34328·6	5
19	35309·9	6	35371·5	7	53	34064·2	5 do	34228·5	7
21	35267·0	6	35335·6	7	55	33956·5	6 d	34128·2	5
23	35220·6	6	35295·4	6	57	33844·9	2	34020·8	8 b
25	35170·7	7 b	35251·5	6	59	33727·7	6 b	33912·2	3 d
27	35116·2	7 b	35203·0	7 b	61	33609·8	3 d	33796·3	7
29	35058·2	7	35151·8	6	63	33486·7	3 b	33677·5	2
31	34996·8	8	35096·1	7	65	33361·3	5 d	33560·3	3 d
33	34930·8	8	35036·7	8	67	33230·3	0 do	33434·8	0 dd
35	34861·5	8	34973·2	8 dv	69			33309·3	5 d
37	34787·5	7	34906·1	8					

(1, 9) band

K	P branch (ν)	*I*	R branch (ν)	*I*	*K*	P branch (ν)	*I*	R branch (ν)	*I*
3	36861·6	6			31	36330·5	7	36430·3	6
5	36850·0	0	36866·7	5	33	36259·6	5	36368·5	6
7	36833·6	3	36857·5	5	35	36191·2	6	36303·4	5 dv
9	36813·5	5	36843·3	6	37	36115·8	5 do	36233·3	5 dv
11	36789·4	5	36826·0	6	39	36035·7	5	36159·6	7 b
13	36761·1	7 b	36804·3	6	41	35952·2	7 b	36083·0	6 d
15	36729·2	6	36778·8	6	43	35864·8	6 b	36000·4	6
17	36693·2	5	36749·1	6	45	35771·3	5	35916·2	6 do
19	36653·6	7	36715·5	6	47	35678·7	7 do	35826·7	7
21	36609·5	7	36678·6	8 b	49	35579·6	8 b	35732·4	4
23	36561·9	7	36636·8	8 b	51	35475·7	7 b	35635·5	8 b
25	36509·5	6	36590·9	7 b	53			35533·5	6 do
27	36454·3	7 b	36541·2	6	55			35428·7	2 dv
29	36394·1	6	36488·1	6					

Table 1 (*cont.*)

(2, 9) band

K	P branch (ν)	*I*	R branch (ν)	*I*
5	37514·7	3		
7	37498·1	4	37521·6	5
9	37477·5	4	37507·7	6
11	37453·0	6	37489·0	5
13	37424·2	6	37466·3	8
15	37391·4	6	37440·0	6
17	37354·6	6	37409·3	6
19	37313·3	6	37374·5	5
21	37268·4	6	37335·8	7
23	37219·4	6	37292·7	6
25	37165·9	6	37245·3	6
27	37108·7	6	37194·6	6
29	37047·6	6	37139·2	6
31	36982·1	5	37080·4	7 b
33	36912·9	7 b	37016·0	7
35	36839·0	6	36949·0	4 do
37	36761·1	7 b	36877·4	6 dv
39	36678·6	8 b	36800·9	6
41	36590·9	7 b	36720·9	5
43	36504·1	6	36636·8	8 b
45	36409·8	5	36549·3	5
47	36312·0	4	36454·3	7 b
49	36209·7	5	36360·6	3 d
51			36262·7	6

(1, 8) band

K	P branch (ν)	*I*	R branch (ν)	*I*
7	38204·3	4		
9	38183·7	4	38221·0	3
11	38159·5	6 dv	38191·1	6 b
13	38130·4	4	38173·3	5
15	38097·5	5	38148·2	8 b
17	38060·7	5	38116·5	6
19	38019·3	5	38081·6	5
21	37974·3	4	38042·7	3
23	37925·1	7	37999·6	5
25	37872·0	4	37952·6	5
27	37814·4	5	37902·0	5 dv
29	37752·5	5	37846·2	7 b
31	37687·3	4	37786·7	5
33	37617·4	4	37723·4	4
35	37543·8	7 b	37655·7	3
37	37466·3	8 b	37583·1	2 dv
39	37383·7	4 d	37507·7	6 b
41	37297·9	5 d	37427·8	2
43	37208·6	2	37343·9	3 d
45	37113·6	5	37255·4	3 b
47	37012·4	2 b	37163·4	2
49	36912·9	7 b	37067·7	4 d
51			36966·7	3 d

(2, 8) band

K	P branch (ν)	*I*	R branch (ν)	*I*
3	38899·8	2	38909·9	3
5	38885·9	6	38903·5	5
7	38869·1	4	38892·7	6 d
9	38847·9	6	38877·9	6
11	38822·7	5	38858·8	6
13	38793·3	5	38835·6	6
15	38759·8	6	38807·9	5
17	38717·4	6	38776·3	6
19	38679·6	6	38740·5	6
21	38633·2	6	38700·4	6
23	38582·6	6	38656·0	6
25	38527·9	6	38607·4	6
27	38468·6	6	38554·5	6
29	38405·9	6	38497·3	6
31	38338·6	6	38436·2	6
33	38266·7	5	38370·8	6
35	38191·1	6 b	38300·6	6
37	38111·2	6	38227·0	6
39	38027·3	6 dv	38148·2	8 d
41	37939·0	5	38066·5	5
43	37846·2	7 b	37979·0	4
45	37749·6	5	37888·9	3
47	37648·4	4	37793·9	5
49	37543·8	7 b	37694·7	3 do
51	37434·0	6	37590·6	9 b*
53	37320·6	6	37482·4	3 d
55	37202·8	1	37370·6	2
57	37080·4	7 b	37255·4	3 b
59	36954·7	1	37136·0	2
61			37012·4	2 b

Table 1 (*cont.*)

(2, 7) band

K	P branch (ν)	I	R branch (ν)	I
3	40293·4	0		
5	40280·6	3	40298·0	5 b
7	40262·9	4	40286·7	3
9	40241·5	5	40271·4	5 b
11	40215·9	4	40251·6	5
13	40185·8	5	40227·7	5
15	40150·8	5	40199·5	5
17	40112·0	5	40166·6	5
19	40068·8	5	40129·6	5
21	40021·2	5	40088·0	6
23	39969·3	5	40042·7	5
25	39913·0	6	39992·5	5
27	39852·5	5	39938·1	5
29	39787·0	5	39879·2	5
31	39718·1	5	39815·3	5
33	39644·7	5	39748·4	5 d
35	39566·5	6 d	39676·3	5
37			39600·1	5

No measures beyond P (35) and R (37)

Abbreviations in Table 1 :—

b—line blended.
b*—blended with a Pt line.
d—line diffuse.
dv—line diffuse to violet.
dr—line diffuse to red.
dd—line very diffuse.
do—line probably double.
†—line on diffuse patch.

Table 2. $\Delta_2 F''(K)$

K	$v''=7$	$v''=8$	$v''=9$	$v''=10$	$v''=11$
4		24·0			23·2
6	35·1	34·4	33·1	34·3	33·3
8	45·2	44·8	44·1	44·0	42·8
10	55·5	55·2	54·3	53·8	53·2
12	65·8	65·5	64·9	63·9	63·3
14	76·9	75·8	75·0	74·3	73·3
16	87·5	87·5	85·5	84·7	83·8
18	97·8	97·0	95·8	94·5	93·9
20	108·4	107·3	106·1	104·5	103·6
22	118·7	117·7	116·6	115·0	113·7
24	129·7	127·9	127·1	125·0	124·0
26	140·0	138·5	136·6	135·1	133·9
28	151·1	149·1	147·1	145·1	143·5
30	161·1	158·8	157·4	155·0	153·4
32	170·6	169·4	167·5	165·0	163·4
34	181·9	179·7	177·2	174·7	172·9
36		189·4	187·8	185·5	182·3
38		199·6	197·6	194·9	193·0
40		209·5	207·4	206·0 ?	202·9
42		219·7	217·5	214·5	212·1
44		229·9	227·0	224·8	221·4
46		240·5	237·4	234·2	231·4
48		250·3	247·1	243·9	241·0
50		260·7	256·7		249·7 ?
52		270·0		264·4	260·1
54		279·6		272·0	271·0
56		290·2		283·3	
58		300·7		293·1	
60				302·4	

Table 3. New Values of B_v''

v''	11	10	9	8	7
B_v''	1·269	1·282	1·298	1·316	1·329

Table 4. Wave-numbers of Band Origins

Band	Formula	Experimental
2, 7	40305·9	40304·6
2, 8	38911·2	38910·1
1, 8	38245·8	38245·2
1, 9	36873·7	36872·8
2, 9	37539·0	37537·9
1, 10	35524·1	35522·7
0, 10	34836·2	34835·7
1, 11	34197·2	34197·3
0, 11	33509·2	33508·9
1, 12	32892·9	32892·2

§3. THE VIBRATIONAL INTENSITY DISTRIBUTION IN THE SCHUMANN-RUNGE SYSTEM

The bands found in the present investigation and in that of Lochte-Holtgreven and Dieke indicate a wide Franck–Condon parabola in the v', v'' array as would be expected since the emission of the system involves a large change in equilibrium inter-nuclear distance. Miss M. E. Pillow has recently been engaged on a theoretical treatment of the vibrational intensity distribution in this system. Though her results are not yet quite complete they are sufficiently extensive for it to be stated that there is good agreement with the present experiments.

§4. BANDS ATTRIBUTED TO PtO

Whilst working with a high voltage arc in oxygen between Pt–Rh electrodes (see Feast 1949 for a discussion of suitable electrodes) a few bands were found in the visible region. These bands also occurred when using Pt electrodes but not with Cu electrodes. In the latter case the CuO bands appeared. The bands are therefore attributed to PtO. The wavelengths of their heads are 5664 A., 5906 A. and 6180 A. They are degraded to the red. There appears to be no previous record of bands due to this molecule.

ACKNOWLEDGMENTS

The author wishes to express his sincere thanks to Professor R. W. B. Pearse for suggesting this work and for giving much encouragement and advice. Miss M. E. Pillow kindly placed the results of her theoretical work at the author's disposal in advance of publication and he is indebted to her both for this and for several useful discussions. The work was made possible by the award of a grant from the Department of Scientific and Industrial Research.

REFERENCES

Babcock, H. D., 1945, *Astrophys. J.*, **102**, 154.
Burns, K., 1913, *Lick Observatory Bulletin*, No. 247.
Curry, J., and Herzberg, G., 1934, *Ann. Phys., Lpz.*, **19**, 800.
Feast, M. W., 1948, *Nature, Lond.*, **162**, 214; 1949, *Proc. Phys. Soc.* A, **62**, 114.
Knauss, H. P., and Ballard, S. S., 1935, *Phys. Rev.*, **48**, 796.
Lal, L., 1948, *Nature, Lond.*, **161**, 477.
Lochte-Holtgreven, W., and Dieke, G. H., 1929, *Ann. Phys., Lpz.*, **3**, 937.
Millon, J, and Herman, L., 1944, *C.R. Acad. Sci., Paris*, **218**, 152.

New O_2^+ Second Negative Bands: a Note on O_3 and O II Emission Spectra

By M. W. FEAST
Imperial College, London S.W.7 *

MS. received 19*th October* 1949

ABSTRACT. The spectrum of an electrodeless discharge in pure oxygen has been studied. New bands of the O_2^+ Second Negative system have been found and the intensity distribution in this system is discussed; subsidiary parabolae as well as the main Franck–Condon parabola are obtained as is predicted by the theory. Emission bands reported by Johnson as due to O_3 are due to O_2^+ and O II. Some abnormal intensities of O II lines excited in the electrodeless discharge are noted. The electrostatic and electromagnetic types of excitation are briefly compared.

§ 1. INTRODUCTION

The O_2^+ Second Negative band system was excited by an electrodeless discharge in pure oxygen. In addition to bands previously reported, others were found which have been shown to belong to this system. When the new bands are taken into account the system is found to show a vibrational intensity distribution with secondary and tertiary parabolae as well as the normal Franck–Condon parabola. These subsidiary parabolae are to be expected for the transition since it involves a large change of equilibrium inter-nuclear distance.

Interest in these bands was originally stimulated by Johnson's observation (1924) of weak bands, which he attributed to O_3, on his spectrograms of the O_2^+ Second Negative system. These bands are not identical with those observed by Janin (1938) in emission from an ozonizer discharge, and also attributed to O_3. It was thus felt desirable to re-examine the oxygen spectrum in order to reach a more definite conclusion with regard to the O_3 emission spectrum. The present work with an electrodeless discharge has revealed no bands that can be attributed to O_3. A study of Johnson's results has shown that his ozone emission spectrum may satisfactorily be accounted for as O II lines and O_2^+ bands. It has not been possible to decide whether or not Janin's bands are a true O_3 spectrum. Finally the relative intensities of the O II lines excited in the high-frequency discharge are discussed, and a complex spectrum obtained from another form of high-frequency discharge is mentioned.

§ 2. EXPERIMENTAL

The spectrum emitted by a glow discharge in oxygen often consists mainly of bands and lines due to impurities in the gas (NO, N_2, CO_2^+, CO). To excite band spectra from oxygen itself it is necessary to remove all sources of impurity from the vacuum system employed. In the present investigation a fused quartz discharge tube 15 cm. long and 3 cm. in diameter with a quartz window fused on one end was used. This tube was evacuated by a mercury diffusion pump with liquid air trap and a 'Hyvac' pump. Pure oxygen was obtained by heating potassium permanganate in a side tube. After the apparatus had been baked out and swept out once or twice with pure oxygen it was found that the spectrum was free from all impurities except faint Mn *raies ultimes* and one or two faint SiO bands.

---

* Now with the National Research Council, Ottawa, Canada.

To excite the spectrum a Metropolitan–Vickers induction furnace was used. The output of this generator was applied to two external electrodes in the form of tin-foil bands wrapped round the outside of the discharge tube. The region 2000 A. to 7000 A. was investigated with a medium quartz (Hilger E.2) spectrograph using Ilford 'Astra III' and 'Q' plates. A prism grating instrument was employed to examine the region 6000 A. to 10,000 A. using Kodak 'I.R.E.R.' and 'I.Q.' plates. These plates were hypersensitized in ammonia before use.

§ 3. APPEARANCE OF THE SPECTRA

At a pressure of about 0 05 mm. Hg a yellow-green glow is obtained, and this consists of bands due to the O_2^+ First and Second Negative systems together with lines due to O II and weaker ones due to O I and O III. This discharge fills the whole of the tube except for the region inside the electrodes, where the luminosity is confined to the axis of the tube. At a slightly higher pressure the discharge is non-luminous except for a mauve glow inside the electrodes and strongest at the walls. The glow shows the same main features in its spectrum as that shown by the lower pressure discharge, but the lines are stronger relative to the bands. At a still higher pressure just prior to extinction of the discharge there is a faint glow along the axis of the tube between the electrodes. This last type of glow gives a continuous spectrum. The continuum was photographed with a small quartz (Hilger E.3) spectrograph because of its weakness and was found to extend from the blue to the ultra-violet region with gradually decreasing intensity.

§ 4. NEW O_2^+ SECOND NEGATIVE BANDS

The Second Negative system of O_2^+ consists of a large number of red-degraded double-headed bands extending from about 2000 A. to 6000 A. The bands have been studied by several workers (Johnson 1924, Ellsworth and Hopfield 1927, Stevens 1931, Mulliken and Stevens 1933, Lal 1948). This work has established that the bands are due to the transition $A^2\Pi_u \rightarrow X^2\Pi_g$ with a doublet separation of about 200 cm^{-1}. It has been tentatively suggested (Lal 1948) that the Franck–Condon parabola of this system may be much narrower than has previously been assumed. However, this suggestion is not supported by the new data given here, which are consistent with the large change in equilibrium inter-nuclear distance involved in the transition ($r_e' = 1{\cdot}41$ A., $r_e'' = 1{\cdot}14$ A.).

The present spectra show, in addition to the bands previously reported for this system, a considerable number of new bands. These new bands are red-degraded and show a 200 cm^{-1} doublet separation. Hence an attempt was made to fit them into the Second Negative system. It was found that all the new bands could be satisfactorily accounted for in this way. Head measurements are presented in Table 1.

In Table 1 λ is the wavelength of the head measured from E.2 spectrograms; over most of the region investigated this should be correct to 0·5 A. The wave numbers obtained from these wavelengths are given in the third column. The vibrational quantum numbers assigned to the bands are given in the last column

In this column i and ii denote the shorter and longer wavelength heads of each band. The analysis was made on the basis of wave-number calculations from the constants of the system. The calculated values given in the column are ν_{cal}; the formula used for these was

$$\nu = \left.\begin{matrix} 38596 \\ 38796 \end{matrix}\right\} + \{898{\cdot}9(v' + \tfrac{1}{2}) - 13{\cdot}7(v' + \tfrac{1}{2})^2\}$$
$$- \{1876{\cdot}4(v'' + \tfrac{1}{2}) - 16{\cdot}53(v'' + \tfrac{1}{2})^2\}.$$

Table 1

λ	I	ν	ν_{cal}	v', v''
2562·5	2	39013	39012	11, 4 ii
2588·9	4	38615	38615	10, 4 i
2602·9	4	38407	38415	10, 4 ii
2677·8	1	37333	37338	8, 4 i
2691·5	1	37143	37138	8, 4 ii
2860·0	3	34955	34947	7, 5 i
2877·3	3	34745	34747	7, 5 ii
2936·9	4	34040	34040	6, 5 ii
3005·0	2	33268	33269	7, 6 i
3022·8	2	33072	33069	7, 6 ii
3070·0	5	32564	32562	6, 6 i
3088·7	5	32367	32362	6, 6 ii
3096 ?	2	32301	32303	8, 7 i
3113·6	2	32108	32103	8, 7 ii
3160·7	a	31629	31624	7, 7 i
3225·8	a	30991	30987	11, 9 i
3257·6	3	30689	30691	8, 8 i
3312·7	a	30178	30182	5, 7 i
3334·2	a	29984	29982	5, 7 ii
3353·5	3	29811	29812	7, 8 ii
3465·9	1	28844	28844	10, 10 i
3542·0	4	28225	28219	9, 10 i
3567·7	4	28021	28019	9, 10 ii
3653·0	2	27367	27367	8, 10 ii
3700·5	a	27016	27019	3, 8 i
3928·9	a	25445	25445	5, 10 i†
3959·1	a	25251	25245	5, 10 ii†
4760	3	21002	21006	5, 13 i
4803	3	20815	20806	5, 13 ii
5102	3	19595	19592	5, 14 i
5143 ?	3	19439	19392	5, 14 ii

i, ii denote shorter and longer wavelength heads.
†, blend with 3, 9 i and 3, 9 ii (see text).
a, difficult to judge intensity due to overlapping structure.
?, wavelength may be inaccurate due to overlapping structure.

This formula uses the constants given by Jevons (1932) and Birge (1929), which differ from those used by Ellsworth and Hopfield (1927). The new measurements do not justify any change in this formula, as deviations from it appear to be random and hence must be attributed to experimental error. A consideration of band intensities suggests that the bands marked † are actually blends of the bands given in the last column with 3, 9 i and 3, 9 ii (25,440 cm^{-1} and 25,240 cm^{-1}). The intensities recorded in the second column are visual estimates. An attempt has been made to keep them on the scale used by Johnson (1924). On this scale the strongest band of the system has an intensity 9.

§ 5. VIBRATIONAL INTENSITY DISTRIBUTION

The Figure shows the distribution of vibrational intensities in the system. It is seen that all the bands previously reported fall on a wide Franck–Condon parabola. However, when the new bands are taken into account, secondary and tertiary parabolae are found. Observation of these extra loci is in accordance with wave-mechanical theory, which predicts them for transitions involving a large change in equilibrium inter-nuclear distance (see for instance Gaydon and Pearse 1939). It will be noted that there are bands falling on the subsidiary loci which have not been observed. Calculations show that all these missing bands would be obscured by main parabola bands.

Miss M. E. Pillow has kindly supplied details in advance of publication of her theoretical work on the intensity distribution in this system. These calculations were made on the assumption of an equal distribution of molecules amongst the vibrational levels of the upper state (i.e. an infinite temperature distribution). Comparison with the results of the present experiments shows that good agreement is to be expected if the distribution of molecules in the upper state is changed to weight the higher v' levels even more heavily that in the infinite temperature distribution. Such a distribution is in fact likely if the system is excited by electron collisions with molecules in the ground state of either O_2 or O_2^+. A consideration of the various potential curves shows that if the Franck–Condon principle is obeyed the higher v' levels of the O_2^+ upper state will be preferentially populated. The agreement of theory and experiment may therefore be stated to be satisfactory.

v' \ v''	0	1	2	3	4	5	6	7	8	9	10	11	12	13	14	15
0						8	7	8	8	6	5	3	1			
1				3	5	6	7	8				3		4	2	
2		1	2	7	8	8	4	2								
3		1	2	8	7	6	a		a	a						
4		3	6	7	7	3										
5		2	8	7				a			a			3	3	
6	a	2	6	4		4	5									
7	a	3	6	1		3	2	a	3							
8	a	1	1		1			2	3		2					
9	a	a									4					
10	a	a			4						1					
11	a	a			2					a						
12	a															
13	a															
14	a															
15	a															

Distribution of vibrational intensities in the Second Negative system of O_2^+.

§6. THE REPORTED O_3 EMISSION SPECTRUM

On Johnson's spectrograms of the O_2^+ Second Negative band system (1924) appear a number of bands which were not fitted into any system. From a comparison of the wavelengths of these bands with the wavelengths of the ozone absorption bands Johnson concluded that these formed an O_3 emission spectrum. On the other hand, Janin (1938) records a large number of bands emitted by an ozonizer discharge in oxygen. These bands are attributed to O_3, but they are not identical with those observed by Johnson. No structure was found on the present spectrograms which could be interpreted as due to O_3. A study of Johnson's measurements and his published photographs has shown that his ozone bands may be accounted for as O_2^+ bands and O II lines. The identification of Johnson's bands is given in Table 2. It should be noted that the O II lines quoted were all found to occur together with the bands on the present spectrograms.

In two cases one O_2^+ band is used to identify two 'O_3' bands. This is justified by the appearance of Johnson's spectrograms, two positions on the band having been measured. Some confusion exists about the wavelengths of the two 'O_3' bands marked †. The wavelengths 4333·3 A. and 4316·5 A. appear in Johnson's list, and if they are indeed correct they may be identified as the O II lines in Table 2. However, on the published spectrogram a band is marked 4316 A. which actually lies near 4240 A. Another band is marked 4216 A. and appears quite strong, though it is not to be found in the table of wavelengths. A comparison of spectrograms indicates that these last-mentioned bands are probably 4238·0 1, 9 ii and 4218·3 1, 9 i O_2^+. Lines are present above 4300 A. in the photograph which are probably the O II lines given in Table 2, but these are not marked 'O_3'. The present interpretation of Johnson's bands still leaves one of them unclassified. This band does not occur in the present spectra, and may possibly be due to an impurity.

Table 2

O_3 band	*I*	Identification	O_3 band	*I*	Identification
4464·7	1	4465·45(4) O II	3337·8	6	3333·8 5, 7 ii O_2^+
4333·3	2	4336·86(6) O II†	3331·5	4	
4316·5	5	4317·16(8) O II†	3313·1	5	3314·3 5, 7 i O_2^+
4276·9	2	4275·52(4) O II	3284·6	2	3287·59(9) O II
3568·9	2	3565·6 9, 10 ii O_2^+	3278·1	2	3277·69(7) O II
3565·2	1		3606·1	5	?
3465·3	0	3465·9 10, 10 i O_2^+	3097·5	4	3093·1 8, 7 i O_2^+
3378·3	1	3377·2(7) O II	3090·4	8	3090·8 6, 6 ii O_2^+

† See text.

It is more difficult to be certain of the origin of the bands reported by Janin (1938). Comparison of the wavelengths shows that many may be due to O_2^+ and O II. However, some strong O_2^+ bands and O II lines do not appear in Janin's list, and thus the correctness of this identification is in doubt.

§7. NOTES ON INTENSITIES IN THE SPECTRUM O II

Emeléus (1934) has pointed out that the following multiplets which are present in the positive column of a condensed discharge are missing in a negative glow of low current density:

$$4956\text{ A.}-4941\text{ A.}(^3P)3p\,^2P^0-(^3P)3d\,^2D$$
$$4406\text{ A.}-4359\text{ A.}(^3P)3p\,^2D^0-(^3P)3d\,^2D$$
$$2419\text{ A.}-2407\text{ A.}(^3P)3p\,^2D^0-(^1D)3d\,^2D$$

An examination of the high-frequency discharge spectrograms shows that these multiplets are missing there; it has revealed that a number of other multiplets are also missing or weakened. The multiplets are listed in Table 3. Since there appears to be no fundamental difference between a line being weakened or completely missing from a particular spectogram, the two types are not distinguished in the table. Lines with a common initial level are grouped together, beginning with those lines whose initial levels are in common with the above three multiplets. The identifications were made using the data of Mihul (1928) and Moore (1933). For each initial level given in Table 3 all known multiplets were studied and they are all listed in the table, showing that there are no inconsistencies in the data. The multiplets marked † are in any case rather weak, and to find them missing on moderately exposed spectrograms is not, of itself, surprising. They are, however, listed for completeness since each has a common initial level with a multiplet which definitely shows the effect.

Table 3

λ (A.)		λ (A.)	
†4871–4861	$({}^1D)3p\,{}^2P^0-({}^1D)3d\,{}^2D$	4448–4443	$({}^1D)3p\,{}^2F^0-({}^1D)3d\,{}^2F$
†4332–4327	$({}^1D)3p\,{}^2D^0-({}^1D)3d\,{}^2D$	4703–4698	$({}^1D)3p\,{}^2D^0-({}^1D)3d\,{}^2F$
2575–2572	$({}^3P)3p\,{}^2P^0-({}^1D)3d\,{}^2D$	2530–2518	$({}^3P)3p\,{}^2D^0-({}^1D)3d\,{}^2F$
4705–4753	$({}^3P)3p\,{}^2D^0-({}^3P)3d\,{}^2F$	4169–4121	$({}^3P)3p\,{}^4P^0-({}^3P)3d\,{}^4P$
4112–3876	$({}^3P)3p\,{}^4P^0-({}^3P)3d\,{}^2F$	4925–4891	$({}^3P)3p\,{}^4S^0-({}^3P)3d\,{}^4P$
3857–3833	$({}^3P)3p\,{}^4D^0-({}^3P)3d\,{}^2F$	3097–3864	$({}^3P)3p\,{}^4D^0-({}^3P)3d\,{}^4P$
4699–4751	$({}^3P)3p\,{}^2D^0-({}^3P)3d\,{}^4D$	†3488	$({}^3P)3p\,{}^2S^0-({}^3P)3d\,{}^4P$
4865–4856	$({}^3P)3p\,{}^4S^0-({}^3P)3d\,{}^4D$	3390–3377	$({}^3P)3p\,{}^2S^0-({}^3P)3d\,{}^2P$
4121–4097	$({}^3P)3p\,{}^4P^0-({}^3P)3d\,{}^4D$	5207–5160	$({}^3P)3p\,{}^2P^0-({}^3P)3d\,{}^2P$
3883–3848	$({}^3P)3p\,{}^4D^0-({}^3P)3d\,{}^4D$	†3985	$({}^3P)3p\,{}^4P^0-({}^3P)3d\,{}^2P$
†3475	$({}^3P)3p\,{}^2S^0-({}^3P)3d\,{}^4D$		

†, weak multiplets (see text).

In the multiplet $({}^3P)3s\,{}^2P-({}^3P)3p\,{}^2D^0$ the line 4452·4 A. is abnormally weak.

There is no very obvious cause for these irregularities. Emeléus (1934) discussed various possible explanations for the behaviour of the multiplets he examined, but reached no very satisfactory conclusion. However, as he pointed out, it is of importance to recognize these irregularities even if no explanation can immediately be found for them, especially since O II lines are met with in astrophysical work (stellar spectra and possibly the aurorae).

§ 8. THE SOLENOID METHOD OF EXCITATION

The work described in the preceding sections was carried out using external electrodes as described in § 2. Some experiments were also carried out using a solenoid wound round the discharge tube as the method of applying the high-frequency impulse to the gas in the discharge tube. At about 0·05 mm. Hg of oxygen a very intense, whitish-blue discharge is obtained. The spectrum of this discharge contains lines of O I and O II but, in contrast to the previous method of excitation, the O I lines predominate. O_2^+ First and Second Negative bands also occur. The Second Negative bands have been observed in detail and show a much higher rotational temperature than in the electrostatic method of excitation; this leads to an almost unrecognizable appearance of the spectrum at the short wavelength end. There also appears to be a lowering of the vibrational temperature.

It is hoped to make a more detailed comparison of the two modes of excitation in the near future.

ACKNOWLEDGMENTS

The author wishes to thank Professor R. W. B. Pearse, who directed this research, for much helpful advice. He is indebted to Miss M. E. Pillow, with whom he has had some discussion on the vibrational intensity distribution in the O_2^+ system, and who kindly communicated to him the results of her theoretical work in advance of publication. The work was made possible by a grant from the Department of Scientific and Industrial Research.

REFERENCES

Birge, R. T., 1929, *International Critical Tables*, **5**, 409.
Ellsworth, V. M., and Hopfield, J. J., 1927, *Phys. Rev.*, **29**, 79
Emeléus, K. G., 1934, *Proc. Nat. Acad. Sci., Wash.*, **20**, 115.
Gaydon, A. G., and Pearse, R. W. B., 1939, *Proc. Roy. Soc.* A, **173**, 37.
Janin, J., 1938, *C.R. Acad. Sci. Paris*, **207**, 145.
Jevons, W., 1932, *Report on the Band Spectra of Diatomic Molecules* (London : The Physical Society).
Johnson, R. C., 1924, *Proc. Roy. Soc.* A, **105**, 583.
Lal, L., 1948, *Phys. Rev.*, **73**, 255.
Mihul, C., 1928, *Ann. Phys., Paris*, **9**, 261.
Moore, C. E., 1933, *A Multiplet Table of Astrophysical Interest* (Princeton, N.J. : The Observatory).
Mulliken, R. S., and Stevens, D. S., 1933, *Phys. Rev.*, **44**, 720.
Stevens, D. S., 1931, *Phys. Rev.*, **38**, 1291.

The Spectra Emitted by the High Voltage Arc in Nitrogen, Hydrogen, Nitrogen–Hydrogen Mixtures and Ammonia

By M. W. FEAST*
Imperial College, London S.W.7

MS. received 19th October 1949

ABSTRACT. The spectra emitted by the high voltage arc in nitrogen, hydrogen, hydrogen–nitrogen mixtures and ammonia have been studied.

The appearance of the N_2 Second Positive bands at various nitrogen gas pressures is discussed and the divergence of rotational and vibrational temperatures is noted. Traces of oxygen greatly reduce the strength of the N_+ bands emitted by the arc in nitrogen. In N_2–H_2 mixtures the NH 3360 A. band is found to be emitted strongly only when hydrogen is present at a very low partial pressure. An attempt is made to explain the various observations.

§ 1. INTRODUCTION

In a previous paper (Feast 1949) a high voltage, low current, arc source was described and its use in the excitation of the O_2 Schumann–Runge bands was discussed. The investigation of this source has now been extended to include several other gases. The present paper reports spectroscopic observations on the excitation of nitrogen, hydrogen, mixtures of these two gases and ammonia. A study, such as this, of the variations produced in band spectra by changing the experimental conditions has become of interest lately, due to the possibility of applying the results obtained to astrophysical and upper atmosphere problems.

§ 2. THE HIGH VOLTAGE ARC IN NITROGEN AT ATMOSPHERIC PRESSURE

Preliminary observations of the spectrum of the high voltage arc were made with a Hilger small quartz spectrograph which covered the region 2000 A. to 6500 A. In the infra-red region a prism-grating instrument was used from 6000 A. to 9000 A. Features of particular interest were later examined in detail in the first order of a 10 ft. Eagle Mounting concave grating (5·5 A/mm.).

---

* Now with the National Research Council, Ottawa, Canada.

When cylinder nitrogen at atmospheric pressure was used in the arc without purification the spectrum in the ultra-violet region was found to consist of strong N_2 Second Positive bands and weak N_2^+ First Negative bands together with NOγ, OH, CN and sometimes NH bands. If, however, a piece of metallic sodium was placed in the arc chamber, the NO and OH bands were removed. The CN bands (the violet system) were very persistent unless the vacuum system was particularly clean, the smallest trace of carbon compounds bringing the bands up strongly. It was noticed that the N_2^+ bands were considerably strengthened by the removal of oxygen from the gas. This is of interest in connection with the theory of the formation of NO_2 in discharges. Brewer and Westhaven (1930 a), by chemical methods, and Wansbrough-Jones (1930 a), by controlled electron experiments, conclude that N_2^+, or N_2^+ (excited), ions are necessary for the production of NO_2. It cannot be said that this point is definitely settled yet—see for instance Willey (1937), and compare with the analogous controversy in the case of O_3 (Wansbrough-Jones 1930 b, Brewer and Westhaven 1930 b, Deegan and Emeléus 1948)—but the present observation links the disappearance of the N_2^+ excited states with the presence of oxygen in the gas, and thus tends to support the N_2^+ theory. It is relevant to remark here that though there is copious production of NO_2 from a high voltage arc in N_2–O_2 mixtures (i.e. air), there is little or no production of O_3 from the high voltage arc in oxygen. This is probably due to the fact that any O_3 that is formed will be almost certainly dissociated at the high temperature of the arc.

In the infra-red region of the spectrum 10-ft. grating spectrograms revealed nitrogen First Positive bands. The appearance of these bands differed considerably from that found in a low pressure discharge. This may be explained as due to the much higher rotational temperature in the arc.

§ 3. THE NITROGEN SECOND POSITIVE BANDS IN THE HIGH VOLTAGE ARC AT VARIOUS PRESSURES

The appearance of the nitrogen Second Positive bands in the high voltage arc at various nitrogen gas pressures has been studied in detail on 10-ft. grating spectrograms.

The general appearance of the Second Positive bands in the arc at atmospheric pressure may be seen from the Plate at *g*. A spectrogram of a positive column discharge in nitrogen at low pressure is included for comparison. The change in structure of the bands may best be illustrated by discussing the (0,0) sequence. It will at once be seen that the rotational temperature of the bands is considerably higher in the arc than in the discharge. A similar result was obtained by Nakamura (1927) who employed a low voltage tungsten arc in nitrogen at 30 to 50 cm. Hg pressure. He used this mode of excitation to measure high rotational lines (up to $J=112$) in the (0,0) band. Microphotometer measurements of the present spectra give rotational temperatures of about 4,000° K. for the arc and 1,000° K. for the discharge.

Further study of the arc and discharge spectra reveals that whilst the rotational temperature of the Second Positive bands has increased from the discharge to the arc, the vibrational temperature has decreased. Thus in the (0,0) progression the bands (3,3), (4,4) are clearly visible in the discharge and entirely absent in the arc spectra. There is, of course, emission from v' levels >0 since sequences to the short wavelength side of the (0,0) sequence do occur, but

PROC. PHYS. SOC. VOL. 63, PT. 6—A (M. W. FEAST)

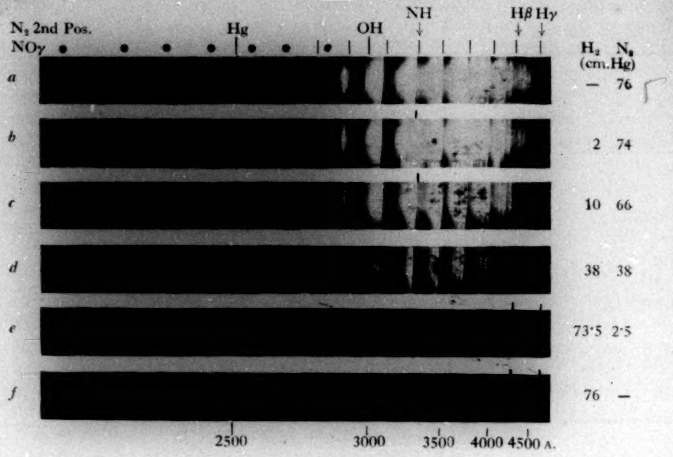

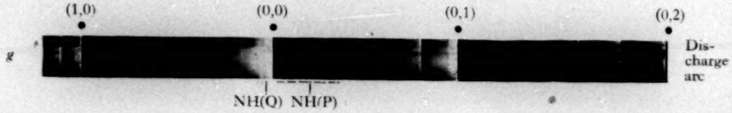

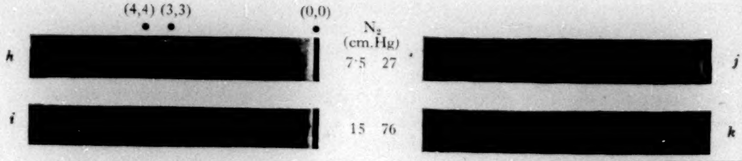

a–f. Spectra of a high voltage arc in H_2–N_2 mixtures. Equal exposure times for all spectrograms. E.3 spectrograph. Spectrogram *f* is too weak to show the H_2 continuum.

g. Spectrum of a high voltage arc in N_2 at 76 cm. Hg pressure with a spectrum of a normal low pressure discharge in N_2 for comparison. 10 ft. Eagle Mounting spectrograph.

h–k. Spectra of a high voltage arc in N_2 at various pressures. Equal exposure times for all spectrograms. 10 ft. Eagle Mounting spectrograph.

the present work shows that they are weakened relative to the discharge spectra. Further evidence of this divergence of rotational and vibrational temperatures has been obtained by photographing the arc in nitrogen at various gas pressures. The Plate (*h*–*k*) shows a set of equal exposures at pressures of 760 mm., 270 mm., 150 mm. and 75 mm. Hg. It will be noted that the strength of the bands increases with decreasing pressure, at first very rapidly. This behaviour should be contrasted with the rapid decrease in intensity of the Schumann–Runge O_2 bands under comparable conditions (Feast 1949). The spectrograms show the increase in vibrational temperature and the decrease in rotational temperature as the pressure is reduced.

It may be noted here that the First Positive bands also show this divergence of rotational and vibrational temperatures. The bands of this system which lie in the visible region correspond to high v' values and are all quite weak compared with the infra-red emissions.

The explanation of the difference in behaviour of the rotational and vibrational structure of the bands is probably to be found in the high collision rate at atmospheric pressure. The excited molecules with $v'>0$ will suffer sufficient collisions before radiating (at these high pressures) for a large number to be reduced to $v'=0$. This assumes of course that vibrational de-activation is more easily affected under these conditions than electronic de-activation; this is probably correct. Since the arc may approach thermal equilibrium at the rotational temperature, rotational de-activation is not to be expected to be important.

Predissociation by rotation has been observed in all levels of the upper state of the Second Positive system except $v'=0$. Coster, Van Dijk and Lameris (1935) have attempted to fix the position of the intersection of the potential curve of the dissociating state with that of the dissociated state. From the levels in which predissociation has been observed they deduce a point, B, on the potential curve of the dissociated state below which this intersection must lie. Measurements of the predissociation can do no more than this since the dissociating state probably has a maximum in its potential curve at large inter-nuclear distances. Coster *et al.* have examined a discharge in nitrogen and measured lines of the (0, 0) band to $J=90$. Since no predissociation occurs up to this level they are able to deduce another point, A, above which the intersection of the two curves must lie. They then tentatively place this intersection mid-way between A and B on the dissociated curve. This is of course somewhat unsatisfactory, especially as the $J=90$ point is completely arbitrary. They have apparently overlooked Nakamura's work in which $J=112$ was attained. No further experiments have yet been made with the present source, but it might be possible to fix the point of intersection of the two curves exactly by photographing the (0, 0) band from the arc at very large dispersion to obtain a limit for predissociation. The very high dispersion would be necessary since the predissociation is probably in the region where the (0, 0) and (1, 0) bands overlap.

§4. THE HIGH VOLTAGE ARC IN HYDROGEN AT ATMOSPHERIC PRESSURE

In hydrogen at atmospheric pressure the high voltage arc between Pt–Rh electrodes is barely visible, being faintly bluish in colour. Spectrograms of this discharge show the Balmer lines, the hydrogen ultra-violet continuum and the H_2 many-lined spectrum. It was often found that absorption bands appeared near 2100 A. in the continuum. These bands became much stronger when a little nitrogen was added to the arc, and they have been identified as due to NH_3. There is apparently sufficient nitrogen in the hydrogen gas cylinders to give these bands.

§ 5. THE HIGH VOLTAGE ARC IN HYDROGEN–NITROGEN MIXTURES

The experiments in hydrogen–nitrogen mixtures were all carried out with a total pressure of one atmosphere. A series of spectra was obtained which covered the whole range from 100% hydrogen to 100% nitrogen. Typical spectrograms for the ultra-violet and blue regions are shown in the Plate (*a–f*); these were all taken with the same exposure times.

The 100% cylinder N_2 spectrum shows NOγ, N_2 Second Positive, OH and CN bands (probably also N_2^+ bands). Introduction of hydrogen (2 cm. Hg pressure) removes the NOγ bands completely. This is presumably due to the hydrogen reducing any NO present. The other alteration in the spectrum is the appearance in great strength of the NH 3360 band (the β band). The most interesting observation which has resulted from these experiments is the peculiar behaviour of the NH β band as the percentage composition of the gas mixture is varied. The Plate shows that as the percentage of hydrogen is increased the band reaches a maximum and then falls in intensity. It is missing, or is at least very weak, in a mixture containing 50% H_2 and 50% N_2, which might have been expected to show the band most strongly. No accurate determination has been made of the pressure of hydrogen at which the band reaches its maximum intensity. A small quantity of hydrogen (a few mm. Hg) produces the band very strongly, and the intensity does not appear to vary appreciably until it starts falling at between 1 and 3 cm.Hg of H_2. Observations in the visible region with a mixture of 50% H_2 and 50% N_2 reveal the presence of the ammonia α band (probably due to NH_2).

With smaller proportions of hydrogen the α band is weaker and is overlapped by nitrogen First Positive bands.

The only other experiments of which the author is aware which are relevant to the present observations on the NH β band are those of Gaviola and Wood (1928) (see also Willey 1934). Gaviola and Wood succeeded in obtaining the NH band in a sensitized fluorescence experiment of the Cario–Franck type. The fluorescence was excited in the normal manner by mixing the gas (H_2 and N_2) with mercury vapour and illuminating it with the mercury line at 2537 A. Atoms of nitrogen and hydrogen were formed by collisions with excited Hg atoms and these combined to give NH and the β band. It was found that the NH band fell in intensity as the hydrogen pressure was raised. This behaviour was attributed to the reaction $NH + H_2 \rightarrow NH_3$, which would reduce the intensity of the band. Such an argument seems plausible, although quantitative confirmation does not appear to be possible. The same reasoning can be applied equally well to the present observations, and the reaction $NH + H \rightarrow NH_2$ may be added to express the increase in strength of the α band with the decrease in strength of the β band, though of course the NH_2 might also be formed in other ways, such as $N + H_2 \rightarrow NH_2$.

§6. THE HIGH VOLTAGE ARC IN AMMONIA

In studying the emission spectrum of ammonia in the high voltage arc at atmospheric pressure it was necessary to use a constant flow of the gas as the arc caused a considerable amount of dissociation into nitrogen and hydrogen. Apart from weak N_2 Second Positive bands and the NH β band (also quite weak) the spectrum of the arc consisted of the so-called α band of ammonia. It has been found possible to photograph the α band in the region 6000 A.–9000 A. on the 10-ft. grating, and it is hoped to communicate measurements of these spectrograms and further details of the work on ammonia at a later date.

ACKNOWLEDGMENTS

This work was carried out in the Spectroscopy Laboratory of Imperial College under the direction of Professor R. W. B. Pearse, who has given the author much helpful advice. Financial support from the Department of Scientific and Industrial Research is acknowledged.

REFERENCES

Brewer, A. K., and Westhaven, J. W., 1930 a, *J. Phys. Chem.*, **34,** 554; 1930 b, *Ibid.*, **34,** 1280.
Coster, D., Van Dijk, E. W., and Lameris, A. J., 1935, *Physica*, **2,** 267.
Deegan, P. J., and Emeléus, K. G., 1948, *Ann. Phys., Lpz.*, **6,** 149.
Feast, M. W., 1949, *Proc. Phys. Soc.* A, **62,** 114.
Gaviola, E., and Wood, R. W., 1928, *Phil. Mag.*, **6,** 1191.
Nakamura, G., 1927, *Jap. J. Phys.*, **4,** 111.
Wansbrough-Jones, O. M., 1930 a, *Proc. Roy. Soc.* A, **127,** 511; 1930 b, *Ibid.*, **127,** 530.
Willey, E. J. B., 1934, *Trans. Faraday Soc.*, **30,** 230; 1937, *Proc. Roy. Soc.* A, **159,** 247.

Rotational Analysis of the (1,0) Band of the N_2 First Positive System

By M. W. FEAST *
Imperial College, London

MS. received 19th October 1949

ABSTRACT. The (1, 0) band of the N_2 First Positive system has been photographed at a dispersion of about 1·2 cm^{-1}/mm. The wave numbers and quantum numbers of the lines, and the rotational term differences in the upper and lower states are given. The spin tripling in the $^3\Sigma$ state and the Λ doubling in the $^3\Pi$ state are evaluated.

§ 1. INTRODUCTION

During the course of other work it was found necessary to have at hand a rotational analysis of the (1, 0) band of the First Positive system of nitrogen. This band lies near 8900 A. in the photographic infra-red and no measurement or analysis of it appear to have been published. Since the photographic infra-red region is becoming of increasing importance both astrophysically and in laboratory spectroscopy, and since the nitrogen molecule is very important for both these fields of study, it seems advisable to make the present analysis available.

The First Positive system of nitrogen is strongly excited by an uncondensed discharge in nitrogen and, much less strongly relative to the Second Positive system, in air. The system consists of several well marked sequences of bands extending from about 5000 A. to beyond 10,000 A. The (5, 2) band at 6705 A. and the (6, 3) band at 6623 A. have been rotationally analysed by Naudé (1932). His work showed that the transition is $^3\Pi \rightarrow {}^3\Sigma$ and that the system has its initial level in common with the final level of the Second Positive system. The 27 branches of each band (of which 9 are main branches) are arranged in three sub-bands. In the present paper wave numbers of the band lines are given together with rotational term differences in the upper and lower states. In the $^3\Sigma$ state the spin tripling has been evaluated for the level $v''=0$ and in the $^3\Pi$ state the Λ doubling has been evaluated for the three sub-levels with $v'=1$.

The (1, 0) band was photographed in the first order of a 20-ft. Eagle Mounting concave grating with 30,000 lines/inch. The dispersion was 1 A/mm. which corresponds to about 1·2 cm^{-1}/mm. in this region of the spectrum. The source used was a simple end-on discharge tube run off a transformer at 3,990 v. and 0·1 amp. The pressure of the nitrogen (which passed continuously through the tube) was adjusted to give maximum brightness of the bands. Kodak I.R.E.R. plates, hypersensitized in ammonia, were used.

§ 2. ANALYSIS OF THE (1, 0) BAND

The lines of the (1, 0) band were measured against iron arc lines (Meggers 1935). Due to the small number of these lines and to their considerable breadth the wavelength measurements are somewhat less accurate than the instrument is capable of giving. Wave numbers of the lines are given here to two decimal places, and for unblended lines they are probably good to $\pm 0{\cdot}01$ cm^{-1}.

---

* Now with the National Research Council, Ottawa, Canada.

In Table 1 are listed the wave numbers of the lines and their estimated intensities (visual scale 0–10). No lines of the following satellite branches were found; ${}^{P}R_{13}$, ${}^{N}P_{13}$, ${}^{T}R_{31}$, ${}^{O}Q_{13}$.

It will be seen from Table 1 that the lines of low K value are often missing. In the (1, 0) band this is very much more noticeable than in the (2, 1) band which has also been studied and it may be due to self-absorption for the metastable lower level with $v'' = 0$. The lines in any one of the branches show alternating intensities in the ratio of about 1 : 2 as predicted for a molecule such as N_2 with a nuclear spin of unity.

(i) *Lower State*, ${}^{3}\Sigma$

The spin fine structure separations in the ${}^{3}\Sigma$ state are given by:

$$\begin{aligned}\Delta f_{21}(K) &= {}^{Q}R_{12}(J) - Q_1(J+1) = {}^{P}Q_{12}(J) - P_1(J+1)\\ &= R_2(J) - {}^{R}Q_{21}(J+1) = Q_2(J) - {}^{Q}P_{21}(J+1)\\ &= {}^{S}R_{32}(J) - {}^{S}Q_{31}(J+1) = {}^{R}Q_{32}(J) - {}^{R}P_{31}(J+1)\\ \Delta f_{23}(K) &= {}^{P}Q_{12}(J) - {}^{P}R_{13}(J-1) = {}^{O}P_{12}(J) - {}^{O}Q_{13}(J-1)\\ &= Q_2(J) - {}^{Q}R_{23}(J-1) = P_2(J) - {}^{P}Q_{23}(J-1)\\ &= {}^{R}Q_{32}(J) - R_3(J-1) = {}^{Q}P_{32}(J) - Q_3(J-1).\end{aligned}$$

In Table 2 the values of these differences that can be obtained from Table 1 are given. The triplet splittings are close to those found by Naudé for the levels $v'' = 2$ and 3. This should be so since the splitting varies slowly with vibrational quantum number. The values are however slightly higher than those found by Naudé.

In Table 3 the rotational term differences $\Delta_2 F''(K)$ are listed. These differences can be obtained from several combinations of branches. In Table 3 they have been computed from the main branches as follows:

$$\begin{aligned}K &= J-1 \qquad \Delta_2 F_1''(J) = R_1(J-1) - P_1(J+1),\\ K &= J \qquad \Delta_2 F_2''(J) = R_2(J-1) - P_2(J+1),\\ K &= J+1 \qquad \Delta_2 F_3''(J) = R_3(J-1) - P_3(J+1).\end{aligned}$$

(ii) *Upper State* ${}^{3}\Pi$

The rotational term differences in the upper state

$$\Delta_2 F'_{ic}(J) = R_i(J) - P_i(J) \qquad i = 1,\ 2 \text{ or } 3,$$

are not given. They agree with those obtained by Hulthén and Johansson (1924) from analysis of the N_2 Second Positive bands as should be the case.

To obtain data on the Λ-type doubling in the ${}^{3}\Pi$ state it is necessary first to obtain the rotational term differences $\Delta_1 F'_{cd}(J)$ and $\Delta_1 F'_{dc}(J)$. These are found by means of the following relationships:

$$\begin{aligned}\Delta_1 F'_{icd}(J) &= R_i(J) - Q_i(J),\\ \Delta_1 F_{icd}(J) &= Q_i(J) - P_i(J) \qquad i = 1,\ 2 \text{ or } 3.\end{aligned}$$

Table 4 gives these differences.

The mean of the Λ doublings ($\delta_{cd}(J+\frac{1}{2})$) for the levels $J = K$ and $J = K+1$ is found from the relationships:

$$\begin{aligned}\Delta_1 F_{cd}(J) - \Delta_1 F_{dc}(J+1) &= \Delta\nu(J+1) - \Delta\nu(J)\\ &= 2\delta_{cd}(J+1).\end{aligned}$$

Table 5 gives the Λ doublings for the three substates of the $^3\Pi$ state. The sign of the values for the $^3\Pi_1$ level is reversed in Table 5 since in the theoretical treatment (Hebb 1936) components which show the same symmetry for a given value of J are grouped together rather than those components with the same designation *c* or *d*.

The Λ doublings in the $v'=1$ level show the same general trends as found by Naudé in the $v'=5$ and 6 levels. That is:

(1) δ_1 large at low J values and decreasing as J increases,
(2) δ_2 and δ_3 small at low J values and increasing as J increases,
(3) $\delta_1>\delta_2>\delta_3$.

The actual values are, as would be expected, slightly different from Naudé's.

Table 1

P_1	I	Q_1	I	R_1	I	$^PQ_{12}$	I	K
11217·47 ?	3							1
11217·20	0·5	11223·96	0·5					2
11217·47	3	11227·20	2·5					3
11217·78	0	11230·69	2·5	11251·31	4			4
11218·23	6	11234·18	3	11257·52	1·5			5
11218·90	1	11237·84	3	11263·91 ?	1·5			6
11219·56	3	11241·71	5	11270·80	5			7
11220·49	1·5	11245·78	3			11221·71	0·5	8
11221·58	3·5	11250·11 ?	5	11285·16	5·5	11222·78	3·5	9
11222·78	3·5	11254·57	4·5	11292·77 b	2	11224·09	1	10
11224·39	4	11259·20	5	11300·40	5·5	11225·61	3·5	11
11226·13	2	11264·11	5	11308·37	4	11227·35	1	12
11228·10	4·5	11269·29	6	11316·60 b	6·5	11229·33	4	13
11230·33	2·5	11274·73	5·5	11325·12	5·5	11231·56	0·5	14
11232·81	4·5	11280·39	7	11333·89	6	11234·03	1	15
11235·56	2	11286·33	5·5	11342·92	5	11236·79	0	16
11238·56 ?	4	11292·53	7	11352·25	7	11239·81	1·5	17
11241·89	1·5	11299·03	5·5	11361·87	5	11243·19	1·5	18
11245·49	5	11305·83	7	11371·77	7			19
11249·44	2	11312·88	6	11381·95	5			20
11253·62	4	11320·26	6·5	11392·44	6			21
11258·09	2	11327·91	5		4			22
11262·81	4	11335·87	7	11414·31	6			23
11267·83	5	11344·13	5·5	11425·70	4·5			24
11273·29	4	11352·71	7					25
11279·00	3	11361·58	5					26
11284·89 ?	3	11370·77	7					27
11290·07	0	11380·26	5					28
11297·35	6	11390·07	6					29
		11400·20	5					30
		11410·62	5					31
		11421·35	6					32

$^OP_{12}$	I	$^QR_{12}$	I	K	$^OP_{12}$	I	$^QR_{12}$	I	K
		11225·09	1	2	11192·06	1	11255·79	0·5	10
11207·35	1	11228·29	0·5	3	11190·55	2·5	11260·43	2	11
11204·76	0·5	11231·73	0	4	11189·24	0·5	11265·32	2·5	12
11202·29	2·5	11235·30	1	5	11188·16	2	11270·50	2	13
11199·92	1	b	—	6	11187·29	0	11275·95	0	14
11197·70	2·5	11242·91	1·5	7	11186·71	2	11281·67	4·5	15
11195·65	1	11246·90	1·5	8	11186·32	1			16
11193·75	2·5	11251·31	4	9			11293·77	1	17

Table 1 (*cont.*)

P_2	*I*	Q_2	*I*	R_2	*I*	$^PQ_{23}$	*I*	*K*
11255·35	2	11260·01	4					2
11252·45	0	11261·13	0					3
11250·32	2	11262·42	0					4
11248·37	1·5	11264·11	5					5
11246·72	1·5	11266·02	1·5		Vis			6
11245·49	5	11268·15	4	11293·39	3·5			7
11244·77	0·5	11270·62 ?	2	11299·03 b	5·5			8
11244·21	4	11273·44	6	11304·95	4			9
11244·02	4	11276·57	4·5	11311·31	6	11242·58	1·5	10
11244·21	4	11280·05	6	11317·92	5·5	11242·75	5·5	11
11244·77	0·5	11283·85	5	11324·87 b	6	11243·32	1·5	12
11245·66	3	11288·01	6	11332·22	7·5	11244·21	4·5	13
11247·03	2·5	11292·53	7	11339·92	5	11245·49	5	14
11248·55	3·5	11297·35	6	11347·92 ?	6	11247·03	2·5	15
11250·47	1	11302·52	5	11356·29	5	11249·04	1	16
11252·83	4	11308·04	6	11364·99	6·5	11251·31	4	17
11255·35	2	11313·89	6	11374·02	4·5	11253·92	0·5	18
11258·30	3	11320·08	6·5	11383·38	6·5	11256·87	1·5	19
11261·56	3	11326·61	4·5	11393·07	5	11260·01	4	20
11265·19	4	11333·47	6		6	11263·76 ?	1	21
11269·16	3	11340·66	6	11413·47	4·5	11267·83	5	22
11273·44	6	11348·15 ?	7	11424·17	6	11271·95	1·5	23
11278·17	3	11356·05	5			11276·74	0	24
11283·15	5	11364·24	6·5			11281·67	4·5	25
11288·50	1	11372·77	6			11287·04	1·5	26
11294·15	4	11381·62	7			11292·77 ?	2	27
11300·16	1	11390·79	5					28
11306·50	3	11400·33	6					29
11313·19	4	11410·17	4					30
11320·26	6·5	11420·34	6					31
11327·57	0							32
11335·24	2							33
11343·25	0·5							34
11351·62	2							35
11360·30	0							36
11369·25	2							37
11378·60	5							38
11388·29	1							39

$^RQ_{21}$	*I*	$^OP_{23}$	*I*	$^QP_{21}$	*I*	$^QR_{23}$	*I*	*K*
11265·51	2							1
11269·16	3							2
11273·09	4			11260·43	2	11259·86	2	3
11277·37	3			11261·56	3	11261·13	0	4
11281·97	5			11263·14 ?	4	11262·65	3	5
11286·91	1·5	11229·33 b	1·5	11264·84	0·5	11264·49	0·5	6
11292·19 ?	4·5	11225·09	1	11266·96	2·5	11266·66	3	7
11297·71	3		Vis	11269·44	0	11269·16 ?	6	8
11303·75	6	11217·45 ?	3	11272·20	1·5	11271·95	1·5	9
11310·05	3	11214·16	0	11275·35	0·5	11275·11	2	10
11316·60 ?	6·5	11211·21	1·5	11278·83	3	11278·52	3	11
11323·69	3	11208·59	0	11282·63	0	11282·39	0	12
11330·91	5	11206·31	1	11286·91 ?	1·5	11286·58	1	13
11338·70	3	11204·36	0·5	11291·31	2	11290·07	0	14
11346·70	5·5	11202·77	1		Vis	11295·86 ?	2	15
11355·11	4		Vis		Vis		Vis	16
11363·76 ?	4	11200·59	0	11306·82	0	11306·50	3	17

Table 1 (*cont.*)

${}^{R}Q_{31}$	*I*	${}^{O}P_{23}$	*I*	${}^{Q}P_{21}$	*I*	${}^{Q}R_{23}$	*I*	*K*
11372·77	6	11199·81 ?	0·5	11312·68	0	11312·34	2·5	18
11382·15	4			11318·85	1·5	11318·53	1·5	19
11391·85	2					11325·12 ?	5·5	20
11402·03 ?	4					11332·06 ?	1·5	21
11412·25	1						Vis	22
11422·97 ?	2							23

${}^{S}R_{21}$	*I*	*K*	${}^{S}R_{21}$	*I*	*K*	${}^{S}R_{21}$	*I*	*K*
11275·11 b	2	1	11321·36 ?	4·5	7	11379·85	4	13
11281·97 b	5	2	11330·27 b	1·5	8	11390·79 b	5	14
11289·16	3	3	11339·50	5	9	11402·05 ?	4	15
11296·65	3	4	11349·08 b	4	10	11413·61	3·5	16
11304·46	1	5	11359·01	4	11	11425·55	4	17
11312·88 b	6	6	11369·25 b	2	12			

P_3	*I*	Q_3	*I*	R_3	*I*	${}^{Q}P_{32}$	*I*	*K*
			Vis					1
	0	11286·71 ?	2					2
			Vis					3
	Vis	11285·08	3	11299·03 b	5·5			4
11270·62	2	11284·76	4	11302·25 b	4			5
	Vis	11284·89	3	11305·83 b	7			6
11264·66	1	11285·54	5·5	11309·82	5			7
11262·42	0	11286·71	2	11314·37	4			8
11260·70	3	11288·35	6	11319·38	6	11289·82	2	9
11259·46	1	11290·76 ?	4·5	11324·87	6	11291·92 ?	0	10
11258·70	3	11293·01	6	11330·73	6	11294·46 ?	2	11
11258·30	3	11296·00	4·5	11337·04	5	11297·35	6	12
11258·44	1·5	11299·43	6	11343·75	6	11300·76	2	13
11259·07	2	11303·25	5	11350·88	5	11304·59	3	14
11259·86	2	11307·47	6	11358·40	7	11308·91	2	15
11261·38	3	11312·09	5	11366·29	6		Vis	16
11263·14	4	11317·10	7	11374·56	7	11318·53	1·5	17
11265·32	2·5	11322·48	6	11383·18	5	11323·69	3	18
11267·83	5	11328·25	6	11392·19	6	11329·66 ?	1	19
11270·80	5	11334·35	6	11401·57	5·5	11335·76 ?	1	20
11274·02	4·5	11340·83	7	11411·28	6	11342·26	0·5	21
11277·67	3	11347·66 ?	6	11421·35	6	11349·08	4	22
11281·67	4·5	11354·99	7			11356·29 ?	5	23
11286·04	0·5	11362·44	5			11363·91	3	24
		11370·36	7			11371·77 ?	7	25
11295·86	2	11378·60	5			11380·02	1	26
11301·28	4·5	11387·21	6·5					27
11307·04	4	11396·15	5·5					28
11313·19	4	11405·46	6					29
11319·67	1	11415·08	4·5					30
11326·50	3	11425·05	6					31
11333·65	2							32
11341·18	1·5							33
11349·08	4							34
11357·25	2							35
11365·15	0·5							36
11374·72	2							37
11383·92 ?	0							38
11393·50	1							39
	Vis							40
11413·61	3·5							41

Table 1 (*cont.*)

$^SQ_{31}$	I	$^SR_{32}$	I	$^RQ_{32}$	I	$^RP_{31}$	I	K
		11312·22	1					3
11317·10 ?	7	11318·25	2·5					4
11323·47	1	11324·62	5	11303·25	5			5
11330·27	1·5	11331·54	3	11307·26	2			6
11337·76	0·5	11338·94	5	11311·31	6			7
		11346·70 b	5·5	11315·85	4			8
11353·92	2·5	11355·11 ?	4	11320·53	5·5	11319·67 ?	1	9
11362·63	1·5	11363·91	3	11326·29	3·5	11325·12 ?	5·5	10
11371·94	0	11373·07	4·5	11332·22 b	7·5	11330·91 ?	1·5	11
11381·62	7	11382·65	3	11338·48	3			12
		11392·63	4	11345·20	5·5	11343·91 ?	0	13
			Vis	11352·25 b	7			14
		11413·75	3·5	11359·83	5	11358·56	1	15
		11424·86 ?	1	11367·72	2			16
				11375·99	4	11374·72	2	17
				11384·62	2	11383·38 ?	6·5	18
				11393·62	3	11392·44 ?	6	19
					4		Vis	20
				11413·60	3			21
				11422·47 ?	0			22

NOTES : ? = Wave number may be inaccurate.
b = Blended line.

Table 2. Spin Triplings in the $^3\Sigma$ state

K	$\Delta f_{23}(K)$	$\Delta f_{21}(K)$	K	$\Delta f_{23}(K)$	$\Delta f_{21}(K)$	K	$\Delta f_{23}(K)$	$\Delta f_{21}(K)$
5	1·46	1·14	13	1·44	1·25	21	1·42	—
6	1·48	1·18	14	1·50	1·22	22	1·42	—
7	1·49	1·19	15	1·47	1·24	23	1·49	—
8	1·47	1·20	16	1·43	1·21	24	1·45	—
9	1·48	1·21	17	1·46	1·23	25	1·45	—
10	1·44	1·26	18	1·47	1·25	26	1·44	—
11	1·48	1·26	19	1·46	1·23	27	1·38	—
12	1·45	1·21	20	1·48	1·22			

Table 3. Rotational Term Differences in $^3\Sigma$ state

K	$\Delta_2F_1''(K)$	$\Delta_2F_2''(K)$	$\Delta_2F_3''(K)$	K	$\Delta_2F_1''(K)$	$\Delta_2F_2''(K)$	$\Delta_2F_3''(K)$
5	32·41			16	95·33	95·09	95·26
6	37·96		37·59	17	101·03	100·94	100·97
7	43·42		43·41	18	106·76	106·69	106·73
8	49·22	49·15	49·12	19	112·43	112·46	112·38
9		55·01	54·91	20	118·15	118·19	118·17
10	60·77	60·74	60·70	21	123·86	123·91	123·90
11	66·64	66·54	66·57	22	129·63		129·61
12	72·30	72·26	72·29	23		135·31	135·31
13	78·04	77·84	77·97	24	141·02	141·02	
14	83·79	83·67	83·89	25	146·70		
15	89·56	89·45	89·50				

Table 4. Rotational Differences $\Delta_1 F'_{1cd}(K)$ and $\Delta_1 F'_{1dc}(K)$ in $^3\Pi$ state

	$^3\Pi_0$		$^3\Pi_1$		$^3\Pi_2$	
K	$\Delta_1 F'_{1dc}(K)$	$\Delta_1 F'_{1cd}(K)$	$\Delta_1 F'_{2dc}(K)$	$\Delta_1 F'_{2cd}(K)$	$\Delta_1 F'_{3dc}(K)$	$\Delta_1 F'_{3cd}(K)$
2			4·66			
3			8·68			
4			12·10			13·95
5			15·74	21·05	14·14	17·49
6	18·94	26·07	19·30			20·94
7	22·16	29·08	22·66	25·23	20·88	24·28
8	25·29		25·85	28·41	24·29	27·66
9	28·53	35·05	29·23	31·51	27·65	31·03
10	31·79	38·20	32·55	34·74	31·30	34·11
11	34·81	41·20	35·84	37·87	34·33	37·72
12	37·98	44·26	39·08	41·02	37·70	41·04
13	41·19	47·31	42·35	44·21	40·99	44·32
14	44·40	50·39	45·50	47·39	44·18	47·63
15	47·58	53·50	48·80	50·57	47·61	50·93
16	50·77	56·59	52·05	53·77	50·71	54·20
17	53·97	59·72	55·21	56·95	53·96	57·46
18	57·14	62·84	58·54	60·13	57·16	60·70
19	60·34	65·94	61·78	63·30	60·42	63·94
20	63·44	69·07	65·05	66·46	63·55	67·22
21	66·64	72·18	68·28		66·81	70·45
22	69·82		71·50	72·81	69·99	73·69
23	73·06	78·44	74·71	76·02	73·32	
24	76·30	81·57	77·89			
25	79·42		81·09			
26			84·27			
27			87·47			

Table 5. Λ Doublings in $^3\Pi$ state, $\delta_{cd}(J+1)$

K	$^3\Pi_0$	$^3\Pi_1$	$^3\Pi_2$	K	$^3\Pi_0$	$^3\Pi_1$	$^3\Pi_2$
4			−0·10 ?	15	1·37	0·74	0·11
5				16	1·31	0·72	0·12
6	1·96		0·03	17	1·29	0·80	0·15
7	1·90	0·31	−0·01	18	1·25	0·83	0·14
8		0·41	0·01	19	1·25	0·88	0·20
9	1·63	0·52	−0·14	20	1·22	0·91	0·21
10	1·70	0·55	−0·11	21	1·18		0·23
11	1·61	0·61	0·01	22		0·95	0·19
12	1·54	0·67	0·03	23	1·07	0·94	
13	1·86	0·65	0·07	24	1·08		
14	1·41	0·71	0·01				

ACKNOWLEDGMENTS

The Author wishes to thank Professor R. W. B. Pearse for his interest in this work and for considerable advice. The work was made possible by the award of a grant from the Department of Scientific and Industrial Research.

REFERENCES

Hebb, M. H., 1936, *Phys. Rev.*, **49**, 610.
Hulthén, E., and Johansson, G., 1924, *Z. Phys.*, **26**, 308.
Meggers, W. F., 1935, *J. Res. Bur. Stand., Wash.*, **14**, 33.
Naudé, S. M., 1932, *Proc. Roy. Soc.* A, **136**, 114.

An Absorption Comparison of the β-Particle Spectra of $^{207}_{81}$AcC″ (allowed), $^{210}_{83}$RaE (second forbidden) and 3·5 yr.-$^{204}_{81}$Tl (third forbidden)

By H. D. EVANS*

Department of Natural Philosophy, University of Edinburgh

Communicated by N. Feather; *MS. received* 24*th August* 1949

ABSTRACT. Experiments are described in which a direct comparison is made by an absorption method of the β-particle spectra of actinium C″, radium E and 3·5 yr. thallium representing allowed, second forbidden and third forbidden transitions respectively.

New values of 623 ± 4 mg/cm^2 and 300 ± 3 mg/cm^2 are proposed for the absorption limits in aluminium of the β particles emitted by actinium C″ and thallium and it is shown that, of the three elements, radium E emits most and actinium C″ least low energy electrons.

An attempt has been made to derive energy distributions from the absorption curves, but the results for radium E depart markedly from those obtained with magnetic spectrographs. The general findings, however, agree with those of other workers who have attempted the same procedure.

The formula used in the derivation of the energy distribution includes an approximation which necessarily leads to an apparent deficiency of low energy particles, but the accuracy of the data is not sufficient to permit the use of a better approximation. Strictly for purposes of comparison, however, the method has obvious applications.

§ 1. INTRODUCTION

There is still very little experimental information on the differences in shape amongst the β-particle spectra of bodies undergoing simple transitions of which the degree of forbiddenness is known. Most of the investigations so far have been carried out by means of magnetic spectrographs (cf. Martin and Richardson 1948), but there is no record of an absorption investigation of the problem, probably because of the difficulty of deriving an energy distribution from an absorption curve. It is desirable, however, that the absorption method should be extended to this work since it allows investigation of radio-elements from which sources cannot yet be made sufficiently strong for spectrographic investigation and it simplifies the apparatus required to a considerable degree.

The first serious attempt to solve the problem of deriving an energy distribution from an absorption curve is that described by Das Gupta and Chaudhury (1948). These workers compare their experimental results for radium E with the theoretical predictions of the Fermi and so-called Konopinski–Uhlenbeck theories and conclude that radium E β-particles follow closely a K.U. form of spectrum. From the results given in their paper, however, it would appear that their absorption measurements are not sufficiently accurate to warrant the analysis to which they are subjected. In addition since the Fermi distribution applies strictly only to allowed transitions it is not to be expected that radium E (second forbidden) should exemplify it—and the K.U. theory has effectively been discarded in recent developments.

A similar method has been described by Hughes, Eggler and Huddleston (1949). These authors compare the energy distributions obtained from the absorption curves with those obtained by spectrographic methods. This is a more realistic approach to the problem in its present state than that adopted by Das Gupta and Chaudhury.

---

* Now at the Royal Cancer Hospital, Fulham Road, London S.W.3

The present paper describes absorption measurements on three β-particle emitters, actinium C″, radium E and thallium (3·5 yr.) known to have effectively simple β-spectra and to emit little or no γ-radiation. These bodies were chosen for investigation as providing examples of allowed, second forbidden and third forbidden transitions respectively, their comparison being the more profitable because their atomic numbers are so nearly the same. As a result of the measurements new values are proposed for the absorption limits of the β-particles from actinium C″ and 3·5 yr. thallium. Range and energy distributions are derived for the β-particles from the three bodies and these distributions are directly compared.

§ 2. APPARATUS

The electronic apparatus was all of A.E.R.E. design and consisted of a power unit, type 200, a scaling unit, type 200A, a timing unit, type 1003K, and a probe unit, type 1014A. The Geiger–Müller counter was a G.E.C. type G.M.4, with a 6 mg/cm² duralumin end window. The counter, sources and absorbers were mounted in a Perspex assembly (Figure 1); the source holders (Figure 2) were also Perspex and were replaceable in a fixed position and orientation in the assembly shown in Figure 1. Perspex was used in an attempt to reduce back-scattering. The active material was contained in the recess in the top of the source holder.

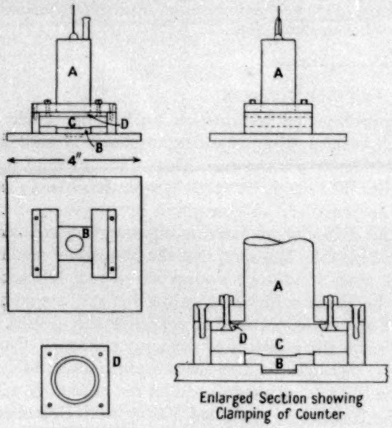

Figure 1.

A. G-M counter. C. Space for absorbers.
B. Source holder. D. Clamping plate.

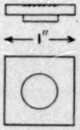

Figure 2.

The short half-value period of actinium C″ (4·76 min.) made it necessary to adopt a method for rapid introduction of fresh sources of this material. A strip of Perspex with a standard source holder suitably built up at each end was rotatable in a horizontal plane about a brass rod supported in an open-sided Perspex box. The source holders projected through 1 in. square holes in the top of the box by the same amount as the single holders in the assembly shown in Figure 1. Over one of the holes was fitted the counter assembly with the bottom square plate removed and over the other was situated a brass pot into which a brass button activated with actinium B could be inserted. The recesses in the two source holders were painted with a suspension of colloidal graphite in acetone and were connected beneath the Perspex strip by a fine wire which was earthed; the actinium B source was connected to a positive 2,000 volt supply. By depressing the brass rod against a light spring and rotating it through 180°, an actinium C″ source could be changed over and counted, two or three seconds after activation was completed, and another source placed in the activator at the same time. Moreover—and this is very important—the conditions prevailing in the experiments with thallium and radium E were reproduced precisely throughout.

§3. PREPARATION OF SOURCES

The thallium was in the form of thallium oxide of high specific activity activated in the pile at Chalk River, Canada. A small amount of the material was spread uniformly in the recess in the top of a source holder and was cemented in with a few drops of chloroform which dissolved the top layer of Perspex. Two sources were used of approximate strengths 1·6 microcuries and 0·016 microcuries and thicknesses estimated at less than 1 mg/cm^2 and much less than 0·1 mg/cm^2 respectively. There was thus practically no self-absorption in the sources.

For radium E, the most satisfactory method of preparation was found to be as follows: a small piece of silver foil was immersed in a solution of 5 microcuries of radium D for 48 hours to remove polonium. A piece of copper foil was then left in the solution for 24 hours collecting radium E; this foil was dissolved in nitric acid and the radium E was precipitated out, with neodymium carrier, as the hydroxide. After several re-precipitations to remove all traces of copper, the active material was washed and dissolved in hydrochloric acid; a portion of the solution was transferred to a source holder, evaporated under an infra-red lamp and cemented in with chloroform. The thickness of this source was estimated to be less than 1 mg/cm^2 and its strength was about 0·5 microcuries immediately after preparation.

The primary source for the preparation of actinium C″ was in the form of actinium fluoride with lanthanum fluoride carrier. Actinium B was collected from this on the face of a ½ in. diameter brass button by the normal recoil method, using a potential of 230 volts. This activated button was then used for the collection of actinium C″ by recoil, in the source changing apparatus described earlier.

§4. THE ABSORPTION CURVES

The experimental procedure followed the normal routine of observing the average counting rate for a number of absorber thicknesses, using aluminium absorbers and applying the usual corrections.

The absorption curve for the 3·5 yr. thallium, shown in Figure 3, curve (*a*), was built up in two sections which were fitted together by taking the two counting rates for an absorber thickness in the region where they overlapped, assigning to them the common value unity and expressing all other readings for both sources as fractions or multiples of this counting rate. All points had standard errors between 1·24% and 0·80%.

A single radium E source was used for the whole absorption curve for this body (Figure 3, curve (*b*)), the readings for small absorber thicknesses being made 16 days after the first reading at maximum absorber thickness. The points on the straight portion of the curve beyond the β-ray end-point have standard errors not greater than 6·3% and all points for absorber thicknesses less than 331·6 mg/cm^2 have standard errors of about 1%; no point has a lower error than 0·86%. Error limits are shown only for some points in the straight lower portion of the curve. In the figure the actual recorded counting rate is plotted, after correction for decay.

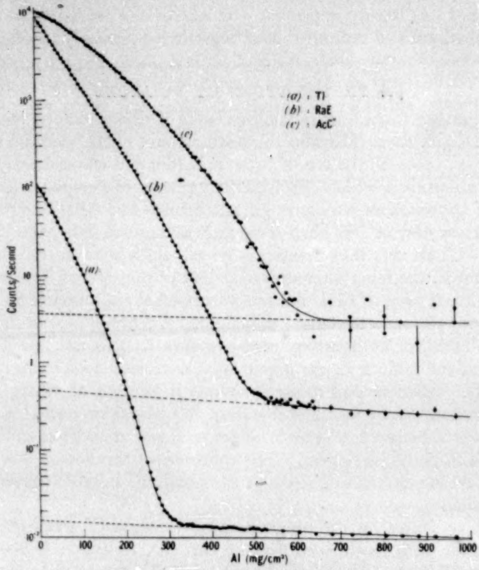

Figure 3. The absorption curves.
The background counting rate has been subtracted in all cases.

Measurements of the half-value period of actinium C″ indicated that it was being collected radioactively pure. A 'control' count was taken for each freshly activated actinium C″ source, with no absorber in place, and the counts taken with absorbers, using the same source and after applying the usual corrections, were expressed as fractions of the 'control' count. Each point on the absorption curve, (*c*) of Figure 3, is the mean of at least 5 readings with different sources and the same absorber thickness. The intensity of the 'control' count, corresponding to the counter window and air gap thickness of 7·7 mg/cm^2, is taken as 10,000 units for the purpose of the figure and all other results are expressed relative to this reading. Though the statistical accuracy of the points decreases towards the lower end of the curve, errors are in general too small to insert without confusing the graph. Three typical points have the following standard errors on the vertical scale: 46·2 mg/cm², 0·56%; 161·7 mg/cm², 0·92%; 324·9 mg/cm², 2·4%; on the part of the curve beyond the β-ray end-point the errors are much greater since the total counting rate was very little in excess of background. The four points shown with their errors were determined to within 30% and were used exclusively for fixing the straight line portion of the curve. With the material available it was not considered worth while to attempt to increase further the accuracy of these points since to reduce the standard error to 5% would necessitate counting for at least 180 hours and the use of more than 1,000 actinium C″ sources. If a more detailed examination of this part of the curve is required a much stronger primary source is desirable.

§ 5. ANALYSIS OF THE RESULTS

The first analytical procedure was to obtain curves for the pure β-activity of the three elements. This was done by extrapolation back to zero absorber thickness of the straight end portions of the curves of Figure 3. Assuming this construction to give the γ-ray and bremsstrahlung effect, this was subtracted from the total intensity of both β- and γ-rays at convenient intervals on the horizontal scale and the resulting β-intensity was replotted on a logarithmic scale, with all three curves passing through the same point on the intensity axis, this point being taken as unity. The ranges in aluminium of the β-particles from 3·5 yr. thallium and actinium C″ were then calculated, using the method described by Feather (1938); radium E was taken as the reference body on account of the well authenticated value of 476 mg/cm² for the absorption limit in aluminium of its β-particles.

This analysis yielded 623 ± 4 mg/cm² for the absorption limit in aluminium of the primary β-particles of actinium C″ and 300 ± 3 mg/cm² for the corresponding limit for the β-particles of 3·5 yr. thallium. The shapes of the 'calculated range' curves indicated that actinium C″ and 3·5 yr. thallium both emit relatively fewer low energy electrons than does radium E, the deficiency being much greater with actinium C″ than with 3·5 yr. thallium. The former result was to be expected since actinium C″ undergoes an allowed transition, but the fact that 3·5 yr. thallium (third forbidden) definitely emits fewer low energy particles than does radium E (second forbidden) is new knowledge.

The results were also treated according to the method of Sargent (1939). This method is based on the conclusion, derived from a limited set of experiments, that beyond an absorber thickness equal to about half the effective range R the form of the absorption curve (logarithm of β-intensity against fraction of effective range) is the same for all simple spectra. The results shown in Figure 4 do not bear out this conclusion in detail. In constructing Figure 4 effective ranges found by Feather's method are used and the three curves are made to be concurrent (at unit intensity) at a point corresponding to two-thirds of the range in each case. Whilst it will be noted that the curves remain indistinguishable for absorber thicknesses greater than $2R/3$, the curve for actinium C″ begins to separate from the other two at about $0{\cdot}65R$ though the curves for radium E and 3·5 yr. thallium do not diverge appreciably until roughly $0{\cdot}45R$ (in agreement with the Sargent conclusion). As was to be expected the Sargent method of comparison gives the same result as the less direct 'calculated range curve' method of Feather regarding the relative proportions of low energy electrons; quite obviously from Figure 4 actinium C″ emits least and radium E most low energy electrons amongst the three bodies investigated.

Very little work has been described in the literature on more detailed methods of analysis of absorption curves. It should, however, be possible to derive range or energy distribution curves from them. This has been attempted by Das Gupta and Chaudhury (1948) and by Hughes, Eggler and Huddleston (1949); independently a similar method was applied to the results above described. In this connection a slight modification in procedure may be claimed as an improvement in the general method of analysis.

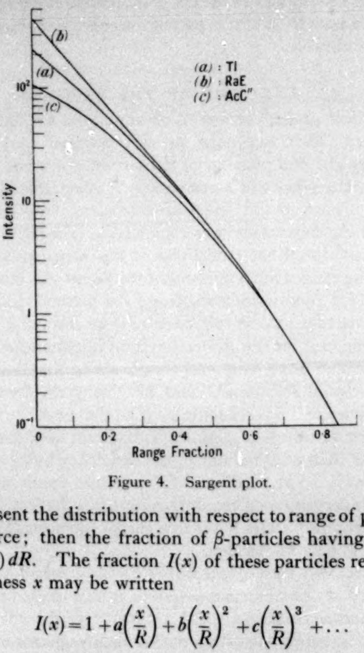

Figure 4. Sargent plot.

Let $f(R)$ represent the distribution with respect to range of primary β-particles emitted by a source; then the fraction of β-particles having ranges between R and $R+dR$ is $f(R)\,dR$. The fraction $I(x)$ of these particles recorded through an absorber of thickness x may be written

$$I(x)=1+a\left(\frac{x}{R}\right)+b\left(\frac{x}{R}\right)^2+c\left(\frac{x}{R}\right)^3+\ldots$$

$a, b, c\ldots$ being constants (Rutherford, Chadwick and Ellis 1930). Experiments with homogeneous β-particles show that to a reasonable first approximation we may take $I(x)=(1-x/R)$. Then if, for a source having a continuous spectrum of primary β-particles as specified above, $A(x)$ is the fraction recorded through a thickness x

$$A(x)=\int_x^\infty\left(1-\frac{x}{R}\right)f(R)\,dR, \qquad \ldots\ldots(1)$$

whence

$$f(x)=xA''(x), \qquad \ldots\ldots(2)$$

dashes denoting differentiation with respect to x.

Equation (2) clearly provides a method of deducing the range distribution when the intensity $A(x)$ is plotted on a linear scale (as in the methods of Das Gupta and Chaudhury and of Hughes *et al.*). It is customary, however, to plot $A(x)$ on a logarithmic scale, as has been done in the present work. In this case, putting $L(x)=\ln A(x)$ it can be shown that

$$F(x)=xA(x)[L''(x)+\{L'(x)\}^2]. \qquad \ldots\ldots(3)$$

Also if $\phi(E)$ is the distribution function with respect to energy, since

$$\phi(E)\,dE=f(x)\,dx,$$

it is only necessary to know the appropriate range–energy relation in order to be able to derive the distribution function relative to energy from the absorption curve.

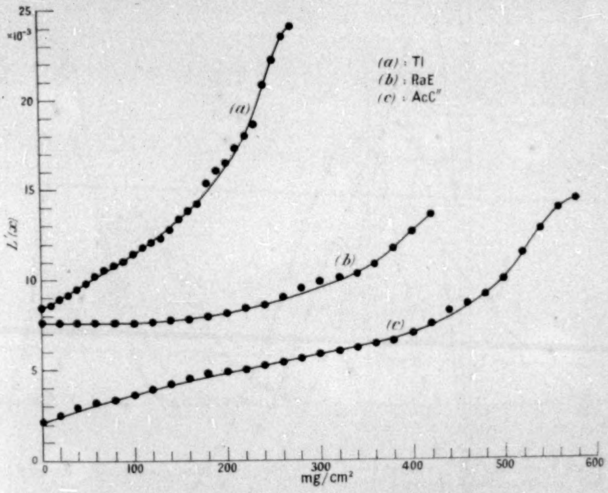

Figure 5. Graphs of $L'(x)$ against absorber thickness.
The numerical values only of $L'(x)$ are plotted; $L''(x)$ must be prefixed by a negative sign for insertion in the formula.

Comparing equations (2) and (3) it will be noted that the former involves the second differential of the experimentally determined $A(x)$ whilst the latter involves both the first and the second differentials of $L(x)$. Formally, this difference represents the improvement in procedure already mentioned: the determination of the second differential of an experimental curve is always attended with very considerable uncertainty, unless the accuracy of the original points is exceptionally high and unless very many points have been taken. An analysis based upon (3) would appear to be preferable to one based upon (2) since $F(x)$ determined from (3) is dependent more upon the value of $L'(x)$ than upon that of $L''(x)$. In applying (3) to the experimental absorption curves of the present investigation it was found that, except at the low energy ends of the curves, $L''(x)$

was generally only of the order of 10% to 20% of $\{L'(x)\}^2$. Thus it seems that there is good reason for preferring such an analysis to the type employed by Das Gupta and Chaudhury, and by Hughes *et al.*, which is based on (2).

The graphs of the first differentials of the β-particle absorption curves are shown in Figure 5. For convenience both Figure 3 and Figure 5 have been plotted using logarithms to the base 10; conversion to the base e was made later in the calculation of $F(x)$.

The calculated distributions with respect to range for the three β spectra are shown in Figure 6. The scale of abscissae gives the fraction of the maximum effective range of the β-particles from each body, the area under each curve being maintained at unity.

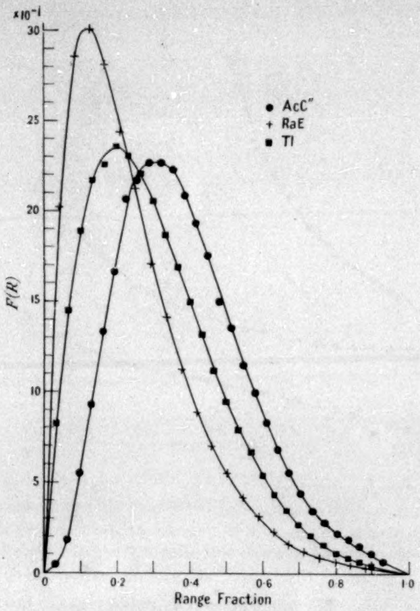

Figure 6. Range distribution curves.

The distribution with respect to energy was calculated with the help of data given by Marshall and Ward (1937) and Curie (1935) from which a range–energy curve was constructed. The three energy distributions so obtained are shown in Figure 7. In Figure 8 the calculated energy distribution for radium E is compared with the currently accepted distributions obtained using a magnetic spectrograph (Flammersfeld 1939, Neary 1940). It was not possible to compare similarly the distributions for 3·5 yr. thallium and actinium C″, there being no reference to magnetic analysis of these spectra in the literature.

§ 6. DISCUSSION

Here the general results of the absorption experiments will be referred to briefly before the calculated distribution curves are discussed in detail. Using the range–energy relation of Feather (1938) the maximum energy of the β-particles of actinium C″ is obtained from the absorption limit of 623 ± 4 mg/cm^2 as 1·442 ± 0·008 Mev. This value is to be compared with 1·47 Mev. deduced by Sargent (by the alternative method already mentioned) from an estimated absorption limit of 0·68 gm/cm^2. The measure of agreement between these values differently determined is not unsatisfactory. For 3·5 yr. thallium the absorption limit of 300 ± 3 mg/cm^2 deduced in the present work is sufficiently close to the less accurate 0·31 gm/cm^2 originally reported by Fajans and Voigt (1941) to support the conclusion that the maximum energy of the β-particles of this body is 0·85 ± 0·01 Mev.

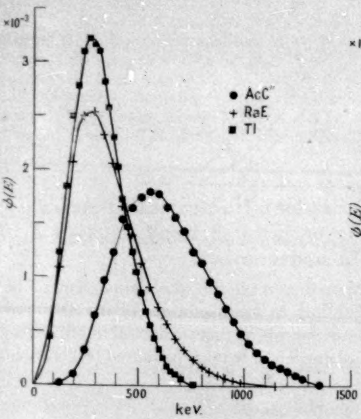

Figure 7. Energy distribution curves.

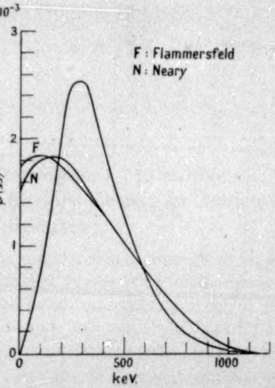

Figure 8. Comparison of the derived energy distribution for RaE with magnetic spectrograph determinations.

The other point of some interest in the results concerns the magnitude of the (γ-ray + bremsstrahlung) effect with the three bodies. From the extrapolations in Figure 3 it will be seen that the values of the 'γ/β ratio' at zero absorber thickness are $(3\cdot6 \pm 0\cdot6) \times 10^{-4}$, $(0\cdot53 \pm 0\cdot01) \times 10^{-4}$ and $(1\cdot38 \pm 0\cdot02) \times 10^{-4}$ for actinium C″, radium E and 3·5 yr. thallium, respectively. Assuming that the value for radium E represents a pure bremsstrahlung effect, and taking count of the difference in average β-particle energy as between the three spectra, it may be concluded that the true γ-ray effect with 3·5 yr. thallium is certainly no greater than that with actinium C″. In the latter case it is known that a γ-ray of 870 kev. energy is emitted about once in 200 disintegrations (Surugue 1941). In any case the assumption that the present work has been concerned with essentially simple β-spectra is fully substantiated.

Turning now to the calculated distribution curves, it will be noted that though they give approximately the correct end-point energies for the three materials, the maximum of the radium E curve certainly falls at too high an energy. It is reasonable to suppose that this is also the case for 3·5 yr. thallium and actinium C″. Such an effect is to be expected since the initial absorption of homogeneous β-particles is slower than that given by the linear relation $I(x)=1-x/R$. Experimental curves obtained by Marshall and Ward (1937) are of the form shown in Figure 9 while the linear relation used is given by the line AB. The line AC might be thought to give a better approximation to the whole curve, and to use it reduces slightly the energy corresponding to the maximum of the distribution but it also reduces greatly the end-point energy, so that no overall improvement is derived. Clearly, the true state of affairs can only be approached by considering more terms in the expression

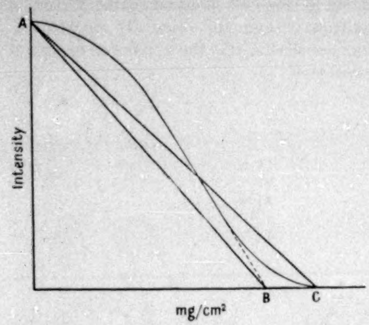

Figure 9. Absorption of homogeneous β-particles (Marshall and Ward).

$$I(x)=1+a\left(\frac{x}{R}\right)+b\left(\frac{x}{R}\right)^2+\ldots.$$

for the absorption of homogeneous β-particles; this, however, introduces differential coefficients of higher order than the second and these cannot be obtained with any reliability from the absorption curves. Hughes *et al.* (1949) have obtained very similar results with ^{64}Cu, ^{178}Au, ^{185}W and radium E comparing the energy distributions derived from absorption curves with magnetic spectrograph data. They found that the end-point energy was correct in all cases, but the maxima of the calculated curves occurred about 100 kev. higher than was expected. To overcome this difficulty, they proposed the empirical method of shifting the calculated distribution by 100 kev. towards lower energies, for an end-point energy of 600 kev., so that the maximum would fall at the correct energy. An obvious objection to this procedure is that the end-point energy is then low by the amount of the shift. The distribution obtained (Figure 7) for radium E agrees fairly well with these findings since the maximum of the curve is about 200 kev. too high; this is double the value reported by Hughes *et al.*, but the end-point energy is also approximately double that for which they propose a shift of 100 kev.

ACKNOWLEDGMENTS

The author wishes to express his sincere thanks to Professor N. Feather for his interest and advice during the course of this work, to Dr. A. G. Maddock of the Cavendish Laboratory, Cambridge, for the separation of the actinium and to Dr. N. Miller for assistance and advice in the preparation of the sources. Thanks are also due to the Department of Scientific and Industrial Research for the provision of a grant during the period of research.

REFERENCES

Curie, P., 1935, *Radioactivité* (Paris : Hermann et Cie).

Das Gupta, N. N., and Chaudhury, A. K., 1948, *Indian J. Phys.*, **22,** 27.

Fajans, K., and Voigt, A. F., 1941, *Phys. Rev.*, **60,** 619.

Feather, N., 1938, *Proc. Camb. Phil. Soc.*, **34,** 599.

Flammersfeld, A., 1939, *Z. Phys.*, **112,** 727.

Hughes, D. J., Eggler, C., and Huddleston, C. M., 1949, *Phys. Rev.*, **75,** 515.

Marshall, J. S., and Ward, A. G., 1937, *Canad. J. Res.* A, **15,** 39.

Martin, D. G. E., and Richardson, H. O. W., 1948, *Proc. Roy. Soc.* A, **195,** 287.

Neary, G. J., 1940, *Proc. Roy. Soc.* A, **175,** 71.

Rutherford, Lord, Chadwick, J., and Ellis, C. D., 1930, *Radiations from Radioactive Substances* (Cambridge : University Press).

Sargent, B. W., 1939, *Canad. J. Res.* A, **17,** 82.

Surugue, J., 1941, *C.R. Acad. Sci., Paris,* **212,** 337.

Excited Electronic Levels in Conjugated Molecules—V: A Valence Bond Estimation of Energy Levels in Aromatic Hydrocarbon Molecules*

By G. R. BALDOCK
King's College, London

Communicated by C. A. Coulson; MS. received 28th November 1949

ABSTRACT. This note is concerned with the calculation of the energy of the ground state and the lowest excited state for hydrocarbons of the condensed ring type. The difference between these two energies is the energy of the first electronic transition. The normal valence bond method is used, taking only the Kekulé structures into consideration. The results are compared with the experimental absorption wavelengths, and are in good agreement, giving a value of the exchange integral α between $-1{\cdot}8$ and -2 electron volts.

§ 1. INTRODUCTION

It is well known that the simple molecular orbital treatment yields a good picture of ground state phenomena in condensed ring molecules, but in calculations on the excited states considerable difficulties arise. At the very least it becomes necessary to use antisymmetrized wave functions (Jacobs 1949), and at present this method is too cumbersome to be applied to large molecules. A similar complexity occurs if the valence bond, or resonance, method is used, unless nearly all the excited structures are neglected. This approximation has therefore been made in all our present calculations, where Kekulé structures alone have been taken into consideration. We used the standard technique, in

---

* This work was supported by a grant from the University of London Research Fund.

Table 1

No.	Compound	$\frac{E_1-Q}{\alpha}$	$\frac{E_2-Q}{\alpha}$	$\frac{E_1-E_2}{\alpha}$	Absorption maximum (in 100 cm^{-1})
5	Hexacene	6·04	5·14	0·90	149
6	Heptacene	6·60	5·84	0·76	—
9	Benznaphthacene	6·13	4·69	1·44	221
10	Benzpentacene	6·88	5·66	1·22	181
12	Dibenzanthracene	6·60	4·82	1·78	253
13	Dibenznaphthacene	7·40	5·84	1·57	231
14	Dibenzpentacene	8·10	6·78	1·32	189
15	Picene	6·70	4·91	1·79	266
16	Benzpicene	7·79	6·05	1·74	267*
19	Benzpyrene	5·68	4·03	1·65	248
20	3489–Dibenzpyrene	6·57	5·11	1·46	222
21	Anthanthrene	5·75	4·27	1·48	231
22	Coronene	6·64	5·07	1·57	232†

* Cook, Schoental and Scott (private communication).

† Patterson (1942).

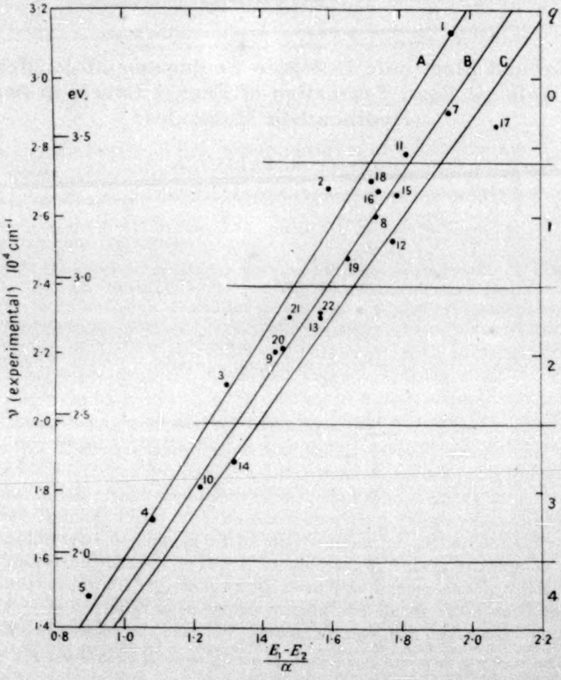

Key to Figure

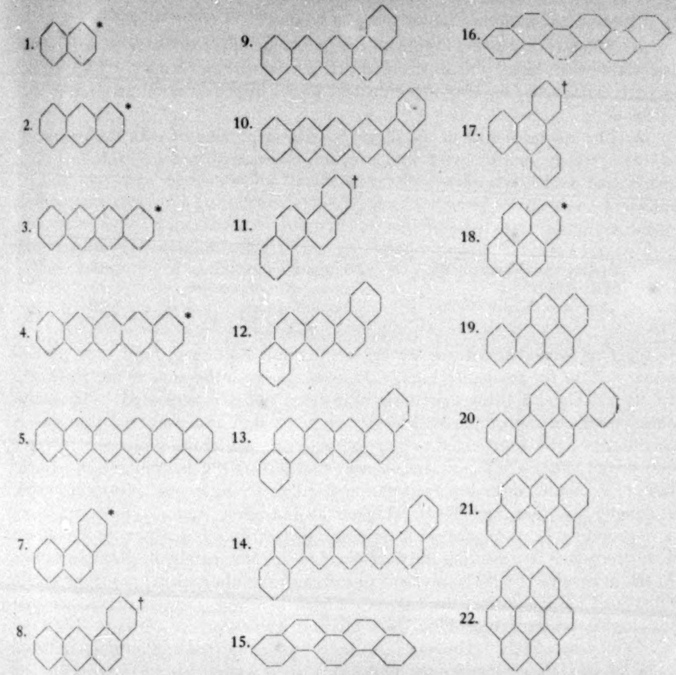

* Calculated by Förster (1938).
† Calculated by Seel (1947).

which the terms of the secular determinant are calculated by means of Pauling's method of superposition diagrams (Pauling 1933). Although this approximation is known to give false values of the ground state energy (Jonsson 1942, Pullman and Pullman 1946), it has been shown by Förster (1938) and Seel (1947) to give in general a good estimate of the energy of the first transition.

§ 2. RESULTS

Table 1 shows the results of the calculations, expressed in terms of the exchange integral α. Q is the coulombic integral, E_1 the ground state energy, E_2 the energy of the lowest excited state, and $E_2 - E_1$ the energy of transition. The last column shows the wave number of the longest wavelength absorption maximum, quoted from Cook, Schoental and Scott (1950) unless otherwise indicated.

In the Figure we have plotted the experimental energy of transition against the calculated values of $(E_1 - E_2)/\alpha$. A few previous results for other molecules are also included.

§ 3. DISCUSSION

The conclusions from this work are as follows:

(*a*) The fact that in the Figure all the points lie approximately on a straight line shows that theory and experiment are in essential agreement. This agreement is unexpected in view of the crudity of the approximation adopted in the calculations.

(*b*) The results shown in the diagram suggest a value of α in the region of $-1{\cdot}9$ ev., which compares well with previous estimates listed in Table 2.

Table 2

Author	Method	$-\alpha$ (ev.)
Pauling and Wheland (1933)	Thermochemical data	1·55
Sklar (1937)	Fluorescence of benzene	1·92
Lloyd and Penney (1939)	Vibration spectra	1·85

(*c*) The excited structures are known to contribute to ground state phenomena, such as the resonance energy, increasingly with the size of the molecule. In our calculations these structures have been entirely neglected. Therefore deviations from the proportionality of the calculated and observed energies of transitions might be expected to increase with the size of the molecule. In fact they do not increase with the size, as can be seen from the diagram, since a single value of α correctly describes a series of molecules varying in size. It is the shape, or 'angularity' (see Seel 1947), which is an important factor, since the points corresponding to molecules with different shapes lie on distinct straight lines. Thus the points representing the polyacenes lie approximately on the straight line A, the molecules 7, 8, 9, 10 give the line B, and the molecules 12, 13, 14 give a third line C, as is shown in the Figure. These three lines (which all pass through the origin) are represented by three distinct values of α, $-1{\cdot}98$, $-1{\cdot}86$ and $-1{\cdot}78$ ev. respectively. The more angular the molecule, the smaller the numerical value of α. (Highly condensed molecules, such as pyrene and coronene, are excluded from this discussion.)

(*d*) The numerals on the right of the figure indicate the minimum number q of non-benzenoid rings in the Kekulé formula for the molecule, i.e. the number of non-benzenoid rings when the structural formula is written according to the Fries rule. It has been remarked by Cook, Schoental and Scott (1950) that there is a correlation between q and the longest wavelength absorption maximum ν. The figure shows that q certainly increases as the experimental value of ν decreases, and that the points representing the molecules may be grouped between horizontal lines as shown. There are two exceptions, picene (15) and benzpicene (16), which lie in the region $q=1$, although in their structural formulae $q=0$. The calculated values of ν also show this effect but not so clearly as the experimental results, for vertical lines cannot be drawn in the figure to separate the points into groups with anything like the distinctness of the horizontal grouping.

(*e*) The symmetry of the polyacene molecules is such that all the Kekulé structures represent states which are symmetrical about the axis parallel to the length of the molecule. Thus the method we have used assumes that the transitions will be polarized along the length of the molecule. This is in direct contradiction with the simplest molecular orbital interpretation. But in view of the present uncertainty in the exact interpretation of the long-wave ultra-violet bands, no clear deduction can be drawn (Jacobs 1949). However, if the transitions we have discussed are not polarized along the length of the molecule, the agreement with experiment becomes all the more difficult to explain.

§ 4. POLYACENES

The polyacene series can be treated generally by the method we have used. If there are n rings in a polyacene molecule, there will be $4n+2$ nuclei, $n+1$ Kekulé structures, $2n+1$ π-bonds in each structure, and $5n+1$ non-vanishing exchange integrals between neighbouring atoms, all supposed equal in magnitude.

The energy E_0 of each separate structure is given by

$$\frac{Q-E_0}{\alpha}+\tfrac{3}{2}(2n+1)-\tfrac{1}{2}(5n+1)=0,$$

i.e.

$$\frac{Q-E_0}{\alpha}+\frac{n}{2}+1=0.$$

Let

$$\frac{Q-E}{\alpha}+\frac{n}{2}+1=x,$$

where E is the energy of the electrons. Then the resonance energy is $E_0-E=x\alpha$.

The secular determinant, of order $n+1$, is conveniently written in terms of $y=2x/9$.

The following equation for y is obtained:

$$\begin{vmatrix} y & y+1 & y+2 & y+3 & \cdots & y+n \\ y+1 & 4^2y & 4^2(y+1) & 4^2(y+2) & \cdots & 4^2(y+n-1) \\ y+2 & 4^2(y+1) & 4^4y & 4^4(y+1) & \cdots & 4^4(y+n-2) \\ y+3 & 4^2(y+2) & 4^4(y+1) & 4^6y & \cdots & 4^6(y+n-3) \\ \vdots & \vdots & \vdots & \vdots & & \vdots \\ y+n & 4^2(y+n-1) & 4^4(y+n-2) & 4^6(y+n-3) & \cdots & 4^{2n}y \end{vmatrix}=0.$$

By subtracting each column from its successor, and performing the same operation on the rows, we eliminate the variable y from the off-diagonal terms. Next, multiplying certain rows and columns by suitable factors and making the substitution $z=15/(15y-17)$, we get

$$\begin{vmatrix} 17z+15 & z & z & z & z & \cdots \\ z & z+1 & z & z & z & \cdots \\ z & z & 4^2(z+1) & 4^2z & 4^2z & \cdots \\ z & z & 4^2z & 4^4(z+1) & 4^4z & \cdots \\ z & z & 4^2z & 4^4z & 4^6(z+1) & \cdots \\ \vdots & \vdots & \vdots & \vdots & \vdots & \end{vmatrix}=0.$$

By similar operations we obtain

$$\begin{vmatrix} \dfrac{17u-16}{15} & \dfrac{4u-17}{60} & 0 & 0 & 0 \cdots\cdots 0 \\ \dfrac{4u-17}{60} & \dfrac{4u-2}{60} & \dfrac{1}{4} & 0 & 0 \cdots\cdots 0 \\ 0 & \frac{1}{4} & u & 1 & 0 \cdots\cdots 0 \\ 0 & 0 & 1 & u & 1 \cdots\cdots 0 \\ 0 & 0 & 0 & 1 & u \cdots\cdots 0 \\ \vdots & \vdots & \vdots & \vdots & \vdots \\ 0 & 0 & 0 & 0 & 0 \cdots\cdots u \end{vmatrix} = 0$$

where $u=(15z+17)/4$.

Putting $u=2\cos\theta$, the equation reduces to

$$\Delta_n \equiv \frac{256\sin(n+2)\theta-256\sin(n+1)\theta+96\sin n\theta-16\sin(n-1)\theta+\sin(n-2)\theta}{\sin\theta}=0 \quad \text{for } n\geqslant 3,$$

where $$\cos\theta=\frac{85x-96}{4(10x-51)} \quad \text{or} \quad x=\frac{12}{5}\,\frac{17\cos\theta-8}{8\cos\theta-17}.$$

Δ_n is a polynominal in $\cos\theta$ of degree $n+1$, with $n+1$ real zeros since it is the determinant of a Hermitian matrix.

Now $\Delta_n=A_nB_n$, where

$$A_n=[16\cos(\tfrac{1}{2}n+1)\theta-8\cos\tfrac{1}{2}n\theta+\cos(\tfrac{1}{2}n-1)\theta]\sec\tfrac{1}{2}\theta$$

and $$B_n=[16\sin(\tfrac{1}{2}n+1)\theta-8\sin\tfrac{1}{2}n\theta+\sin(\tfrac{1}{2}n-1)\theta]\operatorname{cosec}\tfrac{1}{2}\theta.$$

It can easily be verified that A_n and B_n arise from the secular determinants obtained by factorizing the original determinant into two parts involving the coefficients of eigenfunctions respectively symmetrical and antisymmetrical about the central plane normal to the length of the molecule.

From the form of A_n and B_n we see that if n is even A_n has $\frac{1}{2}n+1$ zeros and B_n has $\frac{1}{2}n$ zeros, and for n odd A_n and B_n both have $\frac{1}{2}(n+1)$ zeros. In each case all the zeros are real values of θ, so that the $n+1$ zeros of Δ_n are accounted for and lie in the range $-1\leqslant\cos\theta\leqslant 1$.

Furthermore, for n even or odd, the zeros of A_n and B_n are interlaced throughout, and each zero θ_r is restricted within a range

$$\frac{r\pi/2-\sin^{-1}\frac{9}{16}}{\frac{1}{2}n+1}\leqslant\theta_r\leqslant\frac{r\pi/2+\sin^{-1}\frac{9}{16}}{\frac{1}{2}n+1}.$$

Hence the spacing of the energy levels, which all lie in the range

$$-2{\cdot}4\leqslant x\leqslant 2{\cdot}4,$$

becomes infinitely close (being uniformly dense in terms of θ) at every point as $n\to\infty$.

The ground state resonance energy thus tends steadily to $2{\cdot}4\alpha$ as $n\to\infty$.

The ground state energy corresponds to the lowest root θ_1, and the lowest excited state to the next root θ_2. θ_1 is always a root of $A_n=0$ and θ_2 a root of

$B_n = 0$, so that the first transition is always from a symmetrical to an antisymmetrical state. It is therefore an allowed transition polarized along the length of the molecule.

For large n,
$$\theta_1 \simeq \frac{\pi}{n+\frac{10}{3}} \quad \text{and} \quad \theta_2 \simeq \frac{2\pi}{n+\frac{10}{3}},$$
so
$$\theta_2{}^2 - \theta_1{}^2 \simeq \frac{3\pi^2}{(n+\frac{10}{3})^2}.$$
Now
$$x = -\frac{12}{5}\,\frac{17\cos\theta - 8}{17 - 8\cos\theta} \simeq -\frac{12}{5}\left(1 - \frac{25}{18}\,\theta^2\right) \quad \text{for } \theta \ll 1,$$
so that
$$x_2 - x_1 \simeq \frac{10}{3}\,(\theta_2{}^2 - \theta_1{}^2) \simeq \frac{10\pi^2}{(n+\frac{10}{3})^2} \to 0 \qquad \text{as } n \to \infty.$$

Thus we should expect the longest wavelength absorption maximum to increase proportionately to the square of the number of rings, for long strips. A similar variation would be expected for all other bands in this series, in agreement with Coulson's molecular orbital theory (Coulson 1948).

ACKNOWLEDGMENTS

The author wishes to thank Professor C. A. Coulson for suggesting this work and for many helpful discussions, and Miss R. Schoental and Mr. E. J. Y. Scott for supplying useful experimental data in advance of publication.

REFERENCES

Cook, J. W., Schoental, R., and Scott, E. J. Y., 1950, *Proc. Phys. Soc.* A, **63,** 592.
Coulson, C. A., 1948, *Proc. Phys. Soc.*, **60,** 257.
Förster, Th., 1938, *Z. Phys. Chem.*, **41 B,** 287.
Jacobs, J., 1949, *Proc. Phys. Soc.* A, **62,** 710.
Jonsson, C. V., 1942, *Arkiv. Kemi. Min. Geolog.*, **15 A,** No. 14.
Lloyd, E. H., and Penney, W. G., 1939, *Trans. Faraday Soc.*, **35** (2), 835.
Patterson, J. W., 1942, *J. Amer. Chem. Soc.*, **64,** 1485.
Pauling, L., 1933, *J. Chem. Phys.*, **1,** 280.
Pauling, L., and Wheland, G. W., 1933, *J. Chem. Phys.*, **1,** 362.
Pullman, A., and Pullman, B., 1946, *Experientia*, **2,** 64.
Seel, F., 1947, *Naturwissenschaften*, **4,** 124.
Sklar, A. L., 1937, *J. Chem. Phys.*, **5,** 669.

Relation between Bond Structure and the Longest Ultra-violet Absorption Band of Polycyclic Aromatic Hydrocarbons

By J. W. COOK, R. SCHOENTAL and E. J. Y. SCOTT
Chemistry Department, University of Glasgow

Communicated by C. A. Coulson; MS. received 28th November 1949

ABSTRACT. A comparison has been made between the values expressed in wave numbers of the longest ultra-violet absorption bands of a series of polycyclic aromatic hydrocarbons and the minimum number of quinonoid rings contained in their molecules. It is found that the hydrocarbons fall into series of groups related to this number of quinonoid rings.

In their survey of fluorescence spectra of polycyclic aromatic hydrocarbons Schoental and Scott (1949) noticed a close relation between the position of the maximum of the first (shortest) fluorescence band and the minimum number of quinonoid rings in the molecules, so as to conform to the Fries rule that as many rings as possible should have Kekulé structures. The number of compounds which have been available for the fluorescence studies were, however, too small to allow a satisfactory generalization. These authors have found also that for this series of compounds the shortest fluorescence band coincides approximately in wavelength with the longest absorption band. If this is assumed to be generally true, then it is possible to examine more extensively the relation between the number of quinonoid rings and the wavelength of the maximum of the longest ultra-violet absorption band from the numerous ultra-violet absorption data recorded in the literature.

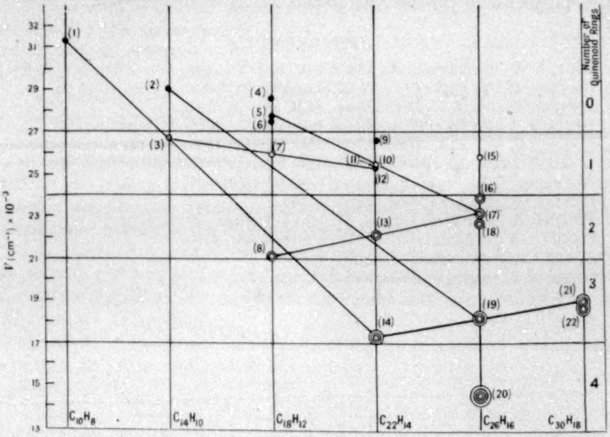

Figure 1.

In the Figures and Table are collected the values of the longest ultra-violet or visible absorption bands, expressed in wave numbers, in relation to the molecular formulae of the respective compounds. (Values referring to hydrocarbons with highly condensed ring-systems are grouped in Figure 2.) It will be noted that values for isomers lie on straight vertical lines.

The horizontal lines divide the figures into zones in which the compounds possess an *equal* number of quinonoid rings *Q* regardless of their structure and total number of rings. There is some overlap between the zone of compounds which have no quinonoid rings (i.e. structures which can be built wholly from Kekulé rings) and that corresponding to one quinonoid ring. With the increase of the number of quinonoid rings the divisions are more striking.

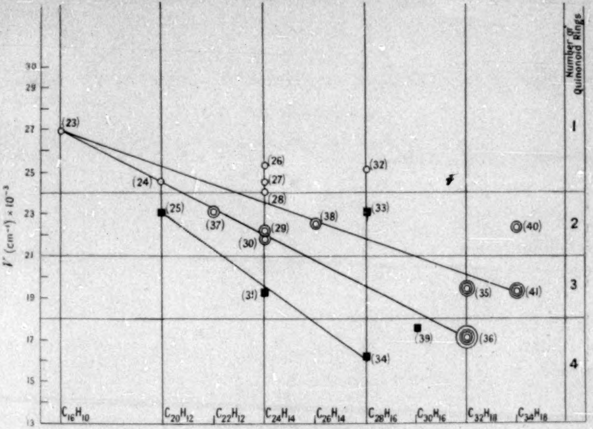

Figure 2.

There is, however, a class of compounds, namely those having the perylene structure in their molecules, where the spectra consistently fall into zones corresponding to one quinonoid ring more than the minimum number derived from the application of the Fries rule. Clar (1932, reference 2) has already drawn attention to the fact that perylene in its chemical behaviour does not correspond to a simple dinaphthyl-derivative. It may be that other excited structures come into play for this class of condensed compounds. Assuming for perylene two quinonoid rings, which would agree with the position of its spectrum, its benzo- and naphthologues exhibit the expected shifts in their spectra.*

The regularities observed by Clar (1941, reference 14) in the ultra-violet absorption spectra of series of aromatic hydrocarbons, built up by linear or angular condensation, find to some extent their expression in the figures. The values of the maxima of the longest ultra-violet absorption bands of each series lie on approximately straight (diagonal) lines. The values corresponding to the linear hydrocarbons lie in the lowest parts of their zones, but that of anthracene is exceptional, in that it is situated in the upper part of its zone.

---

* Data for the longest ultra-violet absorption maximum of several polycyclic hydrocarbons recorded in the literature have not been included in the table and figures. These need checking with the values of their fluorescence spectra; the shortest fluorescence band, being usually the most intense, is not likely to be missed, as may be the case with the longest absorption band, of a low extinction coefficient.

This simple relationship between the number of quinonoid rings and the maximum of the longest ultra-violet absorption (or the shortest fluorescence) band of polycyclic aromatic hydrocarbons seems to reflect some fundamental connection between the chemical reactivity and the spectra of the respective substances, and is worthy of the attention of theoretical chemists.

Table

No.	Substance	Molecular formula	Structure	Q	ν (cm^{-1}) $\times 10^{-2}$	Reference
1	Naphthalene	$C_{10}H_8$	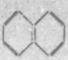	–	313·5	15
2	Phenanthrene	$C_{14}H_{10}$	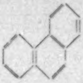	–	289·9	15
3	Anthracene	$C_{14}H_{10}$	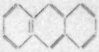	1	267·0	1
4	Triphenylene	$C_{18}H_{12}$	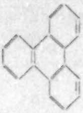	–	285·7	15
5	Chrysene	$C_{18}H_{12}$	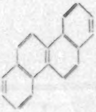	–	277·8	15
6	3 : 4-benzphenanthrene	$C_{18}H_{12}$	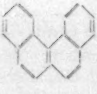	–	268·8	17
7	1 : 2-benzanthracene	$C_{18}H_{12}$	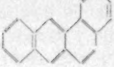	1	259·7	1
8	Naphthacene	$C_{18}H_{12}$	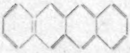	2	211·2	1
9	Picene	$C_{22}H_{14}$	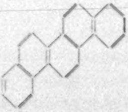	–	266·0	16
10	Naphtho-(2′ : 3′-1 : 2)-phenanthrene	$C_{22}H_{14}$	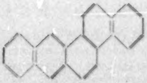	1	254·5	15

Table (*cont.*)

No.	Substance	Molecular formula	Structure	Q	ν (cm^{-1}) $\times 10^{-2}$	Reference
11	1 : 2 : 5 : 6-dibenz-anthracene	$C_{22}H_{14}$	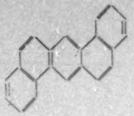	1	253·2	14 (*a*)
12	1 : 2 : 7 : 8-dibenz-anthracene	$C_{22}H_{14}$	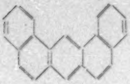	1	253·2	14 (*b*)
13	Naphtho-(2′ : 3′-2 : 3)-phenanthrene	$C_{22}H_{14}$	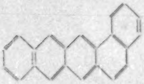	2	221·0	15
14	Pentacene	$C_{22}H_{14}$	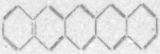	3	173·8	3; 8
15	1 : 2 : 3 : 4 : 5 : 6-tribenzanthracene	$C_{26}H_{16}$	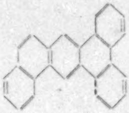	1	257·7	14 (*c*)
16	Anthraceno-(2′ : 1′-1 : 2)-anthracene	$C_{26}H_{16}$	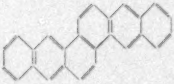	2	238·1	1
17	Phenanthro-(3′ : 2′-2 : 3)-phenanthrene	$C_{26}H_{16}$	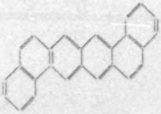	2	230·0	18
18	Anthraceno-(2′ : 3′-9 : 10)-phenanthrene	$C_{26}H_{16}$	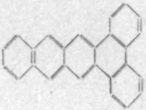	2	226·5	11
19	1 : 2-benzpentacene	$C_{26}H_{16}$	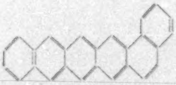	3	181·5	10
20	Hexacene	$C_{26}H_{16}$	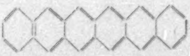	4	144·9	6
21	1 : 2 : 8 : 9-di-benzpentacene	$C_{30}H_{18}$	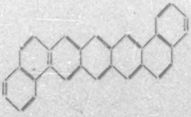	3	189·0	8

Table (*cont.*)

No.	Substance	Molecular formula	Structure	*Q*	ν (cm^{-1}) $\times 10^{-2}$	Reference
22	1 : 2 : 3 : 4-dibenzpentacene	$C_{30}H_{18}$	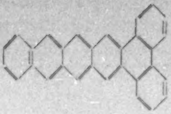	3	185·7	12
23	Pyrene	$C_{16}H_{10}$	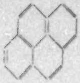	1	269·1	4
24	3 : 4-benzpyrene	$C_{20}H_{12}$	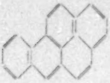	1	248·1	16
25	Perylene	$C_{20}H_{12}$	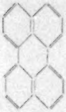	1	230·4	2
26	1 : 2 : 6 : 7-dibenzpyrene	$C_{24}H_{14}$	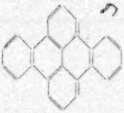	1	253·0*	19
27	Naphtho-(2′ : 3′-1 : 2)-pyrene	$C_{24}H_{14}$	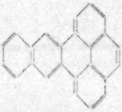	1	245·4	13 (*b*)
28	1 : 2 : 4 : 5-dibenzpyrene	$C_{24}H_{14}$	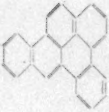	1	240·4	9
29	3 : 4 : 8 : 9-dibenzpyrene	$C_{24}H_{14}$	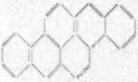	2	221·7	4
30	Naphtho-(2′ : 3′-3 : 4)-pyrene	$C_{24}H_{14}$	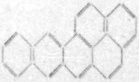	2	218·3	4
31	1 : 2-benzperylene	$C_{24}H_{14}$	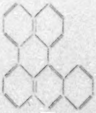	2	193·1	(41*d*)

Table (*cont.*)

o.	Substance	Molecular formula	Structure	Q	ν (cm^{-1}) $\times 10^{-2}$	Reference
2	1 : 2 : 4 : 5 : 8 : 9-tribenzpyrene	$C_{28}H_{16}$	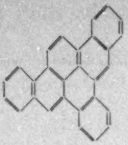	1	250·6	13 (*h*)
33	2 : 3 : 10 : 11 -dibenzperylene	$C_{28}H_{16}$	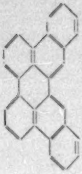	1	230·9	2
34	Naphtho-(2′ : 3′-1 : 2)-perylene	$C_{28}H_{16}$	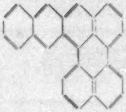	3	163·0*	19
35	Dinaphtho-(2′ : 3′-3 : 4)(2″ : 3″-9 : 10)-pyrene	$C_{32}H_{18}$	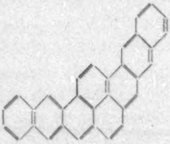	3	194·0*	19
36	Dinaphtho-(2′ : 3′-3 : 4)(2″ : 3″-8 : 9)-pyrene	$C_{32}H_{18}$	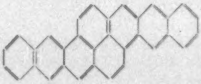	4	171·8	13 (*a*)
37	Anthranthrene	$C_{22}H_{12}$	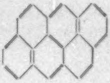	2	230·9	7
38	Peropyrene	$C_{26}H_{14}$	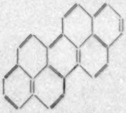	2	225·4	14 (*e*)
39	Rhodacene	$C_{30}H_{16}$	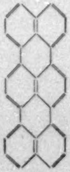	2	175·4	14 (*f*)‡

Table (*cont.*)

No.	Substance	Molecular formula	Structure	Q	ν (cm^{-1}) $\times 10^{-2}$	Referen
40	4 : 5 : 6 : 7- or 4 : 5 : 11 : 12-dibenzperopyrene	$C_{34}H_{18}$	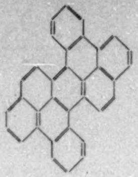	2	223·0	14(*g*)
41	1 : 2 : 8 : 9-dibenzperopyrene	$C_{34}H_{18}$	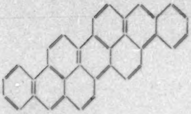	3	193·8	5

Q=number of quinonoid rings.

* Data refer to the shortest fluorescence band maxima.

‡ This structure is assigned by Clar (1948, *Chem. Ber.*, **81,** 52) to a different hydrocarbon (terrylene).

ACKNOWLEDGMENTS

We thank the British Empire Cancer Campaign for a grant (to R.S.) and the Carnegie Trust for the Universities of Scotland for a Scholarship (to E.J.Y.S.).

REFERENCES

1. Clar, E., 1932, *Ber. dtsch. chem. Ges.*, **65,** 503.
2. Clar, E., 1932, *Ber. dtsch. chem. Ges.*, **65,** 846.
3. Clar, E., 1936, *Ber. dtsch. chem. Ges.*, **69,** 607.
4. Clar, E., 1936, *Ber. dtsch. chem. Ges.*, **69,** 1671.
5. Clar, E., 1939, *Ber. dtsch. chem. Ges.*, **72,** 1645.
6. Clar, E., 1939, *Ber. dtsch. chem. Ges.*, **72,** 1817.
7. Clar, E., 1940, *Ber. dtsch. chem. Ges.*, **73,** 596.
8. Clar, E., 1943, *Ber. dtsch. chem. Ges.*, **76,** 257.
9. Clar, E., 1943, *Ber. dtsch. chem. Ges.*, **76,** 609.
10. Clar, E., 1948, *Chem. Ber.*, **81,** 63.
11. Clar, E., 1948, *Chem. Ber.*, **81,** 68.
12. Clar, E., 1948, *Chem. Ber.*, **81,** 163.
13. Clar, E., 1949, *J. Chem. Soc.*, (*a*) p. 2013; (*b*) p. 2168.
14. Clar, E., 1941, *Aromatische Kohlenwasserstoffe* (Berlin : Springer), (*a*) p. 143; (*b*) p. 147; (*c*) p. 148; (*d*) p. 231; (*e*) p. 250; (*f*) p. 267; (*g*) p. 258.
15. Clar, E., and Lombardi, L., 1932, *Ber. dtsch. chem. Ges.*, **65,** 1411.
16. Mayneord, W. V., and Roe, E. M. F., 1935, *Proc. Roy. Soc.* A, **152,** 299.
17. Mayneord, W. V., and Roe, E. M. F., 1937, *Proc. Roy. Soc.* A, **158,** 642.
18. Nicol, J. C., Thorn, G. D., Jones, R. N., and Sandin, R. B., 1947, *J. Amer. Chem. Soc.*, **69,** 376.
19. Schoental, R., and Scott, E. J. Y., 1949, *J. Chem. Soc.*, 1683.

The Scattering of High Energy Charged Particles by Thin Foils of Matter

By S. T. BUTLER
Department of Mathematical Physics, The University, Birmingham

Communicated by R. E. Peierls; MS. received 3rd November 1949

ABSTRACT. The distribution of high energy charged particles scattered by a thin foil has been investigated and compared with the formula for single scattering. It is shown that at sufficiently large angles the distribution approaches that for single scattering and can be expressed in the form of a rapidly convergent series of which the first term is identical with the single scattering formula. The remaining terms of the series form an accurate expression for the deviation from true single scattering. The simplified case of projected scattering has also been considered.

§ 1. INTRODUCTION

When high energy charged particles are scattered by a thin foil of matter, it is well known (see e.g. Williams 1939) that at sufficiently large angles of scattering, the angular distribution of the scattered particles approaches that for scattering by a single atom, multiplied by the surface density of atoms in the foil. Due, however, to the fact that a particle which is scattered once through a large angle always receives, in addition, a large number of deflections through small angles, the actual distribution is never exactly equal to the single scattering distribution. The percentage difference between them is less, at any angle, the smaller the thickness of the foil, and it is often of importance in scattering experiments to know how thick a foil can be used (and thus how great a yield of scattered particles in any one direction can be obtained) without the deviations from single scattering at angles of interest being too great. It is the purpose here to deal with this question by deriving a formula for the angular distribution at angles for which the deviation from single scattering is less than about 100%. The corresponding formula for the projected scattering on a fixed plane is also obtained (cf. Snyder and Scott 1949).

In this treatment small angle approximations are employed, and energy losses by the particles are neglected.

§ 2. GENERAL FORMULAE

Let a particle be incident normally to a scattering foil, and let $f(\mathbf{n}, s)\, d\Omega$ be the probability that at a distance s through the foil, the particle is moving in the direction of the unit vector $\mathbf{n}$ within the element of solid angle $d\Omega$. Let $\mathbf{n}$ make an angle θ with the normal to the foil, and have an azimuthal angle ϕ. We measure s along the normal. Then $f(\mathbf{n}, s)$ satisfies the transport equation

$$\frac{\partial f}{\partial s}(\mathbf{n}, s) = N \int p(\Theta) \left\{ \frac{f(\mathbf{n}', s)}{\cos\theta'} - \frac{f(\mathbf{n}, s)}{\cos\theta} \right\} d\Omega', \qquad \ldots\ldots (1)$$

where Θ is the angle between $\mathbf{n}$ and $\mathbf{n}'$, and p is the differential cross section per unit solid angle for scattering by a single atom. N is the number of atoms per cm^3 in the foil.

Divide p into $g+h$, such that g takes account of most probable deflections through small angles, and h gives the probability of large deflections.* The exact nature in which this splitting is carried out will be unimportant, and for convenience we assume a sudden transition from g to h at some angle θ_1 (Figure 1). Equation (1) now becomes

$$\frac{\partial f}{\partial s}(\mathbf{n},s)=N\int g(\Theta)\left\{\frac{f(\mathbf{n}',s)}{\cos\theta'}-\frac{f(\mathbf{n},s)}{\cos\theta}\right\}d\Omega'+N\int h(\Theta)\left\{\frac{f(\mathbf{n}',s)}{\cos\theta'}-\frac{f(\mathbf{n},s)}{\cos\theta}\right\}d\Omega'. \quad \ldots\ldots(2)$$

For small angles Θ (those for which $g(\Theta)>0$), write $\mathbf{n}'=\mathbf{n}+\boldsymbol{\epsilon}$ and expand $f(\mathbf{n}',s)$ in powers of $\boldsymbol{\epsilon}$. Thus

$$f(\mathbf{n}',s)=\left\{f+\xi\frac{\partial f}{\partial x}+\eta\frac{\partial f}{\partial y}+\tfrac{1}{2}\xi^2\frac{\partial^2 f}{\partial x^2}+\xi\eta\frac{\partial^2 f}{\partial x\partial y}+\tfrac{1}{2}\eta^2\frac{\partial^2 f}{\partial y^2}+\ldots\right\}(\mathbf{n},s), \quad \ldots\ldots(3)$$

where (x,y) are cartesian coordinates of the projection of $\mathbf{n}$ on a plane parallel to the foil, and (ξ,η) the corresponding coordinates for $\boldsymbol{\epsilon}$ such that $\Theta^2=\xi^2+\eta^2$.

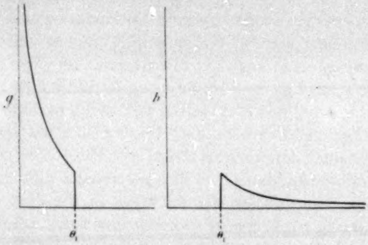

Figure 1. The division of the cross section p into small angle scattering (g) and large angle scattering (h).

We now substitute this expansion in the first integral of (2) and, in this integral, put also $\cos\theta'=\cos\theta$. It is evident, on account of the spherical symmetry of g, that terms containing odd powers of ξ and η vanish and, moreover, that

$$\int\xi^2 g(\Theta)\,d\Omega'=\int\eta^2 g(\Theta)\,d\Omega'=\tfrac{1}{2}\int\Theta^2 g(\Theta)\,d\Omega'$$

and $$\int\xi^4 g(\Theta)\,d\Omega'=\int\eta^4 g(\Theta)\,d\Omega'=3\int\xi^2\eta^2 g(\Theta)\,d\Omega'=\tfrac{3}{8}\int\Theta^4 g(\Theta)\,d\Omega'.$$

Therefore (2) becomes

$$\frac{\partial f}{\partial s}-\frac{k}{2\cos\theta}\nabla^2 f=N\int h(\Theta)\left\{\frac{f(\mathbf{n}',s)}{\cos\theta'}-\frac{f(\mathbf{n},s)}{\cos\theta}\right\}d\Omega'+\frac{k_1}{8\cos\theta}\nabla^4 f, \quad \ldots\ldots(4)$$

in which $$k=\frac{N}{2}\int\Theta^2 g(\Theta)\,d\Omega'=\frac{N}{2}\int\Theta^2 g(\Theta)\,d\Omega,$$

$$k_1=\frac{N}{8}\int\Theta^4 g(\Theta)\,d\Omega,$$

$$\nabla^2=\partial^2/\partial x^2+\partial^2/\partial y^2 \quad\text{and}\quad \nabla^4=\partial^4/\partial x^4+2\partial^4/\partial x^2\partial y^2+\partial^4/\partial y^4.$$

---

* The author is indebted to Professor Peierls for suggesting this procedure.

Although, as will be seen, the only terms of the expansion (3) of importance in (4) are those up to second order, we have considered also the fourth order terms in order to have some guide in our choice of transition angle θ_1. We shall choose θ_1 such that the effect of these terms is small.

If we make the small angle approximation $\cos\theta = 1$ and $\sin\theta = \theta$, the vector **n** becomes identical with the vector $\boldsymbol{\theta}$ having plane polar coordinates (θ, ϕ). In this approximation (4) can be written as the well known diffusion equation

$$\frac{\partial f}{\partial s} - \frac{k}{2}\nabla^2 f = u(\boldsymbol{\theta}, s), \qquad \ldots\ldots (5)$$

where
$$u(\boldsymbol{\theta}, s) = N\int h(\boldsymbol{\theta}-\boldsymbol{\theta}')\left\{f(\boldsymbol{\theta}', s) - f(\boldsymbol{\theta}, s)\right\} d\Omega' + \frac{k_1}{8}\nabla^4 f.$$

The general solution, subject to the condition that it be normalized to unity such that for all s

$$\int f(\boldsymbol{\theta}, s)\, d\Omega = 1$$

is

$$f(\boldsymbol{\theta}, s) = \frac{\exp(-\theta^2/2ks)}{2\pi ks} + \int_0^s\int \frac{\exp\{-(\boldsymbol{\theta}-\boldsymbol{\theta}')^2/2k(s-s')\}}{2\pi k(s-s')} u(\boldsymbol{\theta}', s')\, d\Omega'\, ds'. \qquad \ldots\ldots (6)$$

The gaussian
$$\frac{\exp\{-(x^2+y^2)/2ks\}}{2\pi ks} = \frac{\exp(-\theta^2/2ks)}{2\pi ks} \qquad \ldots\ldots (7)$$

is the solution of the equation

$$\frac{\partial f}{\partial s} - \frac{k}{2}\nabla^2 f = 0$$

and the integral in (6) is a particular solution of (5).

Both terms of the function $u(\boldsymbol{\theta}, s)$ can be made small by suitable choice of θ_1. For $f(\boldsymbol{\theta}, s)$ we thus substitute in u the pure gaussian (7). Then (6) becomes

$$f(\boldsymbol{\theta}, s) = \frac{\exp(-\theta^2/2ks)}{2\pi ks}\left\{1 - z + \frac{k_1 s}{k^2 s^2}\left(1 - \frac{\theta^2}{ks} + \frac{\theta^4}{8k^2s^2}\right)\right\}$$
$$+ N\int_0^s\int\int \frac{\exp\{-(\boldsymbol{\theta}-\boldsymbol{\theta}')^2/2k(s-s')\}}{2\pi k(s-s')} h(\boldsymbol{\theta}'-\boldsymbol{\theta}'')\frac{\exp(-\theta''^2/2ks')}{2\pi ks'}\, d\Omega''\, d\Omega'\, ds', \qquad \ldots\ldots (8)$$

where $z = Ns\int h\, d\Omega$, and is the probability that a particle, on traversal of the foil, undergoes a deflection through an angle greater than θ_1.

The physical interpretation of this solution is clear; the first term represents the multiple scattering due to many collisions through angles smaller than θ_1, and the second term represents the probability of a particle emerging in a direction $\boldsymbol{\theta}$ after traversing a foil of thickness s and having received one major collision (i.e. through $>\theta_1$) somewhere along its path.

Consider the single scattering integral. In general the maximum values of the integrand occur for $\boldsymbol{\theta}''$ small and for $(\boldsymbol{\theta}-\boldsymbol{\theta}')$ small. We expand, therefore, $h(\boldsymbol{\theta}'-\boldsymbol{\theta}'')$ in the neighbourhood of $\boldsymbol{\theta}$:

$$h(\boldsymbol{\theta}'-\boldsymbol{\theta}'') = h(\boldsymbol{\theta}) + (x'-x-x'')\frac{\partial h}{\partial x} + (y'-y-y'')\frac{\partial h}{\partial y} + \frac{(x'-x-x'')^2}{2}\frac{\partial^2 h}{\partial x^2} + \ldots.$$

On carrying out the integration, all terms containing odd powers of $(x'-x)$, $(y'-y)$, x'' and y'' vanish, and we get

$$Ns\left\{h(\theta)+\frac{ks}{2}\nabla^2 h+\frac{k^2s^2}{8}\nabla^4 h+\ldots.+\frac{k^ns^n(2n-1)(2n-3)\ldots.1}{(2n)!}\nabla^{2n}h+\ldots.\right\}. \qquad \ldots\ldots(9)$$

Since h is spherically symmetric, this can also be written

$$Ns\left\{h(\theta)+\frac{ks}{2}\left(\frac{d^2h}{d\theta^2}+\frac{1}{\theta}\frac{dh}{d\theta}\right)+\frac{k^2s^2}{8}\left(\frac{d^2}{d\theta^2}+\frac{1}{\theta}\frac{d}{d\theta}\right)\left(\frac{d^2h}{d\theta^2}+\frac{1}{\theta}\frac{dh}{d\theta}\right)+\ldots.\right\}.$$

It is seen that the first term $Nsh(\theta)$ gives the well known single-scattering probability. The next terms represent the modifications to this probability due to the many small additional deflections which a particle receives.

By substitution for p we shall show that, for suitable adjustment of θ_1, the multiple scattering portion of (8) differs very little from the gaussian (7). At angles for which this gaussian is negligible, f is thus given by (9) which here converges rapidly.

A check on the accuracy of our results can be made by proceeding to the next approximation in which (8) is substituted in (6). In this case the probability of a particle undergoing two major collisions appears. Although this is not carried out here, it can easily be shown that for such angles θ_1 as we shall choose, the results are changed by a negligible amount.

§ 3. SUBSTITUTION FOR THE SINGLE SCATTERING LAW

The single scattering law $p(\theta)$ has the form

$$p(\theta)=\left(\frac{ZZ'e^2}{2Mv^2}\right)^2\left(1-\frac{v^2}{c^2}\right)\frac{1-(v^2/c^2)\sin^2\frac{1}{2}\theta+\ldots.}{\{\sin^2\frac{1}{2}\theta+(\frac{1}{2}\theta_0)^2\}^2},$$

where $Z'e$ is the charge of the particle being scattered, and M its rest mass. In the small angle approximation, and introducing the total energy E of the particle in units of Mc^2, $p(\theta)$ becomes

$$p(\theta)=\left\{\frac{2ZZ'e^2}{Mc^2(E-1/E)}\right\}^2\frac{1}{(\theta^2+\theta_0{}^2)^2}. \qquad \ldots\ldots(10)$$

The effect of the screening of the orbital electrons is taken into account by the factor θ_0 where $\theta_0=\lambda/2\pi a=h/aMc(E^2-1)^{1/2}$, a being the usual screening constant $h^2/me^2Z^{1/3}$. Actually, however, the results are very insensitive to the manner in which screening is considered and would be affected very little if, instead of the above, we had considered the Rutherford scattering law for an unscreened nucleus as merely cut off at the angle θ_0.

Assuming $\theta_1 \gg \theta_0$, we obtain from (10)

$$z=\delta^2/\theta_1{}^2, \qquad ks=\delta^2\xi, \qquad \text{and} \qquad k_1s=\delta^2\theta_1{}^2/8=\delta^4/8z,$$

where

$$\delta^2=\pi Ns\left\{\frac{2ZZ'e^2}{Mc^2(E-1/E)}\right\}^2 \qquad \ldots\ldots(11)$$

and

$$\xi=\log\frac{\theta_1}{1\cdot 82\theta_0}=4\cdot 06+\tfrac{1}{2}\log\left\{\frac{Z^{4/3}Z'^2\rho s}{Wz}\frac{E^2}{E^2-1}\right\}, \qquad \ldots\ldots(12)$$

in which ρ is the density and W the atomic weight of the scattering material.

If we choose $(ks)^{1/2} = \delta\xi^{1/2}$ as unit of angle (and change the unit of solid angle accordingly) (8) becomes, on inserting (9) and substituting for h

$$f(\theta, s) = \frac{1}{2\pi}\left[\exp\left(-\frac{\theta^2}{2}\right)\left\{1 - z + \frac{1}{8z\xi^2}\left(1 - \theta^2 + \frac{\theta^4}{8}\right)\right\}\right.$$
$$\left. + \frac{2}{\xi\theta^4}\left\{1 + \frac{8}{\theta^2} + \frac{72}{\theta^4} + \frac{768}{\theta^6} + \dots\right\}\right]. \qquad \dots\dots (13)$$

The series representation of the single scattering integral diverges for $\theta \gtrsim 3{\cdot}5$, but we shall be considering angles greater than this.

Unless s is extremely small, when our assumption $\theta_1 \gg \theta_0$ breaks down, it is always possible to make both the z and $1/8z\xi^2$ of (13) small (say $<0{\cdot}1$) by adjusting θ_1 such that they are approximately equal. For such values it can easily be verified that these terms are of negligible importance in (13) and can be neglected. Some typical values, for example, of z and $1/8z\xi^2$ are those given in the Table, corresponding to the scattering of high energy electrons by lead.

	$s=0{\cdot}05$			$s=0{\cdot}01$			$s=0{\cdot}005$		
z	0·2	0·1	0·05	0·2	0·1	0·06	0·2	0·1	0·07
$1/8z\xi^2$	0·023	0·042	0·070	0·032	0·056	0·083	0·034	0·064	0·084

ξ takes only a limited range of values (say 2–5) and it is found from (13) that the gaussian always becomes negligible compared with the 'single scattering' portion for $\theta \gtrsim 4$–$4{\cdot}5$. In this range the distribution is thus given by

$$f(\theta, s) = \frac{1}{\pi\xi}\frac{1}{\theta^4}\left(1 + \frac{8}{\theta^2} + \frac{72}{\theta^4} + \frac{768}{\theta^6} + \dots\right), \qquad \dots\dots (14)$$

where the first term is the true single scattering.

The percentage derivation from single scattering is thus given by

$$100\left(\frac{8}{\theta^2} + \frac{72}{\theta^4} + \frac{768}{\theta^6} + \dots\right). \qquad \dots\dots (15)$$

Usually only two terms of (15) are required, but for deviations greater than about 20% more terms must be used.

The unit of angle is $\delta\xi^{1/2}$, where δ and ξ are given respectively by (11) and (12). Although ξ depends on z (which is adjusted so that $z \simeq 1/8z\xi^2$) it is, however, quite insensitive to the exact value of z taken. For example, in the case of high energy electrons being scattered by 0·01 cm. of lead, if we choose $z = 0{\cdot}1$ (and thus $1/8z\xi^2 = 0{\cdot}056$) we find $\xi = 4{\cdot}8$; if however, we choose $z = 0{\cdot}06$ (and thus $1/8z\xi^2 = 0{\cdot}083$), $\xi = 5{\cdot}0$. In fact for all cases, in the evaluation of ξ, z can be taken as something like 0·08.

If the energy of the electrons in the case just considered be taken as 20 MEV., then the unit of angle $\delta\xi^{1/2} = 8{\cdot}7 \times 10^{-2}$, and from (15) the deviation from single scattering is approximately 30% at 30° and 10% at 45°.

Thus, taking $\delta\xi^{1/2}$ as unit of angle, the scattering distrbution per unit solid angle approaches single scattering at angles greater than 4·0–4·5. In this range the distribution is given by (14), and the percentage deviation from single scattering by (15).

§4. PROJECTED SCATTERING

In some cases it may be useful to know the formula corresponding to (14) for the projected scattering on a fixed plane. This can easily be derived in the same way as (14).

In the small angle approximation the transport equation becomes

$$\frac{\partial f}{\partial s}(x,s) = N\int_{-\infty}^{\infty} p_{\text{proj}}(x)\{f(x',s)-f(x,s)\}\,dx',$$

where

$$p_{\text{proj}}(x) = \int_{-\infty}^{\infty} p(\theta)\,dy = \int_{-\infty}^{\infty} p((x^2+y^2)^{1/2})\,dy \qquad \ldots\ldots(16)$$

and x is the angle of scattering on the plane. Dividing $p_{\text{proj}}(x)$ into $g_{\text{proj}}(x)$ and $h_{\text{proj}}(x)$ at angles $+x_1$ and $-x_1$ and proceeding as before, we find

$$f(x,s) = \frac{\exp(-x^2/2k's)}{(2\pi k's)^{1/2}}(1+\text{small terms}) + N\int_0^s\!\!\int\!\!\int \frac{\exp\{-(x-x')^2/2k'(s-s')\}}{(2\pi k'(s-s'))^{1/2}}$$

$$\times\, h_{\text{proj}}(x'-x'')\,\frac{\exp(-x''^2/2k's')}{(2\pi k's')^{1/2}}\,dx''\,dx'\,ds',$$

where

$$k' = N\int_{-\infty}^{\infty} x^2 g_{\text{proj}}(x)\,dx.$$

At angles for which the gaussian is negligible,

$$f(x,s) = Ns\left\{h_{\text{proj}}(x) + \frac{k's}{2}\frac{d^2h_{\text{proj}}}{dx^2} + \frac{k'^2s^2}{8}\frac{d^4h_{\text{proj}}}{dx^4} + \ldots\right\}. \qquad \ldots\ldots(17)$$

Now from (16),

$$p_{\text{proj}}(x) = \frac{\delta^2}{2Ns}\,\frac{1}{\{x^2+\theta_0{}^2\}^{3/2}},$$

and we find $k's = \delta^2\xi'$, where

$$\xi' = \log\frac{|x_1|}{2{\cdot}00\theta_0} = 3{\cdot}62 + \tfrac{1}{2}\log\left\{\frac{Z^{4/3}Z'^2\rho s}{Wz'}\,\frac{E^2}{E^2-1}\right\}.$$

Here z' is the probability of a particle, on traversal of the foil, obtaining a deflection through $>|x_1|$ and can be adjusted to something like 0·05.

In units of $(k's)^{1/2} = \delta\xi'^{1/2}$ (17) becomes

$$f(x,s) = \frac{1}{2\xi' x^3}\left\{1 + \frac{6}{x^2} + \frac{45}{x^4} + \ldots\right\}. \qquad \ldots\ldots(18)$$

The first term is the projected single scattering, and the other terms are corrections.

In a recent treatment of multiple scattering, Snyder and Scott have given an asymptotic formula for the projected scattering on a plane, valid as long as the deviation from the projected single scattering is less than about 20%. Using the ordinary unit of angle (i.e. the radian) their formula can be written

$$f(x,s) = \frac{\delta^2}{2x^3}\left\{1 + \frac{6\delta^2}{x^2}\left(\log\frac{|x|}{\theta_0} - 0{\cdot}884\right) + \frac{45\delta^4}{x^4}\left[\left(\log\frac{|x|}{\theta_0} + 0{\cdot}616\right)^2\right.\right.$$

$$\left.\left. - 3{\cdot}85\log\left(\frac{|x|}{\theta_0} + 0{\cdot}616\right) + 3{\cdot}33\right] + \ldots\right\}. \qquad \ldots\ldots(19)$$

In Figure 2 the percentage deviations as calculated from (18) and (19) are compared for the case of scattering of 20 MeV. electrons by 0·005 cm. of lead. It is seen that the Snyder–Scott formula gives slightly larger deviations than does (18).

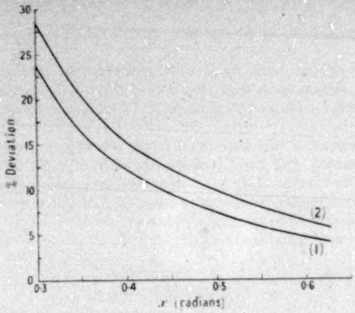

Figure 2. The percentage deviation of the projected scattering from single scattering for the case of 20 MeV. electrons scattered by 0·005 cm. of lead, as calculated (1) from equation (18), (2) from the Snyder–Scott formula (19).

It is of interest to note that we can force (18) into a form almost identical with (19) by choosing x_1 in fact equal to the actual angle x at which a measurement is made. In this case $\xi' = \log|x|/2{\cdot}00\theta_0$, and with the ordinary unit of angle, (18) becomes

$$f(x,s)=\frac{\delta^2}{2x^3}\left\{1+\frac{6\delta^2}{x^2}\left(\log\frac{|x|}{\theta_0}-0{\cdot}693\right)+\frac{45\delta^4}{x^4}\left(\log\frac{|x|}{\theta_0}-0{\cdot}693\right)^2+\dots\right\}. \qquad \dots\dots(20)$$

The similarity between (19) and (20) is evident, and on plotting percentage deviations they are found to be almost indistinguishable. However, when x_1 is adjusted in the manner discussed in § 3, it is always much lower than angles for which the distribution approaches single scattering, and we would expect therefore that (18) be more accurate than (20).

ACKNOWLEDGMENT

It is a pleasure to thank Professor R. E. Peierls for his suggestion of this problem and for many helpful discussions.

REFERENCES

SNYDER, H. S., and SCOTT, W. T., 1949, *Phys. Rev.*, **76**, 220.
WILLIAMS, E. J., 1939, *Proc. Roy. Soc.* A, **169**, 531.

Penetrating Showers at High Altitude

By M. G. NOOH and S. R. HADDARA
The Physical Laboratories, University of Manchester

Communicated by P. M. S. Blackett; *MS. received* 1st *September* 1949

ABSTRACT. A study has been made of cloud chamber photographs of penetrating cosmic-ray showers, originating in lead placed over the cloud chamber and in a lead plate within the cloud chamber, obtained at altitude 3,572 m. in a magnetic field of about 1,000 gauss.

The use of well-separated successive lead layers allowed the association of penetrating events to be demonstrated, and there is some evidence of a general reduction of energy involved in events in the lower lead layers as compared with those in the top layer. Mesons, protons and particles of higher charge were identified in the penetrating showers, and a mean range for non-coulomb scattering of shower particles is given. Evidence is also given of the apparent starting and stopping of charged particles in the lead plate at the centre of the cloud chamber.

§ 1. INTRODUCTION

The existence of penetrating cosmic-ray showers was first demonstrated by Wataghin and his co-workers (1940) and by Jánossy and his co-workers (1940), since which time these showers have been the subject of many detailed researches. In particular Broadbent and Jánossy (1947) distinguished two types of penetrating showers: the local penetrating showers which they considered to be produced by isolated nucleons entering the apparatus, and extensive penetrating showers in which the penetrating events are associated with extensive cascade showers in the atmosphere. In the early work, the multiplicity achieved in the local penetrating showers was mainly attributed to the creation of mesons, and the transition curves for these showers corresponded to a primary range which was in reasonable agreement with the theoretical value given by Hamilton, Heitler and Peng (1943). Recently, the more detailed work of Rochester and Butler (1948 a, b) has thrown doubt on the simplicity of the picture and in particular has shown that many of the fast particles emitted in the local showers are not ordinary mesons and may well be protons.

The present experiment was designed to take advantage of the rapid increase in the nucleon intensity with altitude in order to study large numbers of penetrating shower events. It was also hoped that if the events attributed by Rochester and Butler (1947) to the decay of heavy particles increased with altitude in the same ratio as the local penetrating showers, further examples of these processes would be observed. Work was accordingly carried out at the International High Altitude Research Station at Jungfraujoch (3,572 m. above sea level).

§ 2. APPARATUS

A counter-controlled cloud chamber, 27 cm. diameter and 7·5 cm. deep, and containing a lead plate 2·6 cm. thick, was operated in a magnetic field of 900 gauss. The chamber was contained in a thermally isolated brass box, the whole apparatus being housed in an aluminium cork-lined hut on the roof of the Sphinx meteorological observatory at Jungfraujoch. Although the hut was thermostatically maintained at a uniform temperature, considerable difficulty was encountered in maintaining thermal stability in the cloud chamber. This was due to the large temperature fluctuations of the external air brought into the hut to cool the field solenoids. After the first short period of operation, however, in which track distortion was severe, a condition was reached in which the maximum detectable momentum in either half of the chamber was about 2×10^8 ev/c.

The counter arrangement used, which followed closely an arrangement used by Rochester and Butler (1948 a) is shown in Figure 1. A three-fold counter telescope, built of six 20 cm. × 2 cm. counters, was surrounded by lead (10 cm. above, at least 5 cm. at each side) and selected particles in the central plane of the chamber, which was placed below a further lead layer varying in thickness from 1 cm. to about 3 cm. Below the chamber, and without further shielding, was placed a two-fold counter tray of four 30 cm. × 3·5 cm. counters. The five-fold coincidences of the upper shielded telescope and the lower two-fold tray were used to operate the chamber. This system of selection was, of course, sensitive to 'knock-on' electrons produced by fast incident particles in the lead plate inside the chamber and, to a certain extent, in the lead immediately above the cloud chamber. It is also sensitive to multiple showers of penetrating particles in any of the lead layers: in the lower layers an ionizing primary is required, while in the top lead layer multiple showers arising from a non-ionizing primary would also be recorded.

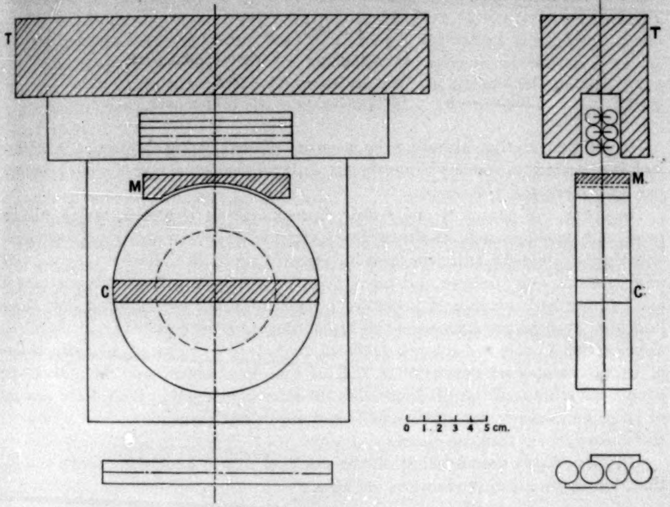

Figure 1.

§ 3. EXPERIMENTAL DATA

3.1. *The Counting Rate*

At sea level (Manchester), the counting rate of the five-fold counter system (Figure 1) was 6·3 counts per hour. At Jungfraujoch 4,700 photographs were taken in 642 hours, i.e. at a rate of 7·3 photographs per hour. In order to compare these rates it is necessary to know the inert time of the cloud chamber, during which cleaning expansions were made and thermal equilibrium restored after each operation. In our apparatus this inert time was 4 minutes. In Table 1 the rates quoted above and the simple counting rate recorded at Jungfraujoch are shown, together with the rate of photographing at sea level deduced from the value of the inert time.

Table 1

	Counting rate	Photographing rate
Sea level	6·3 per hour	(4·4 per hour)
Jungfraujoch	14·3 per hour	7·3 per hour

It will be seen that, although the intensity of penetrating showers at Jungfraujoch is expected to be many times that at sea level, the actual rate of photographing has only increased 1·7 times.

Suppose the counts to arise only from knock-on electrons, which will be produced almost entirely by the ordinary meson component and from penetrating showers. While the latter increase in intensity about 28 times between sea level and Jungfraujoch (George and Jason 1948), the former will scarcely increase at all. This small increase of knock-on counts is due to the fact that only those knock-on events have a large probability of operating the counter system in which the electron is projected at a relatively small angle to its primary, and with radius of curvature at least greater than that of the cloud chamber. Such knock-on events have been shown (Wilson 1938) to arise almost exclusively from mesons of large momentum ($>3\times10^9$ ev/c.), and we estimate their increase in number to be not greater than 1·4 times.

If, then, C_E is the counting rate at sea level due to knock-on events, and C_P that due to penetrating showers, we have

$$C_E + C_P = 6{\cdot}3, \quad \text{(Sea level)}$$
$$1{\cdot}4C_E + 28C_P = 14{\cdot}3. \quad \text{(Jungfraujoch)}$$

Whence

$$C_P/(C_E + C_P) = 0{\cdot}03,$$
$$28C_P/(1{\cdot}4C_E + 28C_P) = 0{\cdot}40.$$

Thus, while the rate of photographing increased 1·7 times, it appears likely that the probability that any operation has been initiated by a penetrating shower has increased from 3% to 40%, and the resultant gain is about 13 times.

3.2. *The Experimental Results*

Of 4,700 photographs taken at Jungfraujoch 92 showed 'penetrating showers' according to the definition of Rochester and Butler (two or more particles penetrating the 2·6 cm. lead plate without measurable loss of momentum and leading to no secondaries), and the main result of the present work is concerned with these events. We shall discuss the angular distribution of the penetrating showers, the association of penetrating showers and of comparable nuclear explosions, and the evidence from our photographs of the nature of the penetrating particles in the showers.

3.3. *Angular Distribution of Particles in Penetrating Showers*

For all penetrating showers, the tracks observed were drawn on a scale diagram of the cloud chamber and the various lead absorbers; it was then found possible, by extrapolating the tracks backwards, to determine the layer of lead in which the shower appeared to have originated. In this way 58 showers were referred to the upper lead layer T and 34 to the layer M immediately above the cloud chamber. The second group formed in M were particularly well defined, and in them the tracks projected back to a point of formation; in the first group the projection was not so successful, probably on account of scattering of the particles in the lower layer M, but this uncertainty was not of a kind which could cause these showers to be attributed, erroneously, to a point of origin in the lower plate.

On inspection, it appeared that the showers from the upper plate T are, on average, more collimated than those from the lower plate M, but it is extremely difficult to establish this fact unambiguously on account of the great diversity of type among the showers. However, several examples existed, for each layer of formation, of showers in which two penetrating particles reach the cloud chamber; the projected angular separation of these penetrating pairs of particles was compared with the distribution of projected angles which could be imposed by the geometry of the cloud chamber, the absorbing plate and the counter array for a distribution of formation which is isotropic at least for the limits of angular spread set by geometry. The results of the comparison are given in Table 2.

Table 2. Angular Distribution of Penetrating Showers of Two Particles in the Cloud Chamber

Layer of Origin	Number	Mean angular separation (deg.)	
		Observed	Calculated (isotropic)
T	11	4·5	10
M	7	18·4	20

We thus have some evidence that the showers from the upper layer T but not those from the layer M are appreciably collimated over angles of the order 10°. It is therefore probable that the energy involved in nuclear collisions in the lower lead layer is significantly less than that in the top block of lead, and that the nucleon spectrum undergoes a transition effect entering lead from the atmosphere. This effect might be expected to arise if the multiplicity in nucleon showers is a function of the number of nucleons in the nuclei in which collision takes place, provided that some at least of the secondary particles in showers are themselves capable of shower production.

The angular distribution of penetrating particles in some events is clearly most complex. In one example of an explosion in the central lead plate (Figure 2), which is probably initiated by an uncharged primary, the penetrating particles emerging fall into three groups: a very narrow group, a, of at least four particles within a total angle of less than 10°, a second group, b, of at least five particles also in an angle of about 10°, the axes of the groups being separated by about 40°, and a third group, c, also narrow and containing about four particles with axis about 20° to that of a. In addition one or two other particles make considerable angles with the main groups. In such an event the final distribution of particles can hardly be regarded as the result of a single stage of interaction, and any argument based on one section only of the event is liable to be misleading.

3.4. *The Association of Penetrating Showers*

Our photographs give evidence that particles in a penetrating shower can themselves lead to further penetrating showers, and are thus in agreement with recent observations (Tinlot and Gregory 1949, and Chao 1949) which show considerable association of showers of the nuclear collision type.

Penetrating showers originating in layer M were observed to be associated either with showers originating in the upper layer T (Figure 3), or else with single penetrating particles passing through M at a point other than the point of origin of the shower but in the same general direction. The occurrence of such a combination as a random association of the single particles with the penetrating event in M is extremely rare (about one, only, in all photographs of penetrating events starting in M); hence we regard these also as indicating the production of a secondary nucleon shower in M.

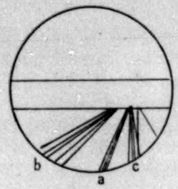

Figure 2.

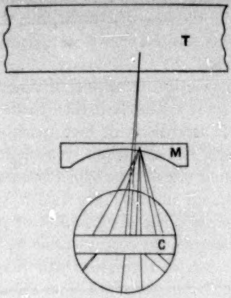

Figure 3.

Nuclear explosions in the lead plate C inside the cloud chamber, whether produced by ionizing or non-ionizing particles were similarly observed to be associated with single penetrating particles traversing some other part of the plate C or with penetrating showers originating in the lead layer T or M. The occurrence of events in these categories is shown in Table 3.

Table 3. Number of Showers associated with pre-existing Penetrating Particles (N_{p})

Summary	N_{p}
Showers in plate M (Total no. 34)	9
Explosions in plate C (Total no. 32)	12
Showers in M Detail	
Possibly large scattering of particles from T	3
Shower + 1 other penetrating particle	3
Shower + shower from T	3
Explosions in C	
Explosion + 1 other penetrating particle	2
Explosion + 1 other penetrating particle + 1 particle stopped	2
Explosion + shower from T	5
Explosion + shower from M	3

3.5. *The Nature of Penetrating Particles*

(*a*) *Particles showing increased ionization in traversing plate C.*

Five penetrating shower particles (Table 4) showed increased ionization after traversing the lead plate C in the centre of the cloud chamber.

Table 4. Estimated Ionization of Particles traversing Chamber and appearing to show Increased Ionization

Top half of chamber	$I/I_{\min}$	2	2	2	>1*	>1*
Lower half of chamber	$I/I_{\min}$	6	6	6	3	3

* Although for the last two particles the ionization in the upper half was judged to be greater than minimum, little weight can be attached to these estimates.

The expected behaviour of particles of mass $200\,m_e$, $300\,m_e$, $1{,}000\,m_e$ and $1{,}840\,m_e$ over a range relevant to the first three particles of Table 4 are shown in Table 5, from which it can be concluded that the masses of these particles are at least of the order $1{,}000\,m_e$.

Table 5. Ionization of Particles traversing 2·6 cm. Lead

Mass		Ionization as multiple of minimum		
$200m_e$	in	1·3	1·4	1·5
	out	2·2	4·6	stopped
$300m_e$	in	1·4	1·5	1·6
	out	2·4	3·5	stopped
$1000m_e$	in	2·2	2·4	2·8
	out	4·4	6·2	stopped
$1840m_e$	in	2·7	2·9	3·0
	out	4·8	6·2	stopped

(*b*) *Particles which are heavily scattered.*

The projection of the angles of scattering in a plane perpendicular to the axis of photography of 230 shower particles traversing the lead plate in the cloud chamber is summarized in Table 6.

Table 6. Scattering of Particles in Penetrating Showers of Momentum $>2 \times 10^8$ ev/c. traversing 2·6 cm. Lead in Cloud Chamber

Angle (degrees)	0–5	5–10	10–20	20–30	>30
Observed no. of particles	183	18	18	6	5
Calculated number	183	18	13	1·2	0·04

The row 'Calculated number' refers to the assumption of coulomb scattering alone when all particles scattered more than 5° are of the lowest possible momentum.

The momentum of the particles concerned is in no case less than about 2×10^8 ev/c. at which momentum the probable angle of multiple coulomb scattering in 2·6 cm. lead would be 7°. Thus with the assumption most favourable to the presence of coulomb scattering only (that is, that the whole of the group of particles scattered in the range of angles 5–10° are of momentum 2×10^8 ev/c. and suffer only coulomb scattering, while the majority of particles scattered

0–5° are of much larger momentum), between 5 and 15 particles of those scattered more than 10° must be considered to show additional scattering of non-coulomb type. We thus find that the particles in the penetrating showers are, on average, heavily scattered once in traversing 40–100 cm. of lead, a scattering range which may be compared with that of 25 cm. lead reported by Rochester and Butler (1948 b). The longer range in the present work is essentially an upper limit, and has almost certainly been increased, as compared with the figure given by Rochester and Butler, on account of the much lower maximum detectable momentum obtained in our apparatus. It is clear, however, that many of the particles near minimum ionization in the penetrating showers are not μ-mesons.

(*c*) *Particles stopped and created in the lead plate C.*

Out of 247 particles with momentum greater than 2×10^8 ev/c. in penetrating showers, 17 showing minimum ionization were stopped in the lead plate C. Twenty other particles appeared under the lead plate without a visible origin above. Reprojecting these photographs through the same stereoscopic lenses used in photographing, the position of these tracks in the cloud chamber was located in order to establish that with normal scattering they would not pass out of the illuminated region. These particles must either be scattered through very large angles or be genuinely stopped or created in the lead plate. Projections in two planes of photographs showing tracks stopping or starting in the lead plate are given in Figures 4 and 5, and show particles stopped or starting which are well inside the illuminated part of the cloud chamber.

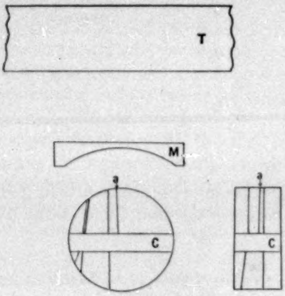

Figure 4.

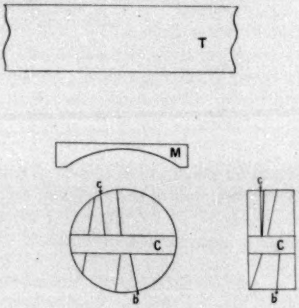

Figure 5.

We can exclude the possibility that the particles which stop are either μ-mesons or electrons, the former because an initial momentum of only about 10^8 ev/c. is required to traverse the plate, and the latter because from an entrant electron $p > 2 \times 10^8$ ev/c. several shower particles are to be expected below 2·6 cm. lead.

It is therefore probable that the particles are of a kind interacting strongly with nuclei, and that they either undergo an exchange transformation of the type proton–neutron in a collision in the plate, or else dissipate the incident energy in such a collision. Similarly, the particles created in the plate are likely to arise from nuclear explosions initiated by a non-ionizing primary or else be derived from a non-ionizing primary by an exchange process.

(*d*) *Heavily ionizing particles.*

A total of 94 heavily ionizing particles were observed, 49 in the upper half of the cloud chamber and 45 in the lower half, under the plate C. The circumstances of occurrence of these particles are summarized in Table 7.

Table 7. Summary of Occurrence of Heavily Ionizing Particles

1. *Particles in Upper Half of Chamber*

No. associated with penetrating particles	21
No. associated with soft component	14
No. identified as multi-charged particles	4
No. identified as μ-mesons	1
No. not associated with other events in the chamber	9
Total	49

2. *Particles in Lower Half of the Chamber*

Single particles associated with explosions	10
Single particles associated with single penetrating particles	4
No. of heavy pairs created in the lead plate (9)	18
No. of particles becoming heavy in traversing the plate	5
No. of particles occurring in showers of more than two particles	6
Single particles not associated with other events	2
Total	45

The great majority of these particles show ionization estimated to be greater than five times minimum and have no measurable curvature: all of these may well be protons. However, two particles occur which are certainly light (π- or μ-) mesons, and five particles which lead to δ-electrons of measurable range will be shown to be multiply charged.

One of the tracks identified as a meson decays to a lightly ionizing particle in the upper half of the cloud chamber, and must be identified as a μ-meson.

The other meson track, which occurs in a explosion from 1 cm. depth in the plate C initiated by an ionizing primary, is identified by ionization and momentum. The measured momentum is $(2{\cdot}2 \pm 0{\cdot}7) \times 10^7$ ev/c. and the ionization is estimated as 5 times minimum. This particle is therefore not identified with certainty, but may be either a μ-meson or π-meson.

Several heavily ionizing tracks are of particular interest because the formation of δ-electrons along the trajectory in the cloud chamber allows an estimate of particle charge to be made.

The probability of production of secondary electrons in elastic collision is given (Jánossy 1948, p. 94) by

$$\psi(E)\,dE = 2\pi r_0^2 zN\,\mathbf{mc}^2 (Z/\beta)^2\,dE/E^2, \qquad \ldots\ldots(1)$$

where $\psi(E)\,dE$ is the probability that a particle of charge Ze traversing material of atomic number z and N atoms/cm^3 will give rise to a secondary electron in the energy range E to $E+dE$ in one centimetre of path length, and where r_0, $\mathbf{m}$, $\mathbf{c}$, β have the usual significance. The number of δ-electrons per centimetre of path, say n, is then given by

$$n = 2\pi r_0^2 zN\,\mathbf{mc}^2 (Z/\beta)^2 \int_{\mathrm{E_{min}}}^{\mathrm{E_{max}}} dE/E^2, \qquad \ldots\ldots(2)$$

where $E_{\min}$ is the minimum energy of δ-electrons which are selected, and $E_{\max}$, the maximum transferable energy, is $2mc^2\beta^2/(1-\beta^2)$. Equation (2) allows us to write Z^2/n as a function of β^2 for the particular medium traversed (in our chamber, oxygen at about 1 atmospheric pressure), and for any chosen value of $E_{\min}$. A typical curve of Z^2/n plotted against β^2 is given in Figure 6 which refers to δ rays

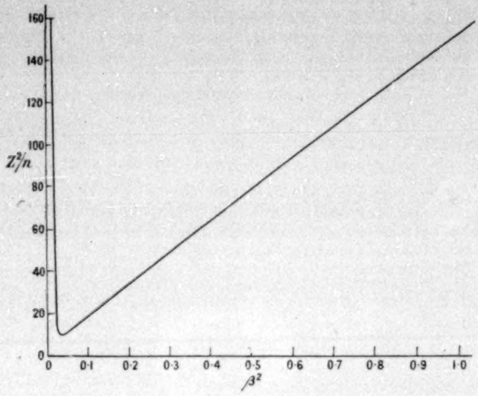

Figure 6.

of minimum energy 15 kev. The charge of the fast particle then lies between limits at the minimum of this curve and the value of Z corresponding to $\beta = 1$. For all of our examples the low velocity limb of the curve is excluded by the range over which the particle has been observed. Results for five particles are given in Table 8.

Table 8. Charge Determinations for Heavily Ionizing Particles producing δ-Electrons

(1)	(2)	(3)	$Z_{\min}$	$Z_{\max}$
5	4	5/5	3	12
6	6	2/6	2	8
6	6	2/6	2	8
4	3	4/4	3	11
8·5	3	5/8·5	2	9

(1) Length of primary track available (cm.); (2) minimum range of δ-electron selected (mm.); (3) n = (no. of δ-electrons)/(cm. track avalable).

No account has been taken in this discussion of the statistical weight to be given to the very small number of secondary electrons observed for each heavy track. However it must be noted that the quantity deduced is actually Z^2/n, and so for the first, fourth and fifth tracks, at least, there is an extremely low possibility that a singly charged particle will give rise to the observed secondaries.

§4. DISCUSSION

The most striking feature of our photographs is the extent to which the results of nuclear interaction, whether they are classified as penetrating showers or as explosions in the lead plate inside the cloud chamber, are associated. The distinction of successive events is assisted by our experimental arrangement in which the lead over the cloud chamber is in two well separated layers: with this arrangement 21 out of 66 events taking place in the lead M immediately over the cloud chamber or in the plate C inside the chamber are associated with penetrating particles in addition to their own primaries. Similar conclusions have been reported by Tinlot and Gregory (1949) and Chao (1949).

The result of the entry of a high energy nucleon-like particle into a layer of matter is thus in some ways similar to an electron–photon cascade, although the process is simpler in so far as multiplication takes place only at a very limited number of collisions. However, the degree of multiplication at a collision as a function of the energy of the incident particles and of the nature of the nucleus which is disrupted is still unknown, and observations have not yet allowed us to estimate how many of the particles produced in a penetrating shower are of a kind with strong nuclear interaction which may be expected to lead to further stages of multiplication. Attention has been drawn to the multiplication process by Rossi (1948).

When the detailed behaviour of collisions leading to penetrating showers is understood, it will no doubt be possible to formulate transition relations for a beam of nucleons (perhaps together with other strongly interacting particles) in equilibrium, analogous to those familiar in cascade theory. In this connection Rossi shows that the energy spectrum of protons (kinetic energy greater than about 100 Mev.) changes only slightly in the greater part of the atmosphere, and this result must certainly be regarded rather as an equilibrium condition than as a pure absorption of the primary beam.

We have given some evidence of a change of energy distribution in the nuclear beam on traversing successive layers of lead, in so far as the mean angle between pairs of penetrating particles from the upper lead plate appears to be smaller than the corresponding angle for pairs from the middle plate. This result would indicate a transition effect towards a different equilibrium particle spectrum in lead. Such a transition might arise either as a result of the change in multiplicity of projected nucleons between air and lead or perhaps as a result of the presence, in the condensed material, of unstable particles capable of nuclear collisions which in air would decay before making further collisions.

ACKNOWLEDGMENTS

The authors are grateful to Professor P. M. S. Blackett for the opportunity of working under his direction and for his constant interest and encouragement. The content of this paper owes much to the continual help and stimulating discussion with Dr. J. G. Wilson to whom they are greatly indebted.

The authors' thanks are also due to Mr. J. A. Newth for his assistance and advice, to Professor A. von Muralt and Dr. R. Stämpfli for the facilities offered them at Jungfraujoch and to Mr. H. Wiederkehr for much assistance. They are also indebted to Professor P. Scherrer for facilities made available to them in his laboratories.

The work was supported by grants to Professor Blackett from the Royal Society and from the Nuffield Foundation.

REFERENCES

Broadbent, D., and Jánossy, L., 1947, *Proc. Roy. Soc.* A, **190,** 497.
Chao, C. Y., 1949, *Phys. Rev.*, **75,** 581.
George, E. P., and Jason, A. C., 1948, *Nature, Lond.*, **161,** 248.
Hamilton, J., Heitler, W., and Peng, H. W., 1943, *Phys. Rev.*, **64,** 78.
Jánossy, L., 1948, *Cosmic Rays* (Oxford : University Press), p. 94.
Jánossy, L., and Ingleby, P., 1940, *Nature, Lond.*, **145,** 511.
Rochester, G. D., and Butler, C. C., 1947, *Nature, Lond.*, **160,** 885; 1948 a, *Proc. Phys. Soc.*, **61,** 307; 1948 b, *Ibid.*, **61,** 535.
Rossi, B., 1948, *Rev. Mod. Phys.*, **20,** 537.
Tinlot, J., and Gregory, B., 1949, *Phys. Rev.*, **75,** 519.
Wataghin, G., de Souza Santos, M. D., and Pompeia, P. A., 1940, *Phys. Rev.*, **57,** 61, 339.
Wilson, J. G., 1938, *Proc. Roy. Soc.* A, **166,** 483.

On the Stresses and Energies associated with Inter-Crystalline Boundaries

By J. H. van der MERWE*
H. H. Wills Physical Laboratory, University of Bristol

Communicated by N. F. Mott; MS. received 13th June 1949, and in amended form 7th October 1949

ABSTRACT. Models, largely based on the assumptions introduced by Peierls and Nabarro in dealing with a single dislocation, are used in calculations on three types of intercrystalline boundaries, namely, (I) a boundary due to a difference of atomic spacing, (II) a twist boundary, and (III) a symmetrical tilt boundary. With these models the resolution of the boundary into a sequence of dislocations is a natural consequence of the analysis, which also yields the expressions for the stresses, atomic displacements and energies associated with the boundary, as functions of the angle of tilt, etc. By allowing the distance between dislocations to tend to infinity, these expressions reduce to the corresponding ones for single dislocations. The outstanding feature of the interfacial energy is that it increases initially very rapidly with the angle of tilt, etc. An application of the results to the theory of oriented overgrowths, developed by Frank and the present author, is described. The validity of the assumptions and approximations involved and the advantages of the treatment as compared with those of other writers are discussed.

§ 1. INTRODUCTION

For the solution of a number of problems in the physics of solids a knowledge of the energy associated with an interface of misfit between two similar or dissimilar crystals would be of considerable assistance. The purpose of the present paper is to calculate the stresses and energy associated with such a boundary. Three simple types of boundary are treated. These are:

I. A boundary at which the lattice spacing changes: e.g., that formed by two crystals of different lattice spacing in contact.

II. A twist boundary, i.e. the boundary between two halves of a crystal rotated with respect to each other about a common axis perpendicular to the boundary.

III. A tilt boundary, which occurs when two portions of the same crystal are symmetrically rotated with respect to each other about a common axis lying in the plane of the boundary.

---

* Now at National Physical Laboratory, Pretoria, South Africa.

Case III has been treated by Burgers (1939, 1940), who points out that the surface between two crystals can be treated as, and is geometrically equivalent to, a row of edge dislocations. In cases I and II the surface can similarly be treated by regarding it as a system of dislocations. This geometrical equivalence of a crystalline boundary and a system of dislocations has been discussed by various authors, namely, Taylor (1934), Bragg (1940), W. G. Burgers (1947), Shockley and Read (1949) and Frank (1950).

Burgers gives no detailed discussion of the singularity, i.e. the infinity, which occurs in the expression for the stress when the surrounding material is treated as a continuum, and he is thus prevented from making an estimate of the energy. Shockley and Read obtain an estimate of the energy by assuming that the energy associated with an element of volume at any point which is nearer to a dislocation than half the distance between dislocations does not vary with this distance, and that the strain energy outside these regions is negligible. Further, they do not calculate the energy associated with the region around the singularity.

We avoid these difficulties by an appropriate choice of the model, depending on two basic assumptions: (*a*) that, at the interface, the potential energy of an element of area of the one may be taken to be a sinusoidal function of its position relative to an element of area of the other; (*b*) that the material elsewhere may be treated as an elastic continuum which obeys Hooke's law.

The assumptions are essentially those used by Peierls (1940) and Nabarro 1947) in dealing with a single dislocation. By using them we introduce certain limitations and approximations. We shall represent the surface interaction by a single sinusoidal function for each of two rectangular position coordinates in the plane and thus restrict ourselves to cases in which the crystal surfaces in contact have square or rectangular symmetry. The magnitude of the error involved in adopting a single sinusoidal term instead of a Fourier series to represent the interaction energy in I and II has been discussed by Mackenzie (1950).

With this model the resolution of the boundary into a sequence of dislocations is a natural consequence of the analysis, and no singularities occur in the expressions for the stresses. The energy density at any point is found to vary with the angle of tilt or its equivalent in the other two cases.

I. BOUNDARY DUE TO DIFFERENCE OF ATOMIC SPACING

§2. THE MODEL

The first problem is to extend the Peierls–Nabarro model of a single dislocation in a perfect crystal to the case where the atomic spacing on one side of the slip plane is different from that on the other and a parallel sequence of dislocations exists in the slip plane.

Such a case is that which arises when two different crystal lattices meet at an interface, e.g. a metal and its adherent oxide film or in general a crystal overgrowth on a different substance.

The model used in the present analysis may be described as follows. Let A and B (Figure 1) be two semi-infinite crystals meeting in the surface S, which is perpendicular to the plane of the paper. The meshes in the atomic planes S_A and S_B adjacent to S are rectangular. Let d be the equilibrium distance between S_A and S_B. Cartesian coordinate axes are taken as shown in the figure, the y axis being perpendicular to the plane of the paper. At S the x spacings of

A and B atoms are different. Let these spacings be a and b respectively. Let the lattice be such that $Pb=(P+1)a=p$, where P is a positive integer. If the atoms C and D are in alignment, then E and F, at a distance p, will also be aligned, and so on. For simplicity, misfit in only one direction has been introduced. However, because the equations are linear to the degree of approximation used, solutions may be superposed and the following treatment easily extended to cover the case of misfit in both the x and y directions. This will be discussed in greater detail in § 6.

In order to express the boundary conditions in a simple manner, it is convenient to introduce a reference lattice L having an x-spacing c. The lattices A and B may be regarded as having been generated from L by a homogeneous compression of one half, in which the distance $(P+1)c$ becomes $(P+1)a=(P+\frac{1}{2})c$ and a homogeneous extension of the other half in which the distance Pc becomes $Pb=(P+\frac{1}{2})c$. The molecular forces are assumed to be zero during this hypothetical deformation and to act again on its completion. The algebraic difference of the final displacements with respect to the reference lattice of an atom in S_B and the nearest atom in S_A will be required. This relative displacement, which we denote by U, is seen to increase in every interval p by c. For example, if C and D remain in alignment throughout the deformation, the relative displacement between E and F is c.

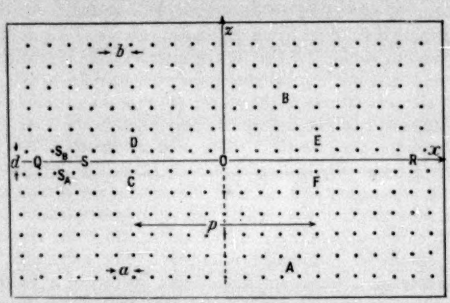

Figure 1. Interface between crystals A and B, having different atomic spacings. Dislocations are shown at Q, O, R.

The atoms in S_B are subjected to two forces: (i) the interaction with atoms in A, particularly those in S_A, which tend to bring the atoms in S_B into correct alignment with the nearest atoms in S_A, and (ii) the interaction with other atoms in B, which tend to keep them in their natural positions. In equilibrium the resultant of these two forces vanishes and the regions of misfit, for example the one at the y axis, are localized. The y axis is thus the axis of a dislocation. Since the dislocation lines extend throughout the crystal parallel to the y axis, the problem will be one of plane strain. The strains are furthermore periodic in x with a period equal to the distance p between dislocations. The lattices of A and B will be slightly distorted under the influence of the force (i), particularly in the neighbourhood of the dislocations. We denote the x and z components of the displacement of a point in the distorted lattice with respect to its position in the undistorted lattice by u and w respectively. If the radial extent of the strains associated with the dislocations is large compared with the interatomic distance, then both u and w will vary slowly from atom to atom. The relative displacement of neighbouring atoms in each half-crystal will then be much smaller than a (or b). (This assumption will be shown later to be reasonable.) In these circumstances each half-crystal may be treated as an elastic continuum. Moreover, for the sake of simplicity the continua will be assumed to be elastically isotropic and to have identical elastic moduli.

We assume that the x component of the force (i) on any particular atom depends only on its tangential separation from the nearest atom in the other slab, and that the z component is similarly a function of the z component of relative displacement only. The tangential forces acting on corresponding points of the opposed surfaces are therefore equal and opposite, in which case their z component of relative displacement is zero and the z component of (i) vanishes. This assumption neglects the change in the equilibrium value of their z component of separation where the atoms are out of alignment in the two planes.

It is convenient to express the x component of the force (i) as a function of U, and we note that it has the period c. We assume the function to be sinusoidal. This is equivalent to neglecting all but the first term of a Fourier series. Some aspects of this approximation have been discussed by Mackenzie (1950). If U varies slowly from atom to atom we may regard S_A and S_B as continuous and express the force in terms of a shear stress acting on S_B, namely,

$$p_{zx}(0,x)=(\mu_0/2\pi)\sin(2\pi U/c), \qquad \ldots\ldots(1)$$

where the constant μ_0 is of the order of magnitude of the shear modulus μ. If $d=c$ and the sine law is a sufficiently good approximation, μ_0 is equal to μ, in accordance with the treatment of Peierls and Nabarro.

§ 3. THE GOVERNING EQUATION AND ITS SOLUTION

The problem is now that of setting up the equation governing the equilibrium of the forces (i) and (ii). This problem, which according to § 2 involves plane strain, may be solved by expressing the stresses in terms of a stress function χ in the usual form (Timoshenko 1934):

$$p_{xx}=\frac{\partial^2\chi}{\partial z^2}, \qquad p_{zz}=\frac{\partial^2\chi}{\partial x^2}, \qquad p_{zx}=-\frac{\partial^2\chi}{\partial x\partial z}. \qquad \ldots\ldots(2)$$

Furthermore, in the case of plane strain, the strain components can be expressed in terms of the stress components by an equation

$$2\mu e_{xx}=(1-\sigma)p_{xx}-\sigma p_{zz}, \qquad \ldots\ldots(3)$$

where σ is Poisson's ratio and e_{xx} is the x component of strain.

χ must further satisfy the equation $\nabla^4\chi=0$. The general expression for a particular solution of this equation may be written in the form (Timoshenko 1934)

$$\chi=(B+zC)e^{\mp mz}{\cos \atop \sin}(mx), \qquad \ldots\ldots(4)$$

where m, B and C are constants. If we take into account that the stresses must vanish at $z=\mp\infty$ and that p_{zx} vanishes at $x=\pm\frac{1}{2}p$ on S_A and S_B, while p_{zz} vanishes everywhere on S_A and S_B in accordance with the assumptions in § 2, we may choose the following proper form of χ:

$$\chi=\zeta C\exp(\mp 2\pi n\zeta/p)\cos(2\pi nx/p), \qquad \ldots\ldots(5)$$

where *n* is a positive integer and where ζ is measured from S_A for A and S_B for B. The upper sign refers to B and the lower one to A. This sign convention will be used throughout. (Where the signs are equal one will be omitted.)

From (2) and (5) we now find

$$\left.\begin{aligned} p_{xx} &= \frac{2\pi n}{p}\left(\frac{2\pi n\zeta}{p} \mp 2\right)\exp\left(\mp\frac{2\pi n\zeta}{p}\right)C\cos\frac{2\pi nx}{p}, \\ p_{zz} &= -\frac{4\pi^2n^2}{p^2}\,\zeta\exp\left(\mp\frac{2\pi n\zeta}{p}\right)C\cos\frac{2\pi nx}{p} \\ \text{and}\qquad p_{zx} &= \frac{2\pi n}{p}\left(1 \mp \frac{2\pi n\zeta}{p}\right)\exp\left(\mp\frac{2\pi n\zeta}{p}\right)C\sin\frac{2\pi nx}{p}. \end{aligned}\right\} \quad \ldots\ldots (6)$$

On the planes S_A and S_B equations (6) reduce to

$$\left.\begin{aligned} p_{xx} &= \mp(4\pi n/p)C\cos(2\pi nx/p), \\ p_{zz} &= 0 \\ \text{and}\qquad p_{zx} &= (2\pi n/p)C\sin(2\pi nx/p). \end{aligned}\right\} \quad \ldots\ldots (7)$$

If we substitute (7) into (3) and carry out the integration, choosing the integration constant such that u is zero at $x = \pm\frac{1}{2}p$, we obtain

$$u = \mp\{(1-\sigma)/\mu\}C\sin(2\pi nx/p). \quad \ldots\ldots (8)$$

This is seen to be in accordance with the fact that the displacements must be equal and opposite, as follows from the assumptions of equal and opposite forces and identical elasticity. It is convenient to put

$$C = -\{\mu c(2\pi(1-\sigma)\}A_n/n, \quad \ldots\ldots (9)$$

where the constant A_n depends on n. Finally we may express the most general form of (8) in terms of the Fourier series

$$u = \pm\frac{c}{2\pi}\sum_{n=1}^{\infty}\frac{A_n}{n}\sin\frac{2\pi nx}{p}. \quad \ldots\ldots (10)$$

On using this we find

$$U = \tfrac{1}{2}c + \frac{cx}{p} + \frac{c}{\pi}\sum_{n=1}^{\infty}\frac{A_n}{n}\sin\frac{2\pi nx}{p}, \quad \ldots\ldots (11)$$

where U is taken to be zero at $x = -\frac{1}{2}p$. The first two terms in (10) represent the linear variation which exists when the lattices A and B are rectangular, i.e. before the force (i) is allowed to act. If we substitute (9) into (7) the general expression for the shear stress is seen to be

$$p_{zx}(0, x) = -\frac{\mu c}{p(1-\sigma)}\sum_{n=1}^{\infty}\mathrm{A}_n\sin\frac{2\pi nx}{p}. \quad \ldots\ldots (12)$$

The problem is now that of finding U from (1), (11) and (12). We put

$$\beta = \pi\mu c/p\mu_0(1-\sigma), \quad X = 2\pi x/p, \quad \psi = U/c, \quad \ldots\ldots (13)$$

in which case the differentiation of (11) and the combination of (1) and (12) respectively yield

$$\left.\begin{aligned} &\sum_{n=1}^{\infty} A_n \cos nX = \pi\left(\frac{d\psi}{dX} - \frac{1}{2\pi}\right) \\ \text{and}\qquad &\sum_{n=1}^{\infty} A_n \sin nX = -\frac{1}{2\beta}\sin 2\pi\psi. \end{aligned}\right\} \qquad \ldots\ldots(14)$$

If we represent the function conjugate to $f(X)$ by Conjugate$\{f(X)\}$ and make use of the fact that a function and its conjugate are respectively the real and imaginary parts of an analytic function of a complex variable, then it is seen that Conjugate$\{\cos mX\} = \sin mX$ and Conjugate$\{\sin mX\} = -\cos mX$. By using this we may finally write the governing equations (14) in the form

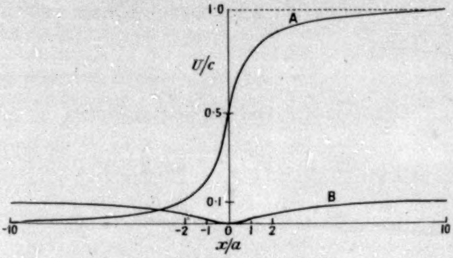

Figure 2.

Curve A. Relative displacement of an atom in S_B with respect to the nearest atom in S_A ($U/c = \psi$).
Curve B. Displacement of boundary perpendicular to itself (w/c). The curves are calculated for the case in which each dislocation is 20 atoms from the next ($p = 20a$). σ is taken to be 0·3 and μ_0 to be equal to μ.

$$2\pi\left(\frac{d\psi}{dX} - \frac{1}{2\pi}\right) = \text{Conjugate}\,\{\beta^{-1}\sin 2\pi\psi\}. \qquad \ldots\ldots(15)$$

This can be expressed as an integral equation (Hardy and Rogosinski 1944):

$$2\pi\left(\frac{d\psi(X)}{dX} - \frac{1}{2\pi}\right) = -\frac{1}{2\pi\beta}\int_0^{\pi}\{\sin 2\pi\psi(X+t) - \sin 2\pi\psi(X-t)\}\cot\tfrac{1}{2}t\,dt. \qquad \ldots\ldots(16)$$

A method of iteration yielded the solution of this equation as a power series in $1/\beta$. The sum-function

$$\psi = \tfrac{1}{2} + (1/\pi)\arctan\{[(1+\beta^{-2})^{\frac{1}{2}} + \beta^{-1}]\tan\tfrac{1}{2}X\} \qquad \ldots\ldots(17)$$

of this series is defined for all values of β, whereas the series converges only for a limited range of the variable. A graph of $\psi(x)$ is shown in Figure 2. Differentiation of (17) gives

$$d\psi/dX = (1/2\pi)\{(1+\beta^{-2})^{\frac{1}{2}} - \beta^{-1}\cos X\}^{-1}. \qquad \ldots\ldots(18)$$

This solution can be verified by substituting (17) and (18) into (15). We find, as we should, that $\beta^{-1}\sin 2\pi\psi$ and $2\pi(d\psi/dX-1/2\pi)$ are respectively the real and imaginary parts of an analytic function of a complex variable. This function is

$$-2i\{1-[(1+\beta^2)^{\frac{1}{2}}-\beta]e^{iX}\}^{-1}. \qquad \ldots\ldots(19)$$

The Fourier coefficients A_n can now be obtained by expanding (19) into a Fourier series and comparing the coefficients of its imaginary part with those of $2\pi(d\psi/dX-1/2\pi)$ in (14). We find

$$A_n=\{(1+\beta^2)^{\frac{1}{2}}-\beta\}^n=A^n \quad \text{(say)}. \qquad \ldots\ldots(20)$$

§4. STRESSES AND DISPLACEMENTS

If we use the notation

$$X=2\pi x/p \quad \text{and} \quad Z=2\pi\zeta/p \qquad \ldots\ldots(21)$$

and substitute (9) and (20) into (5) and (6), we may deduce

$$\left.\begin{aligned}
\chi&=\frac{\mu cpZ}{4\pi^2(1-\sigma)}\sum_{n=1}^{\infty}\frac{A^n}{n}e^{\mp nZ}\cos nX,\\
p_{xx}&=-\frac{\mu c}{p(1-\sigma)}\sum_{n=1}^{\infty}\mathrm{A}^n(nZ\mp 2)e^{\mp nZ}\cos nX,\\
p_{zz}&=\frac{\mu cZ}{p(1-\sigma)}\sum_{n=1}^{\infty}nA^n e^{\mp nZ}\cos nX\\
\text{and}\qquad p_{zx}&=-\frac{\mu c}{p(1-\sigma)}\sum_{n=1}^{\infty}A^n(1\mp nZ)e^{\mp nZ}\sin nX.
\end{aligned}\right\} \qquad \ldots\ldots(22)$$

These Fourier forms of the stresses are useful in calculating the displacements and the strain energies in each half-crystal.

The expressions for the sums of these series are also useful. The sum for χ can be written down from the sum of the complex series of which χ is the real part. The other sums concerned are easily treated by differentiation of this series. The expression for the stresses may, of course, also be determined from χ by differentiation according to (2). We find

$$\left.\begin{aligned}
\chi&=\{\mu cp/4\pi^2(1-\sigma)\}Z\ln R,\\
p_{xx}&=-Q\{Z[(1+A^2e^{\mp 2Z})\cos X-2Ae^{\mp Z}]\mp 2R^2(\cos X-Ae^{\mp Z})\},\\
p_{zz}&=QZ\{(1+A^2e^{\mp 2Z})\cos X-2Ae^{\mp Z}\},\\
\text{and}\qquad p_{zx}&=-Q\sin X\{R^2\mp Z(1-A^2e^{\mp 2Z})\},
\end{aligned}\right\} \qquad \ldots\ldots(23)$$

where $Q=\mu cAe^{\mp Z}/(1-\sigma)pR^4$ and $R^2=1+A^2e^{\mp 2Z}-2Ae^{\mp Z}\cos X$.

The displacements u and w can be determined by using (3) and the analogous expression for e_{zz}. The integration of (3), for example, gives

$$2\mu u=(1-\sigma)\int p_{xx}\,dx-\sigma\int p_{zz}\,dx+\text{const.}$$

The integrals in this and the analogous equation for w are most easily obtained by using (22). If we sum the integrated series we find

$$\left.\begin{aligned} u &= \pm\frac{c}{2\pi}\arctan\left\{\frac{Ae^{\mp Z}\sin X}{1-Ae^{\mp Z}\cos X}\right\} - \frac{cZe^{\mp Z}\sin X}{4\pi(1-\sigma)R^2} \\ \text{and}\qquad w &= \frac{(1-2\sigma)c}{4\pi(1-\sigma)}\ln\left(\frac{R}{1-A}\right) \mp \frac{cZAe^{\mp Z}(\cos X - Ae^{\mp Z})}{4\pi(1-\sigma)R^2}, \end{aligned}\right\} \quad \ldots\ldots (24)$$

where the integration constants are chosen such that both u and w vanish at the dislocation line.

The graph of

$$w(x)/c = \frac{(1-2\sigma)}{8\pi(1-\sigma)}\ln\left\{\frac{1+A^2-2A\cos(2\pi x/p)}{(1-A)^2}\right\}$$

shown in Figure 2 is of particular interest as it describes the shape of the boundary.

An interesting feature of the present treatment is that it provides another method of deriving the stresses and displacements associated with a single Peierls–Nabarro dislocation. This is done by expanding the radicals, and the exponential and sinusoidal functions contained in (17), (23) and (24) as Taylor series and taking the limits of the resulting expressions as p tends to infinity. We find

$$\left.\begin{aligned} \psi &= \tfrac{1}{2} + (1/\pi)\arctan(x/\zeta_0), \\ u &= \frac{a}{2\pi}\left\{\arctan\left(\frac{x}{\zeta\pm\zeta_0}\right) - \frac{x\zeta}{2(1-\sigma)r^2}\right\}, \\ w &= \frac{a}{2\pi}\left\{\frac{1-2\sigma}{2(1-\sigma)}\ln\left(\frac{r}{\zeta_0}\right) - \frac{\zeta(\zeta\pm\zeta_0)}{2(1-\sigma)r^2}\right\}, \\ p_{xx} &= q\{2r^2(\zeta\pm\zeta_0) - \zeta[(\zeta\pm\zeta_0)^2 - x^2]\}, \\ p_{zz} &= q\zeta\{(\zeta\pm\zeta_0)^2 - x^2\} \\ \text{and}\qquad p_{zx} &= qx\{r^2 - 2\zeta(\zeta\pm\zeta_0)\}, \end{aligned}\right\} \quad \ldots\ldots (25)$$

where $q = \mu a/2\pi(1-\sigma)r^4$, $r^2 = x^2 + (\zeta\pm\zeta_0)^2$, $\zeta_0 = a\mu/\mu_0 2(1-\sigma)$ and $a = b = c$.

Leibfried and Lücke (1949), who have also treated the Peierls–Nabarro case in which $\mu_0 = \mu$, discuss in detail the relation between its solution and the pure elastic solution.

§ 5. THE INTERFACIAL ENERGY

The energy associated with the boundary between the two half-crystals consists of two parts, namely, the strain energy in each half-crystal and the potential energy of attraction due to the sinusoidal force at the interface. The mean total energy per unit area of the interface is called the interfacial energy and denoted by τ.

The total strain energy residing in a slab extending a distance p in the x direction, unit distance in the y direction and to infinity in the positive and negative z directions is given by

$$E_e = 4\int_0^\infty\int_0^{\frac{1}{2}p}\frac{1}{4\mu}\{(1-\sigma)(p_{xx}^2 + p_{zz}^2) - 2\sigma p_{xx}p_{zz} + 2p_{zx}^2\}\,dx\,d\zeta,$$

where, as we are dealing with plane strain, the integrand is the strain energy per unit volume in each half-crystal (Timoshenko 1934). The integral is easily evaluated by using the series (24). We find

$$E_e = \frac{\mu c^2}{4\pi(1-\sigma)} \sum_{n=1}^{\infty} \frac{A^{2n}}{n} = -\frac{\mu c^2}{4\pi(1-\sigma)} \ln\{2\beta(1+\beta^2)^{\frac{1}{2}} - 2\beta^2\}. \quad \ldots\ldots (26)$$

The energy of attraction per unit area of the interface follows from (1),

$$\int_0^U p_{zx}(0,x)\, dU = \frac{\mu_0 c}{4\pi^2}\left(1 - \cos\frac{2\pi U}{c}\right).$$

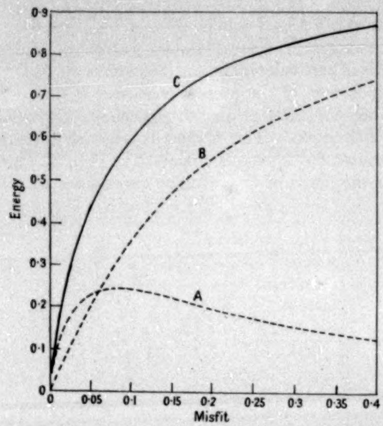

Figure 3. Interfacial energy as a function of misfit (c/p) between the two surfaces in contact (misfit in one direction only). Energy in units of $\mu c/4\pi^2$ per unit area, where c is the lattice parameter, μ the rigidity modulus of the bulk material and p the distance between dislocations.

Curve A. The elastic energy of the two half-crystals (E_e/p).
Curve B. Energy resulting from sinusoidal force at interface (E_a/p).
Curve C. Total energy of interface $\{\tau = (E_e + E_a)/p\}$.

The total energy of attraction connected with the interface of the slab considered above is therefore

$$E_a = \frac{\mu_0 c}{4\pi^2} \int_{-\frac{1}{2}p}^{\frac{1}{2}p} (1 - \cos 2\pi\psi)\, dx.$$

If we substitute (17) in this integral and carry out the integration, we find

$$E_a = (\mu_0 c p/4\pi^2)\{1 + \beta - (1+\beta^2)^{\frac{1}{2}}\}. \quad \ldots\ldots (27)$$

The interfacial energy may now be written as

$$\tau = (\mu_0 c/4\pi^2)\{1 + \beta - (1+\beta^2)^{\frac{1}{2}} - \beta \ln[2\beta(1+\beta^2)^{\frac{1}{2}} - 2\beta^2]\}, \quad \ldots\ldots (28)$$

the logarithmic term being E_e/p and the remaining part E_a/p. The graph of $\tau(c/p)$ in Figure 3 shows that τ increases initially very rapidly with the density of dislocations c/p.

§ 6. A CROSS GRID OF DISLOCATIONS

We still have to show that the preceding treatment also covers the case in which there is in addition a difference of spacing in the y direction, as will usually be the case. There is then an additional sequence of dislocations parallel to the x axis and associated with it a force analogous to (i) in § 2. We take a term of the form (1) to represent the force acting parallel to each axis. This is equivalent to neglecting all but the first two terms of a surface Fourier series, each being a function of one coordinate only. Even when the sinusoidal approximation is not a good one, the resulting error in the interfacial energy will be small as long as the distance between dislocations is large compared with the interatomic distance, for then only a small proportion of the atoms at the interface are in bad alignment, i.e. outside the regions where the sinusoidal law approximates to Hooke's law.

To the degree of approximation of the sinusoidal law we may take U and V to be of the forms $U(x)$ and $V(y)$, in which case u and v must also be of the forms $u(x, z)$ and $v(y, z)$, and hence w of the form $w = w_1(x, z) + w_2(y, z)$, where V and v are analogous to U and u but refer to the y direction. That w has this form can easily be shown by substitution in the differential equations for u, v, and w. To the degree of approximation used, the equations are therefore linear, which allows the superposition of solutions and the addition of the energies associated with the two sequences of dislocations.

II. BOUNDARY DUE TO TWIST

§ 7. THE MODEL

The second problem is that of finding the stresses and energies associated with a twist boundary, i.e. the plane boundary between the halves of a crystal which are rigidly rotated with respect to each other about a common axis perpendicular to the boundary.

The model used in treating this problem may be described as follows. Let a perfect crystal be cut along a plane S which is midway between the adjacent atomic planes S_A and S_B of the half-crystals A and B respectively. Let the meshes of S_A and S_B have square symmetry, the side of an elementary square being a. Cartesian coordinate axes are chosen in such a way that the plane $z = 0$ is coincident with S and that the x and y axes are parallel to atomic rows in S_A (and hence in S_B). For convenience we call these rows the x and the y rows respectively. Let B be twisted rigidly through an angle $\frac{1}{2}\theta$ in one sense and A through $\frac{1}{2}\theta$ in the opposite sense. A force, analogous to force (i) of § 2, now comes into play and is balanced by a force analogous to (ii). If we do not allow force (i) to act, the meshes of S_A and S_B will remain square as indicated by the dots and crosses in Figure 4 (*a*), which represent the atomic positions in S_A and S_B respectively. Let S be the plane of the paper, S_A being below and S_B above. If we now allow the force (i) to act, it causes a distortion which is particularly marked in the meshes of S_A and S_B but also extends some distance into A and B. The new atomic positions in S_A and S_B are as indicated by the circles and plus signs respectively. We may now define u, v and w as in § 2. We further define the x component of relative displacement of two atoms in S_B and S_A which were in alignment when θ was zero to be the algebraic difference of their x components of displacement from the aligned position and denote it by U. We may similarly define V as the y component of relative displacement. The distortion gives rise to a state of affairs analogous to that existing at the boundary with a difference of spacing in the two directions as in I. The dislocations are, however, now of the screw type introduced by Burgers (1939). We note that the distance between dislocations is

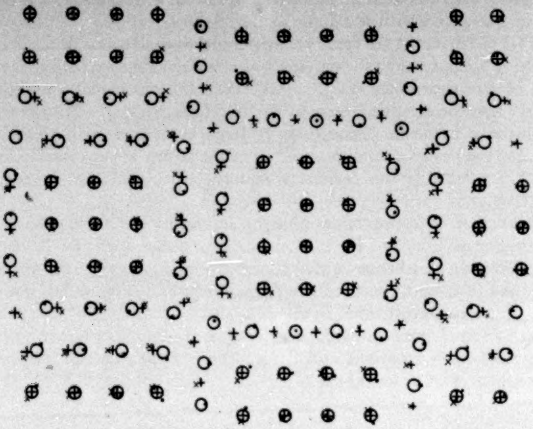

Figure 4(a). Diagram of the atomic configurations on either side of a twist boundary. The dots, circles, crosses and plus signs represent atomic positions. The dots are the positions on one side of the boundary and the crosses the positions on the other side before relaxation. During relaxation the dots and crosses become the nearest circles and plus signs respectively. The two perpendicular sequences of dislocations are most easily distinguished by viewing the figure at grazing angle.

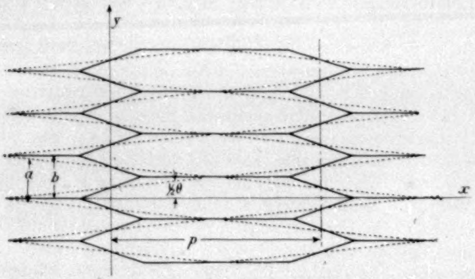

Figure 4 (b). Diagram showing only the sequence of dislocations which is parallel to the y axis. The broken and full lines represent the atomic rows on either side of the twist boundary, before and after relaxation respectively.

$$p = \tfrac{1}{2} a \operatorname{cosec} \tfrac{1}{2}\theta, \qquad \ldots\ldots (29)$$

that V (or U) increases in every interval p along the x axis (or y axis) by

$$b = a \sec \tfrac{1}{2}\theta, \qquad \ldots\ldots (30)$$

and that, as in I, the state of strain of A and B is periodic in x and y with period p.

It may be shown, by an argument similar to that of § 6, that the equations which we use to solve this problem are linear to the degree of approximation used and therefore allow superposition of the solutions corresponding to the two sequences of dislocations. It is therefore only necessary to treat one sequence, say the sequence parallel to the y axis, and for this purpose we fix our attention on the atomic rows which were originally parallel to the x axis, the corresponding picture being that of Figure 4 (*b*). As we are considering only one sequence of dislocations, we take u and U to be zero and V to be a function of x only. Further, v must vanish at points far from the interface, i.e. at $z = \pm\infty$. Since we are concerned with screw dislocations, we may also take w to be zero. This approximation, like that of § 2, whereby the z component of relative displacement vanishes, also neglects the change in the equilibrium value of the z component of separation where the atoms in S_A and S_B are out of alignment and consequently the corresponding term in the interfacial energy. The z component of the force (i) is therefore assumed to vanish. We treat A and B as elastic isotropic continua, the conditions for the validity of this being the same as before. We must also assume that the overall amplitude of the potential energy of an atom in S_B (or S_A) with respect to the atoms in S_A (or S_B) is independent of the angle of twist. In the continuum approximation, this implies that the overall amplitude of the surface density of potential energy at a point in S_B (or S_A) with respect to S_A (or S_B) is independent of θ. If we further adopt the assumptions of § 2 relating to the force (i), we may express (i) in terms of the shear stress,

$$p_{zy}(0, x) = (\bar{\mu}/2\pi)\sin(2\pi V/b), \qquad \ldots\ldots (31)$$

where

$$\bar{\mu} = \mu_0 \cos \tfrac{1}{2}\theta. \qquad \ldots\ldots (32)$$

Equation (32) is the condition for the overall amplitude $\bar{\mu}b/2\pi^2$ of the potential energy density, as obtained from (31), to be independent of θ.

§ 8. THE GOVERNING EQUATION AND ITS SOLUTION

The next step in the solution of this problem is to set up the equation governing the equilibrium of the forces (i) and (ii). To do this we require expressions for the displacements and stresses which we obtain by solving the differential equations for the displacements in the elastic continua. In our problem u and w are zero, and so these equations (Timoshenko 1934) reduce to Laplace's equation in two dimensions, namely $\partial^2 v/\partial x^2 + \partial^2 v/\partial z^2 = 0$. The appropriate solution must vanish at $z = \pm\infty$ and on S_A (and S_B) at $x = \pm\frac{1}{2}p$, and must have equal and opposite values at opposite points on S_A and S_B.

The most general solution satisfying these conditions may be expressed as a Fourier series:

$$v = \pm\frac{b}{2\pi}\sum_{n=1}^{\infty}\frac{A_n}{n}e^{\mp nZ}\sin nX, \qquad \ldots\ldots (33)$$

where X, Z (and ζ) and the sign convention are the same as before. We find by differentiation

$$p_{zy} = \mu\frac{\partial v}{\partial z} = -\frac{\mu b}{p}\sum_{n=1}^{\infty}A_n e^{\mp nZ}\sin nX,$$

and

$$p_{xy} = \mu\frac{\partial v}{\partial x} = \pm\frac{\mu b}{p}\sum_{n=1}^{\infty}A_n e^{\mp nZ}\cos nX. \qquad \ldots\ldots (34)$$

On S_A and S_B v and p_{zy} reduce to

$$v = \pm \frac{b}{2\pi} \sum_{n=1}^{\infty} \frac{A_n}{n} \sin nX \qquad \ldots\ldots(35\,a)$$

and

$$p_{zy} = -\frac{\mu b}{p} \sum_{n=1}^{\infty} A_n \sin nX. \qquad \ldots\ldots(35\,b)$$

Using (35 *a*), we may construct

$$V = \tfrac{1}{2}b + \frac{bX}{2\pi} + \frac{b}{\pi} \sum_{n=1}^{\infty} \frac{A_n}{n} \sin nX, \qquad \ldots\ldots(36)$$

the zero of V being taken at $x = -\tfrac{1}{2}p$ and the first two terms having the same significance as in (11).

The problem is now that of finding V from equations (31), (35 *b*) and (36). These equations are seen to be of the same forms as (1), (12) and (11) respectively, and the solution is, therefore,

$$V = \tfrac{1}{2}b + (b/\pi) \arctan \{[(1+\beta^{-2})^{\frac{1}{2}} + \beta^{-1}] \tan \tfrac{1}{2}X\}. \qquad \ldots\ldots(37)$$

The parameter β and the Fourier coefficient A_n are similarly seen to be

$$\left.\begin{aligned} \beta &= \pi u b/\bar{\mu} p = 2\pi\mu\mu_0^{-1} \tan \tfrac{1}{2}\theta \sec \tfrac{1}{2}\theta \\ \text{and} \qquad A_n &= \{(1+\beta^2)^{\frac{1}{2}} - \beta\}^n = A^n \ \text{(say).} \end{aligned}\right\} \qquad \ldots\ldots(38)$$

We may likewise determine the sums of the series in equations (33) and (34). We find

$$\left.\begin{aligned} v &= \pm \frac{b}{2\pi} \arctan \left\{ \frac{Ae^{\mp Z} \sin X}{1 - Ae^{\mp Z} \cos X} \right\}, \\ p_{zy} &= -(\mu b A/pR^2) e^{\mp Z} \sin X \\ \text{and} \qquad p_{xy} &= \pm(\mu b A/pR^2) e^{\mp Z} \{\cos X - Ae^{\mp Z}\}, \end{aligned}\right\} \qquad \ldots\ldots(39)$$

where

$$R^2 = 1 + A^2 e^{\mp 2Z} - 2Ae^{\mp Z} \cos X.$$

The expressions for the stresses and displacements associated with a single screw dislocation may be deduced by the method described in § 3. They are found to be

$$\left.\begin{aligned} V &= \tfrac{1}{2}a + (a/\pi) \arctan (x/\zeta_0), \\ v &= (a/2\pi) \arctan \{x/(\zeta \pm \zeta_0)\}, \\ p_{zy} &= -(\mu a/2\pi) x/r^2 \\ \text{and} \qquad p_{xy} &= (\mu a/2\pi)(\zeta \pm \zeta_0)/r^2, \end{aligned}\right\} \qquad \ldots\ldots(40)$$

where

$$r^2 = x^2 + (\zeta \pm \zeta_0)^2 \quad \text{and} \quad \zeta_0 = \tfrac{1}{2}a\mu\mu_0^{-1}.$$

§ 9. THE INTERFACIAL ENERGY

The interfacial energy τ again consists of two parts as in § 5. These may be calculated in the same way as before except that the strain energy density is now given by $V_0 = (p_{zy}^2 + p_{xy}^2)/4\mu$. We must take the second sequence of dislocations into account. This is a simple matter as the energies associated with the two sequences are additive to the degree of approximation used. We find

$$\tau = (\mu_0 a/2\pi^2)\{1 + \beta - (1+\beta^2)^{\frac{1}{2}} - \beta \ln [2\beta(1+\beta^2)^{\frac{1}{2}} - 2\beta^2]\} \ldots\ldots(41)$$

A graph of $\tau(\theta)$ is shown in Figure 5, curve C.

Expression (41) reveals a shortcoming of the treatment, namely, that the interfacial energy does not come back to zero when θ becomes $\pi/2$, as it should on account of the square symmetry of the meshes in S_A and S_B. Instead it tends to a value $\mu_0 a/2\pi^2$, which will be the value of the potential energy density when the meshes in S_B and S_A remain undistorted. At $\theta=\pi/4$, τ is somewhat less than $\mu_0 a/2\pi^2$. A value of this order of magnitude is to be expected, for the average frequency with which the force (i) changes sign is now approximately the reciprocal of the interatomic distance, and the departure of the meshes from their undistorted forms will therefore be small. We may therefore take the formula (41) to be a good approximation when θ is less than $\pi/4$, and to be particularly good when θ is small.

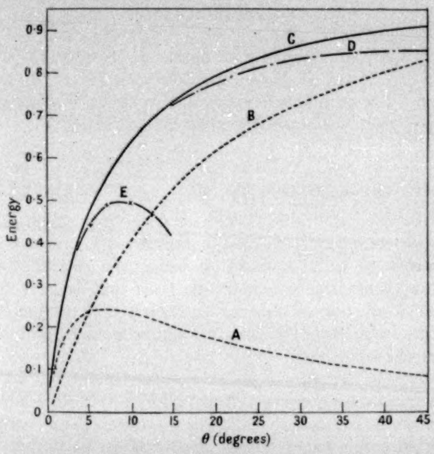

Figure 5. Interfacial energy as a function of the angle θ through which the two faces in contact are twisted with respect to each other. Energy in units of $\mu a/2\pi^2$ per unit area, where μ is the rigidity modulus and a the lattice parameter. (The curves are calculated for $\mu_0=\bar{\mu}$.)

Curve A. Elastic energy in the half-crystals (E_e/p).
Curve B. Energy resulting from sinusoidal force at misfitting interface (E_a/p).
Curve C. Total energy of interface $\{\tau=(E_e+E_a)/p\}$: (41).
Curve D. Total energy according to the symmetrical formula (42).
Curve E. Total energy according to the approximate formula (43).

The fact that τ does not return to zero at $\pi/2$ is due to the approximation involved in expressing the force (i) in the form (31). This approximation implies that we treat the atomic rows in S_A and S_B as though they were continuous (see Figure 4(*b*)) and the force between them as though it acted only between a point in a row of S_B and the nearest point in a row of S_A, and then only if the two rows were parallel when θ was zero. Furthermore, the interaction may be described as a tendency to keep these points as close as possible to the zx plane (or zy plane) through the nearest point of complete alignment. The approximation is a good one when θ is small. The interaction between rows which were initially perpendicular, though negligible when θ is small, becomes greater than the interaction between the rows which were initially parallel as soon as θ exceeds $\pi/4$. As a first approximation we take the interaction energy between a row in S_B and the two sets of rows in S_A to be additive and construct the symmetrical formula

$$\tau_s = \tau(\theta) + \tau(\tfrac{1}{2}\pi - \theta) - \tau(\tfrac{1}{2}\pi) \qquad \ldots\ldots (42)$$

for the interfacial energy. This gives a zero value at both $\theta = 0$ and $\theta = \pi/2$. The graph of $\tau_s(\theta)$ in Figure 5 (curve D) is seen to differ only slightly from the graph of $\tau(\theta)$ (curve C).

The equivalent assumptions to those used by Shockley and Read (1949) in deriving equation (55)—see § 13 below—will lead in the case of a twist boundary to the formula

$$\tau = (\mu a/2\pi)\theta(C - \ln\theta). \qquad \ldots\ldots (43)$$

Equation (43), like (55), is intended to be a good approximation when θ is small; we may therefore evaluate C by comparison with (41). It is found to be $C = \ln(e\mu_0/\mu 2\pi)$. The corresponding curve E is shown in Figure 5, and is seen to depart seriously from our curve for values of θ exceeding 5°.

§10. AN APPLICATION TO ORIENTED OVERGROWTH

Frank and the present author (1949) have developed a theory which explains the formation of completely oriented overgrowths on crystalline substrates when the difference in lattice spacing is smaller than a certain critical value. According to this theory, the first molecular layer that deposits deforms homogeneously in such a way that its atoms are in the potential troughs of the substrate field. The second monolayer deforms in a similar manner, and so on, to form a completely oriented overgrowth.

However, when the overgrowth attains a certain thickness it becomes unstable because of the increased strain energy. This energy may be released by the breaking away of the deposited film from the substrate. If there is no change of structure by recrystallization at this stage, the new state of affairs being that described in I, then, provided the overgrowth does not swing round, the initial orientation will be maintained. The considerations of this paper may be used to show that if we assume the thick overgrowth has the same symmetry properties as its first molecular layer with respect to rotations about the normal to the contact plane, then it at least cannot swing round freely, since this is certainly accompanied by an increase in the energy. That this is so may be deduced as follows: the maximum value which the interfacial energy can attain in a rotation is probably not less than the maximum interfacial energy τ_m in a pure twist boundary (Figure 5). The maximum increase in energy during a rotation is therefore probably not less than $\tau_m - \tau_1$, where τ_1 is the interfacial energy when the deposit has broken away from the substrate. Since the maximum value of τ in I is less than in II, $\tau_m - \tau_1$ is always positive. The magnitude of τ_1 depends on the density of dislocations, i.e. on the degree of misfit. Since the degree of misfit with which we are concerned is small—less than the critical value of 9% to 14% below which the initial layer is oriented—τ_1 is small, and the increase in energy $\tau_m - \tau_1$ is therefore large.

III. BOUNDARY DUE TO TILT

§ 11. THE MODEL

The third problem is that of finding the stresses and energies associated with a symmetrical tilt boundary, i.e. the boundary between the halves of a crystal which are symmetrically rotated with respect to each other about a common axis in the boundary.

Consider the case in which the undisturbed crystal lattice is of simple rectangular structure, the lattice parameters being a_1, a_2 and a_3, and in which the axis of tilt is parallel to a crystal axis (corresponding parameter a_1 say), the planes (a_1, a_2) of the two portions making angles $\frac{1}{2}\theta$ with the boundary. We restrict ourselves to the case $a_2 = a_3 (= a)$, a_1 being unrestricted; the extension to the case in which a_2 and a_3 are different is quite simple. Let the boundary be the xy plane of a Cartesian coordinate system, the y axis being the axis of rotation. We denote the half-crystals by A and B. As in I and II, two forces, which we may call (i) and (ii), act on A and B. The force (ii) may be defined as in §2, but the force (i) now acts essentially perpendicular to the boundary. The effect of the forces is again to reproduce a configuration which may be described

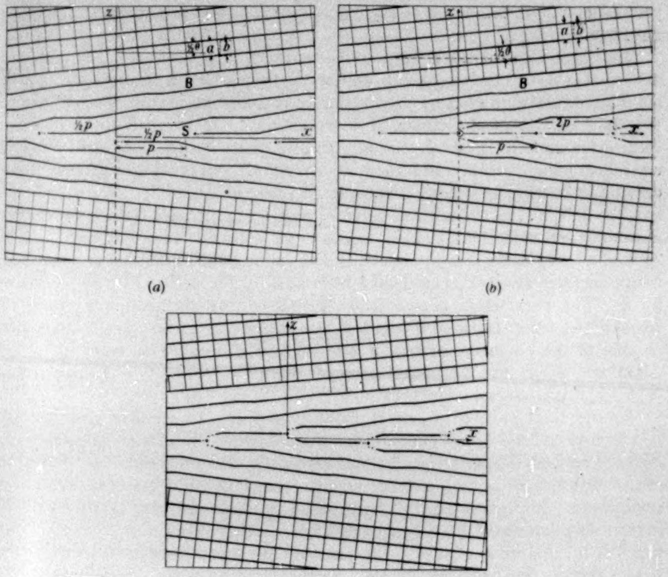

(a) (b)

(c)

Figure 6. Diagram showing three possible configurations of tilt boundaries.

as a sequence of dislocations, the dislocation lines being along the edges of the atomic planes terminating in the boundary. Three possible configurations are shown in Figures 6 (*a*), (*b*) and (*c*).

The form 6 (*a*) is the one shown in Burgers' diagram (1939); 6 (*b*) and 6 (*c*) are alternative forms suggested by F. C. Frank (private communication). The form (*b*) contains dislocations in their two possible symmetrical positions and (*a*) and (*c*) each contains dislocations in only one of the possible positions. Since by using (*b*) we obtain a precisely planar boundary, this should be a configuration of lower energy than (*a*) or (*c*) if the energies of the dislocations in their two possible positions are equal, as appears from the calculations of Nabarro (1947). The latter result is presumably a consequence of the approximations used. If the energies in these two positions differ, the configuration of lowest energy may well depend on θ, being that of Figure 6 (*a*) or (*c*) when θ is small, and (*b*) when θ is large.

We define a conventional normal displacement W as follows. The deformed half-crystals A and B, lying below and above the surface S respectively, may be considered to define systems of curvilinear coordinates in the two half-spaces. Standard mathematical methods of interpolation could be used, firstly to define continuous surfaces passing through all the atom centres on each principal crystallographic 'plane', and then to define all intervening surfaces of the curvilinear coordinate system. In these coordinate systems let $Z_A^1 = 0, 1, 2 \ldots.$ and $Z_B^1 = 0, 1, 2 \ldots.$ denote those surfaces which, at a distance from the boundary S become atomic planes making angles $\pm \frac{1}{2}\theta$ with S. Now, in each interval $2p$ of x, where p is the distance between dislocations, the separation of continuous lattice surfaces across the boundary increases by $2b$, while $Z_A^1 + Z_B^1$ decreases by 2. The parameters p and b are given by the formulae (29) and (30) respectively. Let surfaces S_A and S_B be described in the two half-crystals, parallel to the boundary surface S and each at a distance $\frac{1}{2}b$ from it. Let $Z_A^1(x)$ and $Z_B^1(x)$ be the coordinates of points in these two surfaces, then $W = -b\{Z_A^1(x) + Z_B^1(x)\}$.

Between each successive pair of dislocations there is a value of x, which may be taken to be half-way between them and for which W/b is an integer. The distance between atoms in the two half-crystals is there the same as it would be in the undeformed crystal, and the normal force (i) should therefore be zero at such points: it changes sign at these points, and should vary linearly with W in their neighbourhood. It changes sign again at each dislocation, corresponding to a half-integral value of W/b. We assume the normal force to be proportional to $\sin(2\pi W/b)$, this being the simplest function which has the desired properties; our knowledge of the inter-atomic forces is insufficient to justify use of any more elaborate function. We accordingly replace the half-crystals above S_B and below S_A by Hookian isotropic elastic continua which have suffered small displacements at these surfaces. The accompanying tangential displacements (and corresponding forces), excluding those which are a consequence of the normal force, are disregarded. The error thus introduced is only serious when θ is large: an approximate way of compensating for it is indicated below (§ 13). We also adopt the assumption that the overall amplitude of the surface potential energy density is independent of θ.

As before, we express the sinusoidal force (i) in terms of a stress $p_{zz}(0, x)$. We fix the amplitude of the sine-function such that this function approximates to Hooke's law in the linear region half-way between dislocations. We further make use of the fact that p_{xx} and p_{zz} are equal at S where p_{zx} vanishes according to our assumptions and of the equation for e_{zz} which is analogous to (3). We find

$$p_{zz}(0,x)=\{\bar{\mu}/\pi(1-2\sigma)\}\sin(2\pi W/b), \qquad \ldots\ldots(44)$$

where $\bar{\mu}$ is given by equation (32). Certain aspects of the sinusoidal approximation are discussed in § 14.

§ 12. THE GOVERNING EQUATION AND ITS SOLUTION

The next steps in the solution of this problem are very much the same as those in I. The proper stress function must now be chosen from (4) in accordance with the assumptions of § 11, i.e. in such a way that the stresses vanish at $z=\pm\infty$, that p_{zx} vanishes at S, that w vanishes at S where $x=\pm\frac{1}{2}p$, and that w has equal and opposite values at opposite points on S_A and S_B. The most general form of the stress function can be expressed as a Fourier series. If we use a convenient form for the Fourier coefficients, the nth term of the series is of the form

$$\chi_n=\frac{\mu p b}{4\pi^2(1-\sigma)}\frac{A_n}{n^2}(1\pm nZ)e^{\mp nZ}\sin nX, \qquad \ldots\ldots(45)$$

where X, Z (and ζ) and the sign convention are the same as before. By differentiation according to (2) we find

$$\left.\begin{aligned} p_{xx}&=-\frac{\mu b}{p(1-\sigma)}A_n(1\mp nZ)e^{\mp nZ}\sin nX,\\ p_{zz}&=-\frac{\mu b}{p(1-\sigma)}A_n(1\pm nZ)e^{\mp nZ}\sin nX\\ \text{and}\qquad p_{zx}&=\frac{\mu b}{p(1-\sigma)}A_n nZe^{\mp nZ}\cos nX.\end{aligned}\right\} \qquad \ldots\ldots(46)$$

If we now substitute from (45) into the equation analogous to (3), integrate with respect to ζ, let ζ tend to zero and choose the integration constant such that $w(x)$ vanishes at $x=\pm\frac{1}{2}p$, we find

$$w(x)=\pm(bA_n/2\pi n)\sin nX. \qquad \ldots\ldots(47)$$

By using this we may now construct

$$W=\tfrac{1}{2}b+\frac{bX}{2\pi}+\frac{b}{\pi}\sum_{n=1}^{\infty}\frac{A_n}{n}\sin nX, \qquad \ldots\ldots(48)$$

where the different terms have the same significance as before. From (45) we may also write down the Fourier representation of (44), namely

$$p_{zz}(0,x)=-\frac{\mu b}{p(1-\sigma)}\sum_{n=1}^{\infty}A_n\sin nX. \qquad \ldots\ldots(49)$$

We must solve equations (44), (48) and (49). These are of the same forms as before and the solution is, therefore,

$$W=\tfrac{1}{2}b+(b/\pi)\arctan\{[(1+\beta^{-2})^{\frac{1}{2}}+\beta^{-1}]\tan\tfrac{1}{2}X\}. \qquad \ldots\ldots(50)$$

The parameter β and the Fourier coefficient A_n are similarly seen to be

$$\left.\begin{aligned}&\beta=\pi\mu(1-2\sigma)\tan\tfrac{1}{2}\theta\sec\tfrac{1}{2}\theta/\mu_0(1-\sigma)\\ \text{and}\qquad &A_n=\{(1+\beta^2)^{\frac{1}{2}}-\beta\}^n=A^n\quad\text{(say).}\end{aligned}\right\}\quad\ldots\ldots(51)$$

The nth terms of the Fourier series representing the stresses are given in (46). The displacements and the sums of these series can be obtained as described in § 4. We find

$$\left.\begin{aligned}p_{xx}&=-Q\sin X\{R^2\mp[1-A^2e^{\mp 2Z}]\},\\ p_{zz}&=-Q\sin X\{R^2\pm[1-A^2e^{\mp 2Z}]\},\\ p_{zx}&=QZ\{[1+A^2e^{\mp 2Z}]\cos X-2Ae^{\mp Z}\},\\ w&=\frac{b}{2\pi}\left\{\pm\arctan\left[\frac{Ae^{\mp Z}\sin X}{1-Ae^{\mp Z}\cos X}\right]+\frac{ZAe^{\mp Z}\sin X}{2(1-\sigma)R^2}\right\}\\ \text{and}\qquad u&=-\frac{b}{4\pi}\left\{\frac{1-2\sigma}{1-\sigma}\ln\left(\frac{R}{1-A}\right)\pm\frac{ZA}{(1-\sigma)R^2}e^{\mp Z}[\cos X-Ae^{\mp Z}]\right\}\end{aligned}\right\}\quad\ldots\ldots(52)$$

where $Q=\mu bAe^{\mp Z}/p(1-\sigma)R^4$ and $R^2=1+A^2e^{\mp 2Z}-2Ae^{\mp Z}\cos X$ and where u and w are taken to be zero at the origin.

The stresses and displacements associated with a single dislocation may be deduced from (52) by the method described in § 4. We find

$$\left.\begin{aligned}p_{xx}&=-qx\{r^2-2\zeta(\zeta\pm\zeta_0)\},\\ p_{zz}&=-qx\{r^2+2\zeta(\zeta\pm\zeta_0)\},\\ p_{zx}&=q\zeta\{(\zeta\pm\zeta_0)^2-x^2\},\\ u&=-\frac{a}{2\pi}\left\{\frac{1-2\sigma}{2(1-\sigma)}\ln\left(\frac{r}{\zeta_0}\right)+\frac{\zeta(\zeta\pm\zeta_0)}{2(1-\sigma)r^2}\right\},\\ w&=\frac{a}{2\pi}\left\{\arctan\left(\frac{x}{\zeta\pm\zeta_0}\right)+\frac{x\zeta}{2(1-\sigma)r^2}\right\}\\ \text{and}\qquad W&=\tfrac{1}{2}a+(a/\pi)\arctan(x/\zeta_0),\end{aligned}\right\}\quad\ldots\ldots(53)$$

where $q=\mu a/2\pi(1-\sigma)r^4$, $r^2=x^2+(\zeta\pm\zeta_0)^2$ and $\zeta_0=a(1-2\sigma)\mu/4\mu_0(1-\sigma)$.

§ 13. THE INTERFACIAL ENERGY

The interfacial energy consists of two parts and is calculated as in § 5. We find

$$\tau=\{\mu_0 a/2\pi^2(1-2\sigma)\}\{1+\beta-(1+\beta^2)^{\frac{1}{2}}-\beta\ln[2\beta(1+\beta^2)^{\frac{1}{2}}-2\beta^2]\}.\quad\ldots\ldots(54)$$

The formula (54), like (41), gives a non-vanishing value of τ at $\theta=\pi/2$. We may also correct this error by constructing a symmetrical formula of the form (42) for the interfacial energy of the tilt boundary.

Shockley and Read (1949) obtained an estimate of the interfacial energy of a tilt boundary by assuming that the energy associated with an element of volume which is nearer to a dislocation than the distance between dislocations does not vary with the tilt and that the strain energy outside these regions is negligible They find

$$\tau=\{\mu a/4\pi(1-\sigma)\}\theta(B-\ln\theta), \qquad \ldots\ldots(55)$$

where the quantity B, which they do not evaluate, depends on the energy in the region surrounding the dislocation line, where Hooke's law becomes invalid. (55) is meant to be a good approximation when θ is small, and may therefore be evaluated from (54) by comparison with (55). We find $B=\ln\{e(1-\sigma)\mu_0/2\mu(1-2\sigma)\}$. The graph of (55), shown in Figure 7 (curve E), together with graphs of (54) (curve C) and (42) (curve D), is seen to be comparable with (54) and (42) over a wider range of θ than was found for the corresponding curves in II.

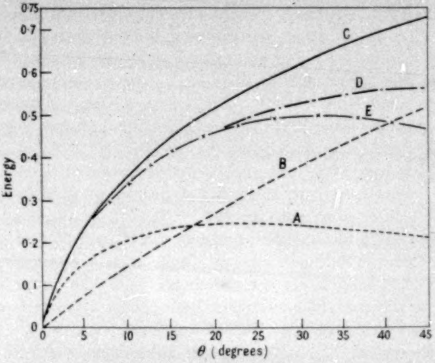

Figure 7. Interfacial energy as a function of the angle of tilt θ. Energy in units of $\mu a/2\pi^2(1-2\sigma)$ per unit area, where a is the lattice parameter, μ the rigidity modulus and σ Poisson's ratio. (The curves are calculated for $\sigma=0{\cdot}3$ and $\mu_0=\mu$.)

Curve A. Elastic energy in the two half-crystals (E_e/p).
Curve B. Energy resulting from sinusoidal force at misfitting interface.
Curve C. Total energy of interface $\{\tau=(E_e+E_a)/p\}$; formula (54).
Curve D. Symmetrical expression for total energy; formula (42).
Curve E. Total energy according to the formula (55) of Shockley and Read.

For the values $\mu_0=\mu$ and $\sigma=0{\cdot}3$, used in plotting the graphs, B is equal to 0·415. Shockley and Read found that when they take B equal to 0·5 their curve is in good agreement with the experimental observations of Dunn and Lionetti (1949). According to our formula B is equal to 0·5 when $\mu_0=\mu$ and $\sigma=0{\cdot}322$.

§ 14. DISCUSSION

It is appropriate to consider now what are the advantages and disadvantages of the present treatment, particularly as compared with the calculations of Shockley and Read and of Burgers, and what is the general significance of the results.

To begin with, the resolution of the boundary into a sequence of dislocations is a natural consequence of the present analysis. The lattice fault of I is a state of bad alignment between nearest atoms on either side of the boundary and is almost wholly contained in the distance in which U varies from $c/4$ to $3c/4$. This interval, which is given by $(2p/\pi)\arctan\{(1+\beta^{-2})^{\frac{1}{2}}-\beta^{-1}\}$, may be termed the width of a dislocation, and analogous definitions may be used for dislocation width in the cases II and III. The width, thus defined, as well as the energy density at all points, varies with the distance between dislocations. The treatment of Shockley and Read does not allow for this variation. When the distance between dislocations becomes large, the dislocation widths approximate to $a\mu/\mu_0(1-\sigma)$, $a\mu/\mu_0$ and $a(1-2\sigma)\mu/\mu_0 2(1-\sigma)$ for dislocations of the types I, II and III respectively.

The width of a dislocation of the type III may be regarded as a measure of the rapidity with which the sinusoidal approximation allows for the atomic 'planes' which terminate in the boundary. In the case of a single dislocation, for example, the separation of atomic 'planes' on either side of S increases in a distance ζ_0 by $\frac{1}{2}a$, or in a distance a by $a(2/\pi)\arctan(a/2\zeta_0)$, as can be seen from (53). The latter increase in separation and the distance ζ_0 respectively approximate to $5a/6$ and $0{\cdot}35a$ when $\mu_0=\mu$ and $\sigma=0{\cdot}3$. The corresponding allowances are of the order which is to be expected and may therefore be regarded as partly justifying the use of the sinusoidal approximation.

It is also to be counted an advantage of this treatment that singularities are avoided, and the departure from Hooke's law in regions of high strain is allowed for, even if only in an approximate manner.

The question should be considered whether in the regions treated as continua there are strains too large for the validity of Hooke's law. In I the strain associated with the relative displacement of the two atoms in S_B on either side of a single dislocation may be taken as the maximum strain occurring in this case. From (25) it is seen that this is $\{u(\frac{1}{2}a)-u(-\frac{1}{2}a)\}/a=\arctan(a/2\zeta_0)$, which, for $\mu_0=\mu$ and $\sigma=0{\cdot}3$, is approximately $1/5$. Analogous definitions may be used for the corresponding quantities in II and III which are then found to be approximately $1/4$ and $1/2{\cdot}5$ respectively. The strains of I and II probably are, and those of III certainly are, beyond the limit at which Hooke's law becomes invalid.

One necessary condition to permit our treating the half-crystals as elastic continua is, as given in § 2, that the relative displacement of neighbouring atoms in each half-crystal must change only slowly from atom to atom. The difference between the relative displacement of the two atoms considered in the previous paragraph and the relative displacement between one of these and its opposite neighbour is approximately the maximum variation that exists in case I. From (25) this difference is seen to be $u(3a/2)-2u(\frac{1}{2}a)+u(-\frac{1}{2}a)$, which is approximately $-a/9$. The corresponding differences in II and III are about $-a/7$ and $-a/2{\cdot}6$. The continuum approximation is therefore reasonable everywhere in the half-crystals of I and II, but is certainly bad for III in the neighbourhood of a dislocation.

The assumption that we may treat the surfaces of the half-crystals as continuous may be regarded as a separate assumption. It allows us to express the force (i) in terms of stresses and requires U, V and W to vary slowly from atom to atom, i.e. it requires the width of a dislocation to be large. The dislocation widths, which are respectively $1{\cdot}4a$, a and $0{\cdot}35a$ for $\mu_0=\mu$ and $\sigma=0{\cdot}3$, are rather small; this is the main objection to the treatment and other treatments in which the Peierls assumptions are used.

A further objection is the uncertainty as to whether the sinusoidal law of force is good enough in the region where it does not approximate to Hooke's law, i.e. in the small region around a dislocation where, for example, $\sin 2\pi\psi$ cannot be replaced by either $2\pi\psi$ or $-2\pi(1-\psi)$. If the approximation is bad it will introduce appreciable errors into the interfacial energy and in particular into that part associated with the potential energy of the atoms which lie in this region of high potential energy. The width of a dislocation may be regarded as a relative measure of the extent of this region. The error will be large when the dislocations are close together since the fraction of the total number of atoms at the boundary which are in the regions of high potential energy becomes large. A consideration of the width alone would predict that the smallest error is obtained in case III. However, it is very likely that the sinusoidal approximation is the worst for this case.

We finally conclude that a single mathematical treatment enables us to calculate the stresses and energies associated with three different types of boundaries and that these results are in all probability good approximations when the distance p between dislocations is large compared with the interatomic distance a. The errors, depending particularly on the sinusoidal approximation, may become appreciable when p is comparable with a and are certainly greatest in III. The outstanding feature of the interfacial energy is its rapid initial increase with the density of dislocations. It is unfortunate that, except for the work of Dunn and Lionetti (1949), no experimental observations with which the present results could be compared have been made. In view of the importance of boundaries of misfit in questions concerning oriented overgrowths or the physics of polycrystals further experimental measurements are much to be desired.

ACKNOWLEDGMENTS

The writer is greatly indebted to Professor N. F. Mott for suggesting problem I and for valuable discussions. He also wishes to express his gratitude to Professor H. Heilbronn for fruitful suggestions regarding the relationship (15). His thanks are further due to Dr. F. C. Frank, Mr. F. R. N. Nabarro, Mr. W. K. Burton and Dr. N. Cabrera for valuable discussions and constructive criticism.

The author also desires to thank the South African Council for Scientific and Industrial Research for a grant and special leave which rendered it possible to do this research.

REFERENCES

Bragg, W. L., 1940, *Proc. Phys. Soc.*, **52,** 54.
Burgers, J. M., 1949, *Proc. K. Ned. Akad. Wet.*, **42,** 293; 1940, *Proc. Phys. Soc.*, **52,** 23.
Burgers, W. G., 1947, *Proc. K. Ned. Akad. Wet.*, **50,** 452.
Dunn, G. G., and Lionetti, F., 1949, *J. Metals*, **1,** 125.
Frank, F. C., 1950 (in preparation).
Frank, F. C., and van der Merwe, J. H., 1949, *Proc. Roy. Soc.* A, **189,** 205.
Hardy, G. H., and Rocosinski, W. W., 1944, *Fourier Series* (Cambridge: University Press), p. 45.
Leibfried, G., and Lücke, K., 1949, *Z. Phys.*, **126,** 50.
Mackenzie, J. K., 1950, *Proc. Phys. Soc.* B, **63,** 2.
van der Merwe, J. H., 1949, *Faraday Society's General Discussion on Crystal Growth* (in the press).
Nabarro, F. R. N., 1947, *Proc. Phys. Soc.*, **59,** 256.
Peierls, R., 1940, *Proc. Phys. Soc.*, **52,** 34.
Shockley, W., and Read, W. T., 1949, *Phys. Rev.*, **75,** 692.
Timoshenko, S., 1934, *Theory of Elasticity* (New York: McGraw-Hill Book Co.).
Taylor, G. I., 1934, *Proc. Roy. Soc.* A, **145,** 362.

The Theory of the Propagation of First and Second Sound in Helium II.—Energy Theorems and Irreversible Processes

By R. B. DINGLE
Royal Society Mond Laboratory, Cambridge

Communicated by H. N. V. Temperley; MS. received 26th August 1949

ABSTRACT. The first part of this paper contains a discussion of the conditions determining whether sound waves in helium II are propagated isothermally or adiabatically. In the remainder of this part an expression is found for the energy flux from a closed region, and the impedance concept is applied to waves of second sound.

The second part of the paper is devoted to the study of the effects of irreversible processes on the propagation of waves of first and second sound. The irreversible processes discussed are those due to viscosity and thermal conduction, both in an extended fluid and in a narrow tube.

---

§ 1. INTRODUCTION

The work given here is a continuation of that of an earlier paper of similar title (Dingle 1948, referred to as I). In the present paper, the emphasis is on a unified theory of the propagation of first and second sound in helium. The interactions between the two types of sound are included in the theory. The first part of the paper contains a discussion of the thermodynamical nature of the fluctuations due to sound in helium II, and some considerations on the flow of energy; these will be required in the second part of the paper. The proof of the energy theorem of § 3 is based on some results of a paper on the hydrodynamics of helium II (Dingle 1949).

The irreversible processes discussed in the second part are those due to well-established effects—viscosity and thermal conduction. In efforts to find expressions for the thermal *convection*, other irreversible processes have been postulated. Meyer and Band (1947, 1948) have assumed the existence of a time of relaxation inversely proportional to the square of the heat flow, and Gorter and Mellink (1949) have assumed the existence of a mutual force of friction between the normal fluid and the superfluid proportional to the cube of their relative velocity. In the present paper we shall not discuss these possible causes of irreversibility, since in the absence of theoretical justification they must be regarded as empirical formulae describing the additive result of many irreversible effects. In any case both these postulated effects will vanish for sufficiently small amplitudes.

PART I.—GENERAL CONSIDERATIONS AND ENERGY THEOREMS

§ 2. THE THERMODYNAMICAL NATURE OF THE SOUND FLUCTUATIONS

In normal fluids the fluctuations in density and pressure due to the passage of sound waves are adiabatic, because of the small thermal conductivity of the medium. However, helium II transports heat very easily, and we must inquire whether the fluctuations may still be considered as adiabatic.* The situation is by no means the same as that which would exist in the hypothetical case of a liquid with a very high heat conductivity of the familiar type (i.e. a heat transfer not involving movement of the fluid), but otherwise normal. For in helium II the transfer of heat is itself due to a wave motion—second sound. Quantitatively, the problem may be investigated as follows. Neglecting the corrections due to viscous effects, we obtain the following equation for the sound velocities (cf. (A3) of the Appendix, also Landau 1941):

---

* This problem was discussed by Groenewold (1939) before the nature of heat flow in helium II was fully understood.

$$u^4 - u^2\left\{\frac{\rho_s}{\rho_n}\frac{TS^2}{C_v} + \left(\frac{\partial p}{\partial \rho}\right)_S\right\} + \frac{TS^2}{C_v}\frac{\rho_s}{\rho_n}\left(\frac{\partial p}{\partial \rho}\right)_T = 0. \quad \ldots\ldots (2.1)$$

The two solutions are given by

$$2u^2 = u_{20}^2 + u_{1S}^2 \pm [(u_{1S}^2 - u_{20}^2)^2 + 4u_{20}^2(u_{1S}^2 - u_{1T}^2)]^{\frac{1}{2}}, \quad \ldots\ldots (2.2)$$

where $u_{20}^2 = TS^2\rho_s/C\rho_n$; $u_{1S}^2 = (\partial p/\partial \rho)_S$ and $u_{1T}^2 = (\partial p/\partial \rho)_T$. ......(2.3)

The difference between the adiabatic and isothermal compressibilities is small, so that $u_{1S}^2 \sim u_{1T}^2$. Expanding in terms of their difference, we obtain for the velocity of first sound, given by the solution corresponding to the positive sign of (2.2),

$$u_1^2 = u_{1S}^2 + \frac{u_{20}^2(u_{1S}^2 - u_{1T}^2)}{u_{1S}^2 - u_{20}^2} = u_{1T}^2 + \frac{u_{1S}^2(u_{1S}^2 - u_{1T}^2)}{u_{1S}^2 - u_{20}^2}. \quad \ldots\ldots (2.4)$$

Thus first sound in helium II is propagated neither quite isothermally nor adiabatically, the precise nature of the fluctuations depending on the ratio of the velocity of first sound to that of second sound. In the temperature region so far investigated experimentally, ($T > 1°$ K.), $(u_2)_{\max} \sim u_1/13$, so that $u_{20}^2 \ll u_{1S}^2$. In this case, we see from the first of the alternative formulae (2.4) that $u_1 = u_{1S}$, and thus first sound will be propagated adiabatically, as in other fluids.

If, on the other hand, there exists a temperature region in which the velocity of second sound is considerably greater than that of first sound, as is unlikely, the second relation of (2.4) shows that the first sound fluctuations would be isothermal.

The velocity of second sound is given by the solution corresponding to the negative sign in (2.2), i.e. by

$$u_2^2 = u_{20}^2\left[1 - \frac{u_{1S}^2 - u_{1T}^2}{u_{1S}^2 - u_{20}^2}\right] = u_{20}^2\left[\frac{u_{1T}^2 - u_{20}^2}{u_{1S}^2 - u_{20}^2}\right]. \quad \ldots\ldots (2.5)$$

The deviations of the actual velocities from those calculated on the assumption of isothermal or adiabatic propagation may be calculated thermodynamically, the ratio of u_{1S} to u_{1T} being given by

$$\frac{u_{1S}^2}{u_{1T}^2} = \frac{C_p}{C_v} = 1 + \frac{T\alpha^2}{C_v}u_{1T}^2, \quad \ldots\ldots (2.6)$$

where α is the coefficient of thermal expansion. Thus ignoring terms of the second order,

$$u_1^2 = u_{1S}^2\left[1 + \frac{u_{20}^2 u_{1S}^2}{u_{1S}^2 - u_{20}^2}\frac{T\alpha^2}{C_v}\right] = u_{1T}^2\left[1 + \frac{u_{1T}^4}{u_{1T}^2 - u_{20}^2}\frac{T\alpha^2}{C_v}\right] \ldots\ldots (2.7)$$

and

$$u_2^2 = u_{20}^2\left[1 - \frac{u_{1S}^4}{u_{1S}^2 - u_{20}^2}\frac{T\alpha^2}{C_v}\right]. \quad \ldots\ldots (2.8)$$

Hence in the temperature region so far investigated, and probably at all temperatures, the velocity of first sound is greater than that calculated from either the adiabatic or the isothermal compressibility, and the velocity of second sound is less than that calculated from the usual formula $u_2^2 = TS^2\rho_s/C\rho_n$. It was shown by Stokes (cf. Rayleigh 1896) that in ordinary liquids sound waves would suffer extreme attenuation if propagated under conditions which were not very nearly adiabatic, or very nearly isothermal. It is interesting to note that this conclusion does not apply to the propagation of sound in helium II; in fact we have shown above that there is no attenuation in spite of the fact that the waves are propagated neither isothermally nor adiabatically. This difference in behaviour exists because the transfer of heat in helium II is primarily due not to conduction but to a *convection* current, which in this liquid is itself propagated as a wave motion.

The actual magnitudes of the corrections to the velocities are negligible. For instance, at 1·5° K. we may take $\alpha \sim -3\times 10^{-3}\,\mathrm{deg}^{-1}$, $C_v \sim 0{\cdot}28\,\mathrm{cal.\,gm}^{-1}$, $u_1 \sim 2{\cdot}5\times 10^4\,\mathrm{cm.\,sec}^{-1}$, giving $T\alpha^2 u_1^2/C_v \sim 7\times 10^{-4}$, showing that the difference between the two compressibilities is minute.

§ 3. A THEOREM ON THE FLOW OF ENERGY

In the theory of electricity there is a well-known theorem that the energy flowing per second from a region enclosed by a surface A is given by the surface integral $\int_A (c/4\pi) E\wedge H\,.\,dA$: the integrand is the Poynting vector. In this section we find an analogue to this vector representing the energy flux due to waves of first and second sound.

As was shown in a recent paper (Dingle 1949)† simple expressions may be found for the derivatives of the potential energy of unit mass of helium. With W as the potential energy per unit mass, these may be written, (cf. (6) and (7) of *loc. cit.*),

$$(\partial W/\partial\rho)_S = p'/\rho^2 \qquad \ldots\ldots (3.1)$$

and

$$(\partial W/\partial S)_\rho = T', \qquad \ldots\ldots (3.2)$$

where p' and T' are the fluctuations in pressure and temperature respectively.

Next we introduce the coordinates x and y defined by the relations

$$\rho x = \rho_n x_n + \rho_s x_s \qquad \ldots\ldots (3.3)$$

and

$$\rho^2 S y = \rho_n \rho_s S^*(x_n - x_s), \qquad \ldots\ldots (3.4)$$

where x_n and x_s are the displacements of the normal and superfluid respectively, S the total entropy per unit mass and S^* the difference in entropies of the two fluids. The coordinate x gives the position of the centre of gravity of the fluids and y is a coordinate proportional to their relative displacement. In this system, the conservation equations may be written

$$\partial\rho/\partial t + \rho\nabla.x = 0 \qquad \ldots\ldots (3.5)$$

and

$$\partial S/\partial t + S\nabla.y = 0. \qquad \ldots\ldots (3.6)$$

---

† For the remainder of this section 'loc. cit.' refers to this paper.

Thus the rate of change of the potential energy per unit volume is

$$-\frac{\partial(\rho W)}{\partial t} = -\left(\frac{\partial W}{\partial \rho}\right)_S \frac{1}{\rho}\frac{\partial \rho}{\partial t} - \left(\frac{\partial W}{\partial S}\right)_\rho \frac{1}{\rho}\frac{\partial S}{\partial t} = p'\nabla . \dot{x} + \rho S T' \nabla . \dot{y} \qquad \ldots\ldots (3.7)$$

by (3.1), (3.2), (3.5) and (3.6).

The rate of change of the density of kinetic energy is

$$-\frac{\partial}{\partial t} . \tfrac{1}{2}(\rho_n v_n^2 + \rho_s v_s^2) = -(\rho_n \dot{v}_n . v_n + \rho_s \dot{v}_s . v_s)$$

$$= \frac{\nabla p}{\rho} . (\rho_n v_n + \rho_s v_s) + \frac{\rho_n \rho_s}{\rho} S^* \nabla T . (v_n - v_s) \qquad \ldots\ldots (3.8)$$

(by (17) and (18) of *loc. cit.*),

$$= \dot{x} . \nabla p + \rho S \dot{y} . \nabla T \qquad \ldots\ldots (3.9)$$

by (3.3) and (3.4) of the present paper. Hence the rate of change of energy in a region of volume τ enclosed by a surface A is given by

$$-\frac{\partial}{\partial t}(\text{total energy}) = \int_A [(p'\nabla . \dot{x} + \rho S T' \nabla . \dot{y}) + (\dot{x} . \nabla p + \rho S \dot{y} . \nabla T)]\, d\tau$$

$$= \int_A \nabla . (p'\dot{x} + \rho S T' \dot{y})\, d\tau = \int_A (p'\dot{x} + \rho S T' \dot{y}) . dA. \qquad \ldots\ldots (3.10)$$

Thus the analogue of the Poynting vector of electromagnetism is the vector $(p'\dot{x} + \rho S T' \dot{y})$. The physical meaning of this result is clear: $p'\dot{x}$ is the rate at which 'mechanical' work is done in moving the centre of gravity of the two fluids against a pressure excess, whilst $\rho S T' \dot{y}$ is the rate at which 'thermal' work is done in moving entropy (relative to the centre of gravity) against a temperature excess.

§ 4. THE CONCEPT OF IMPEDANCE APPLIED TO SECOND SOUND

In I, it was shown that the rate of flow of energy per unit area is, for a plane wave of second sound,

$$\frac{1}{2}\frac{\rho_n \rho (V_n{}^0)^2 u_2}{\rho_s} = \frac{1}{2}\frac{\rho \rho_s S^2 (T^0)^2}{\rho_n u_2} = \frac{1}{2}\frac{\rho u_2 C (T^0)^2}{T} = \tfrac{1}{2} T^0 \rho V_n{}^0 S), \qquad \ldots\ldots (4.1)$$

where $V_n{}^0$ and $T_n{}^0$ specify respectively the peak values of the velocity of the normal fluid and the temperature excess. $\phi^0 = \rho V_n{}^0 S$ is the peak value of the flux of entropy, and $H^0 = \rho V_n{}^0 S/T$ is the peak value of the flux of heat. Hence

Flux of energy of second sound = ½ (peak fluctuation in temperature)
× (peak flux of entropy) ...... (4.2)

= ½ (peak fluctuation in temperature/actual temperature)
× (peak heat flux). ...... (4.3)

Comparing (4.2) and (4.3) with the well-known expression for the electrical energy flux, i.e.

Flux of electrical energy = ½(peak voltage) × (peak current density) we see that for second sound there are two convenient ways of defining the impedance; either

$$Z = \text{Impedance} = \frac{\text{Fluctuation in temperature}}{\text{Actual temperature}} \Big/ \text{Heat flux}$$

giving

$$\text{Flux of energy of second sound} = \frac{1}{2}\frac{T^0}{T}H^0 = \tfrac{1}{2}Z\left(\frac{T^0}{T}\right)^2 = \frac{1}{2}\frac{(H^0)^2}{Z} \qquad \ldots\ldots(4.4)$$

or

$$Z = \text{Impedance} = \text{Fluctuation in temperature}/\text{flux of entropy}$$

giving

$$\text{Flux of energy of second sound} = \tfrac{1}{2}T^0\phi^0 = \tfrac{1}{2}(T^0)^2/Z = \tfrac{1}{2}Z(\phi^0)^2. \qquad \ldots\ldots(4.5)$$

These results may also be deduced from (3.10) of the preceding section. The energy flux vector $(p'\dot{x} + \rho ST'\dot{y})$ may be divided into a 'mechanical' energy flux vector

$$p'\dot{x} = p'(\rho_{\rm n}V_{\rm n} + \rho_{\rm s}V_{\rm s})/\rho \qquad \ldots\ldots(4.6)$$

and a 'thermal' energy flux vector

$$\rho ST'\dot{y} = \rho_{\rm s}ST'(V_{\rm n} - V_{\rm s}). \qquad \ldots\ldots(4.7)$$

In first sound the 'thermal' energy flux is negligible, and hence the flux of energy is $p'V = \tfrac{1}{2}p^0V^0$, if the vibrations are simple harmonic. In second sound the 'mechanical' energy flux vector is negligible, and hence the flux of energy is $\rho_{\rm s}ST'(V_{\rm n} - V_{\rm s}) \simeq \rho ST'V_{\rm n}$, since $j = \rho_{\rm n}V_{\rm n} + \rho_{\rm s}V_{\rm s} \simeq 0$; thus for simple harmonic waves of second sound the energy flux is $\tfrac{1}{2}\rho ST^0V_{\rm n}^0$, in agreement with (4.1).

Of the two equivalent definitions of the impedance for second sound propagation, the second brings out clearly the nature of the work done—i.e. work done in transporting entropy through differences in temperature. Corresponding to ordinary mechanical power given by the product of force and fluid velocity, in second sound we have the thermal power given by the product of the temperature fluctuation and the entropy flux.

PART II.—IRREVERSIBLE PROCESSES

§ 5. THE VISCOUS ATTENUATION OF PLANE WAVES OF SOUND IN AN EXTENDED MEDIUM

We assume that normal fluid has viscosity μ, and that the superfluid is non-viscous*. Then, as has been shown in a previous paper (Dingle 1949) the equations to be satisfied are

$$\frac{\partial j}{\partial t} + \nabla p - \mu(\nabla^2 V_{\rm n} + \tfrac{1}{3}\nabla\nabla . V_{\rm n}) = 0, \qquad \ldots\ldots(5.1)$$

$$\frac{\partial \rho}{\partial t} + \nabla . j = 0, \qquad \ldots\ldots(5.2)$$

$$\frac{\partial(\rho S)}{\partial t} + \rho S\nabla . V_{\rm n} = 0, \qquad \ldots\ldots(5.3)$$

$$\frac{\partial V_{\rm s}}{\partial t} - S\nabla T + \frac{\nabla p}{\rho} = 0. \qquad \ldots\ldots(5.4)$$

---

* The supposition of a non-zero value of the superfluid viscosity would be incompatible with the assumption that the superfluid has no entropy.

These are respectively (28), (1), (2) and (4) of the paper quoted above, with V_n written for $\dot{x}_n$, the velocity of the normal fluid, and V_s written for $\dot{x}_s$, the velocity of the superfluid. By definition we have also $\rho = \rho_n + \rho_s$ and $j = \rho_n V_n + \rho_s V_s$.

Representing fluctuations by symbols with a dash, (5.1)–(5.4) reduce to

$$V_n(\rho_n - \epsilon\rho) + \rho_s V_s - p'/u = 0, \qquad \ldots\ldots (5.5)$$

$$up' - \rho_n V_n - \rho_s V_s = 0, \qquad \ldots\ldots (5.6)$$

$$u(\rho' S + \rho S') - \rho S V_n = 0, \qquad \ldots\ldots (5.7)$$

$$uV_s + ST' - p'/\rho = 0, \qquad \ldots\ldots (5.8)$$

where u is the velocity of propagation and $\epsilon = 4i\mu\omega/3u^2\rho$, ω being the pulsatance. Eliminating V_n and V_s from these equations, we obtain

$$u^2\rho'(1-\epsilon) - p' = \epsilon u^2 \rho S'/S \qquad \ldots\ldots (5.9)$$

and

$$u^2 S'(\rho_n/\rho_s - \epsilon) - S^2 T' = \epsilon u^2 S \rho'/\omega\rho. \qquad \ldots\ldots (5.10)$$

We shall obtain approximate solutions of (5.9) and (5.10) by neglecting the right-hand terms, these giving only the coupling between first and second sound. This procedure will be justified in the Appendix. To this approximation we may also neglect the coefficient of thermal expansion, so that it is legitimate to take $p' = \rho' \partial p/\partial\rho$ and $S' = T'\partial S/\partial T = CT'/T$, where C is the specific heat and T the actual temperature of the fluid. Thus

$$u^2(1-\epsilon) - \partial p/\partial\rho = 0 \qquad \ldots\ldots (5.11)$$

and

$$\frac{u^2 C}{T}\left(\frac{\rho_n}{\rho_s} - \epsilon\right) - S^2 = 0. \qquad \ldots\ldots (5.12)$$

Since $\epsilon u^2 = 4i\mu\omega/3\rho$, we obtain as our two solutions

$$u_1{}^2 = \partial p/\partial\rho + 4i\mu\omega/3\rho \qquad \ldots\ldots (5.13)$$

and

$$u_2{}^2 = \frac{TS^2\rho_s}{C\rho_n} + \frac{4i\mu\omega}{3\rho}\frac{\rho_s}{\rho_n}. \qquad \ldots\ldots (5.14)$$

Thus the real parts of u_1 and u_2 are altered only in the second order of approximation. The distance in which the amplitude falls to $1/e$ of its initial value is given by $1/I(\omega/u_1) \simeq 3u_1{}^3\rho/2\mu\omega^2$ for first sound, and by $1/I(\omega/u_2) \simeq (3u_2{}^3\rho/2\mu\omega^2)(\rho_n/\rho_s)$ for second sound. Hence the attenuation of first sound due to this cause will not vary appreciably with temperature, since u_1 is approximately constant, but that of second sound will alter considerably with temperature, the attenuation being very large near the λ-point, where $u_2{}^3/\rho_s \sim 0$.

A rough calculation of the magnitude of the distance in which the amplitude falls to $1/e$ of its initial value may be made for a specific temperature. For example, at 1·5° K. we may take $u_1 = 2{\cdot}5 \times 10^4$ cm. sec^{-1}; $u_2 = 2 \times 10^3$ cm. sec^{-1}; $\rho = 0{\cdot}145$ gm. cm^{-3}, $\rho_s/\rho_n = 7{\cdot}4$ and $\mu = 10^{-5}$ poise, obtaining for the characteristic distance a value $8{\cdot}8 \times 10^{17}/f^2$ cm. for first sound propagation, and $6{\cdot}1 \times 10^{15}/f^2$ cm. for second sound: f is the frequency in cycles per second. At this temperature the attenuation is important only at extremely high frequencies. Near the point, however, the attenuation of second sound will be serious for lower equencies also.

§ 6. THE VISCOUS ATTENUATION OF FIRST AND SECOND SOUND IN A THIN TUBE[*]

We assume that the tube is sufficiently wide for the 'shell' of fluid near the walls, which is affected by the boundary condition $V_n=0$ at the surface, to be considered as thin. Then the forces acting on the bulk liquid are those due to the pressure gradient and to the force transmitted by this shell of fluid near the boundary. The latter force may easily be calculated if we consider the walls as effectively flat; this approximation, and also that of assuming the 'shell' to be thin, may be justified *a posteriori*. If the sound wave is taken to be travelling along the x axis, we have

$$\rho_n \partial V_n/\partial t = \mu\, d^2V_n/dx^2,$$

since the viscous force acts only on the normal fluid. Taking $\partial/\partial t \equiv i\omega$,

$$d^2V_n/dx^2 = i\omega\rho_n V_n/\mu.$$

The solution satisfying the boundary condition $V_n=0$ at $x=0$ is

$$V_n = V_n^0[1-\exp\{-x(1+i)(\omega\rho_n/2\mu)^{\frac{1}{2}}\}], \qquad \ldots\ldots (6.1)$$

where V_n^0 is the velocity of the normal fluid well away from the shell of liquid dragging at the perimeter of the tube. If this shell is thin enough to be considered as located at the plane $x=0$, the force transmitted by it is, per unit area,

$$\mu\left(\frac{dV_n}{dx}\right)_{x=0} = \mu(1+i)V_n^0(\omega\rho_n/2\mu)^{\frac{1}{2}}. \qquad \ldots\ldots (6.2)$$

Thus the viscous force per unit volume is

$$\frac{P}{A}\left(\frac{\omega\rho_n\mu}{2}\right)^{\frac{1}{2}}(1+i)V_n,$$

where P/A is the ratio of perimeter to cross section, and V_n has been written for V_n^0. This force opposes the acceleration. Writing

$$\epsilon' = \frac{P}{\rho A}\left(\frac{\rho_n\mu}{2\omega}\right)^{\frac{1}{2}}(i-1) \qquad \ldots\ldots (6.3)$$

the equation of motion of the bulk liquid reduces to (5.5) with ϵ' replacing ϵ of § 5. The elimination of the variables proceeds as before until the equivalents of (5.11) and (5.12) are obtained. However, unlike ϵ, ϵ' does not involve u, and the solutions are now given by

$$u_1^2 = (1-\epsilon')^{-1}\partial p/\partial\rho \qquad \ldots\ldots (6.4)$$

and

$$u_2^2 = (1-\epsilon'\rho_s/\rho_n)^{-1}TS^2\rho_s/C\rho_n. \qquad \ldots\ldots (6.5)$$

Thus the real part of the velocity of first sound is altered by a factor of approximately

$$1-\frac{1}{2\rho}\frac{P}{A}\left(\frac{\rho_n\mu}{2\omega}\right)^{\frac{1}{2}}$$

and that of second sound by a factor[†]

$$1-\frac{\rho_s}{2\rho_n\rho}\frac{P}{A}\left(\frac{\rho_n\mu}{2\omega}\right)^{\frac{1}{2}}.$$

---

[*] The steady flow of helium II through thin tubes has been discussed by F. London and Zilsel (1948).

[†] The results for second sound which were given in I are erroneous, as the increased coupling between the sounds due to the viscous effects was not taken into account. The equation

$$-\epsilon'\rho V_n + u^2\rho' - p' = 0,$$

obtained by elimination of j between (5.5) and (5.6), appeared to show that the effects of viscosity (contained in ϵ') are associated with density and pressure fluctuations, i.e. with first sound, and thus with second sound only through thermal expansion.

For first sound, the distance in which the amplitude falls to $1/e$ of its initial value is $1/I(\omega/u_1) = u_1 \rho r (2/\rho_n \mu\omega)^{\frac{1}{2}}$ for a circular tube of radius r. The corresponding distance for second sound is $(u_2 \rho r/\rho_s)(2\rho_n/\mu\omega)^{\frac{1}{2}}$. The attenuation of second sound due to this cause will be serious near the λ-point, where $u_2 \sim 0$, and at very low temperatures, where $\rho_n \sim 0$. With the values given in §5, the distance in which the amplitude falls to $1/e$ of its initial value is, at 1·5° K., $1{\cdot}6 \times 10^6 r f^{-\frac{1}{2}}$ cm. for first sound, and $5{\cdot}3 \times 10^4 r f^{-\frac{1}{2}}$ cm. for second sound; r is the radius of the tube in centimetres and f the frequency in cycles per second.

§7. THE COUPLING COEFFICIENTS BETWEEN FIRST AND SECOND SOUND

We have seen in §5 that the coupling between the sounds is caused by at least two different factors: the existence of thermal expansion (which means that the temperature fluctuations of second sound will be accompanied by slight pressure and density changes), and the viscosity μ of the normal fluid. In this section we calculate the magnitude of this coupling by a method due to Lifshitz (1944).

Introducing parameters a, b and c defined by the relations $V_n = aV_s$, $p' = bV_s$, $T' = cV_s$, we have from (5.8)

$$b/\rho - Sc = u \qquad \ldots\ldots (7.1)$$

and by (5.5)

$$au(\rho_n - \epsilon\rho) - \rho Sc = u\rho_n. \qquad \ldots\ldots (7.2)$$

Finally by (A1) of the Appendix,

$$b\left[\left(\frac{\partial\rho}{\partial p}\right)_T u^2(1-\epsilon) - 1 - \frac{\epsilon u^2 \rho}{S}\left(\frac{\partial S}{\partial p}\right)_T\right] + c\left[u^2(1-\epsilon)\left(\frac{\partial \rho}{\partial T}\right)_p - \frac{\rho\epsilon u^2}{S}\left(\frac{\partial S}{\partial T}\right)_p\right] = 0. \qquad \ldots\ldots (7.3)$$

Since $(\partial\rho/\partial T)_p$ and $(\partial S/\partial p)_T = -(\partial V/\partial T)_p$ are proportional to the coefficient of thermal expansion, the products of these quantities with ϵ may be neglected. Noting also that $u_1^{-2} = (\partial\rho/\partial p)_T(1-\epsilon)$, we have

$$b(u^2/u_1^2 - 1) - \rho u^2 c(\alpha + \epsilon C/ST) = 0. \qquad \ldots\ldots (7.4)$$

Thus by (7.1)

$$b \simeq -\frac{u^3\rho(\alpha + \epsilon C/ST)}{S(u^2/u_1^2 - 1)}. \qquad \ldots\ldots (7.5)$$

In a similar way, we obtain the following values for a, b and c:

$$a_1 = 1 + \frac{\epsilon_1\rho}{\rho_n} + \frac{\sigma_1\rho u_1^2 u_2^2}{S\rho_s(u_1^2 - u_2^2)}; \quad b_1 = \rho u_1\left(1 + \frac{S\sigma_1 T u_1^2}{\rho C(u_1^2 - u_2^2)}\right); \quad c_1 = \frac{\sigma_1 T u_1^3}{C(u_1^2 - u_2^2)}, \qquad \ldots\ldots (7.6)$$

$$\left.\begin{aligned} a_2 &= -\frac{\rho_s}{\rho_n}\left(1 + \frac{\epsilon_2\rho}{\rho_n}\right) + \frac{\rho\sigma_2}{S\rho_n}\frac{u_1^2 u_2^2}{(u_1^2 - u_2^2)}; \quad b_2 = \frac{\sigma_2\rho u_1^2 u_2^3}{S(u_1^2 - u_2^2)}; \\ c_2 &= -\frac{u_2}{S}\left(1 - \frac{\sigma_2}{S}\frac{u_1^2 u_2^2}{(u_1^2 - u_2^2)}\right), \end{aligned}\right\} \qquad \ldots\ldots (7.7)$$

where $\epsilon_1 = 4\mu i\omega/3\rho u_1^2$, $\epsilon_2 = 4\mu i\omega/3\rho u_2^2$, $\sigma_1 = \alpha + C\epsilon_1/TS$, and $\sigma_2 = \alpha + C\epsilon_2/TS$.

At 1·5° K., ϵ_1 and ϵ_2 may be calculated using the values of §5, giving $\epsilon_1 = 9{\cdot}2 \times 10^{-13} if$ and $\epsilon_2 = 1{\cdot}5 \times 10^{-10} if$. With $C = 0{\cdot}28$ cal.gm^{-1} and $S = 0{\cdot}06$ cal.gm^{-1} the additions to be made to the thermal expansion coefficient $\alpha \sim -3 \times 10^{-3}$ deg^{-1}

to take account of viscosity are $C\epsilon_1/TS = 2{\cdot}8 \times 10^{-13} if$ and $C\epsilon_2/TS = 4{\cdot}7 \times 10^{-11} if$ for first and second sound respectively.

The additional coupling due to viscosity is negligible except for second sound waves of very high frequency, or at temperatures close to the λ-point, where ϵ_2 becomes very large since $u_2 \sim 0$.

When the liquid is contained in a narrow tube, the additional coupling due to viscosity may be calculated merely by replacing ϵ_1 and ϵ_2 by ϵ', where

$$\epsilon' = \frac{2}{\rho r}\left(\frac{\rho_{\rm n}\mu}{2\omega}\right)^{\frac{1}{2}}(i-1).$$

At 1·5° K., $\epsilon' = 135(i-1)r^{-1}f^{-\frac{1}{2}}$ and $C\epsilon'/TS = 42(i-1)r^{-1}f^{-\frac{1}{2}}$. Thus when the liquid is contained in a tube, the coupling between the sounds may be much greater than that calculated from thermal expansion alone, especially if the tube is narrow and the frequency low.

§8. THE RATIO OF THE AMPLITUDES OF THE FIRST AND SECOND SOUND PRODUCED BY DIFFERENT PROCESSES*

(*a*) *A surface fluctuating in temperature.*

Let A_1 and A_2 be the amplitudes of the velocities of the superfluid in first and second sound respectively, these being produced by a source consisting of a plate undergoing fluctuations in temperature of amplitude T'. The boundary conditions to be satisfied are: (i) The sum of the temperature fluctuations due to the two sounds must equal the temperature fluctuation T'. Since

$$T = cV_{\rm s}, \qquad c_1A_1 + c_2A_2 = T'. \qquad \ldots\ldots (8.1)$$

(ii) There must be no net flow of fluid at the surface; i.e. $j = \rho_{\rm n}V_{\rm n} + \rho_{\rm s}V_{\rm s} = 0$. Since $V_{\rm n} = aV_{\rm s}$ this gives

$$(\rho_{\rm s} + a_1\rho_{\rm n})A_1 + (\rho_{\rm s} + a_2\rho_{\rm n})A_2 = 0. \qquad \ldots\ldots (8.2)$$

From (8.2) we obtain the relation

$$\frac{T_2'}{T_1'} = \frac{c_2}{c_1}\frac{A_2}{A_1} = -\frac{c_2}{c_1}\frac{\rho_{\rm s} + a_1\rho_{\rm n}}{\rho_{\rm s} + a_2\rho_{\rm n}} = \frac{C}{T\sigma_1\sigma_2}\frac{(u_1^2 - u_2^2)^2}{u_1^5u_2} \simeq \frac{C}{T\sigma_1\sigma_2u_1u_2}. \qquad \ldots\ldots (8.3)$$

At 1·5° K., taking $\sigma_1 \sim \sigma_2 \sim \alpha \sim -3 \times 10^{-3}$ deg^{-1}, $T_2'/T_1' \simeq 1{\cdot}38 \times 10^4$.

(*b*) *A surface vibrating in its own plane.*

Let V be the velocity of the plane. Then, since only the normal fluid drags, our boundary conditions are

$$\text{(i) } a_1A_1 + a_2A_2 = V \quad \text{and} \quad \text{(ii) } A_1 + A_2 = 0.$$

Hence the relations

$$\frac{T_2'}{T_1'} = \frac{c_2}{c_1}\frac{A_2}{A_1} = -\frac{c_2}{c_1} = \frac{u_2C(u_1^2 - u_2^2)}{S\sigma_1Tu_1^3} \simeq \frac{C}{\sigma_1TS}\frac{u_2}{u_1}. \qquad \ldots\ldots (8.4)$$

At 1·5° K., taking $\sigma_1 \sim \alpha$, $T_2'/T_1' \simeq 0{\cdot}83 \times 10^2$.

These numerical values of T_2'/T_1' are minimum estimates, as the increased coupling due to viscosity has not been taken into account. This additional coupling decreases the efficiency of these methods of second sound production.

---

* The method of this section is also due to Lifshitz (1944).

§ 9. THE RATIO OF THERMAL TO MECHANICAL ENERGY IN SOUND

If we consider a volume enclosed by a spherical surface of unit area, the rate of loss of energy is given by the product of the velocity of the sound concerned and the energy density within the sphere, i.e. by $u(\rho_n V_n^2 + \rho_s V_s^2)$. Hence by (4.6), the proportion of 'mechanical' energy emerging from the sphere is, in the notation of § 7,

$$\frac{p'(\rho_n V_n + \rho_s V_s)}{u\rho(\rho_n V_n^2 + \rho_s V_s^2)} = \frac{b(\rho_n a + \rho_s)}{u\rho(\rho_n a^2 + \rho_s)}. \qquad \ldots\ldots (9.1)$$

For second sound this is equal to

$$\frac{\sigma_2^2}{S^2} \cdot \frac{\rho_n}{\rho_s} \cdot \left(\frac{u_1^2 u_2^2}{u_1^2 - u_2^2}\right)^2. \qquad \ldots\ldots (9.2)$$

The proportion of 'thermal' energy is, by (4.7),

$$\frac{\rho_s S T'(V_n - V_s)}{u(\rho_n V_n^2 + \rho_s V_s^2)} = \frac{\rho_s S c(a-1)}{u(\rho_n a^2 + \rho_s)}. \qquad \ldots\ldots (9.3)$$

For first sound this is equal to

$$\frac{\sigma_1^2}{S^2} \cdot \frac{\rho_n}{\rho_s} \cdot \left(\frac{u_1^2 u_2^2}{u_1^2 - u_2^2}\right)^2. \qquad \ldots\ldots (9.4)$$

When $\sigma_1 \sim \sigma_2$ (there is exact equality if the only coupling taken into account is that due to thermal expansion), the proportion of 'thermal' energy in first sound is almost identical with the proportion of 'mechanical' energy in second sound. At 1·5° K. this proportion is 3×10^{-6} if only thermal expansion coupling is taken into account.

§ 10. THE ATTENUATION OF SOUND DUE TO THERMAL CONDUCTION IN AN EXTENDED MEDIUM*

We shall assume that in addition to the heat flow caused by convection there is a heat flow due to conduction which is directly proportional to the temperature gradient, with a factor of proportionality K per unit cross section per unit time.

Considering unit volume, the rate of loss of entropy is $-\partial(\rho S)/\partial t$. This must be equated to the sum of the loss $\rho S \nabla . V_n$ due to convection (assuming that only the normal fluid carries entropy), and the loss due to conduction

$$T^{-1}\partial Q/\partial t = -KT^{-1}\nabla^2 T',$$

where T is the mean temperature of the liquid. Hence

$$\partial(\rho S)/\partial t + \rho S \nabla . V_n - KT^{-1}\nabla^2 T' = 0. \qquad \ldots\ldots (10.1)$$

The equations describing the hydrodynamics of helium II (cf. § 5) are now

$$\rho_n V_n + \rho_s V_s - p'/u = 0, \qquad \ldots\ldots (10.2)$$

$$u\rho' - \rho_n V_n - \rho_s V_s = 0, \qquad \ldots\ldots (10.3)$$

$$\rho' S + \rho S' - \rho S V_n/u + iK\omega T'/Tu^2 = 0, \qquad \ldots\ldots (10.4)$$

$$u V_s + ST' - p'/\rho = 0. \qquad \ldots\ldots (10.5)$$

---

* The elementary theory of this effect for second sound alone was given in I. § 5.

By the methods of the Appendix, we obtain

$$u^4 - u^2 \left[\frac{\rho_s}{\rho_n} \cdot \frac{TS^2}{C_v} - \frac{iK\omega}{\rho C_v} + \left(\frac{\partial p}{\partial \rho} \right)_S \right] + \left[\frac{TS^2}{C_v} \cdot \frac{\rho_s}{\rho_n} - \frac{iK\omega}{\rho C_v} \right] \left(\frac{\partial p}{\partial \rho} \right)_T = 0. \qquad \ldots\ldots (10.6)$$

Writing

$$u_{20}^2 = \rho_s TS^2/\rho_n C_v, \qquad \eta = iK\omega/\rho C_v, \qquad u_{1S}^2 = (\partial p/\partial \rho)_S, \qquad u_{1T}^2 = (\partial p/\partial \rho)_T, \qquad \ldots\ldots (10.7)$$

we have

$$2u^2 \simeq u_{20}^2 - \eta + u_{1S}^2 \pm \left[u_{1S}^2 - u_{20}^2 + \eta + \frac{2(u_{20}^2 - \eta)(u_{1S}^2 - u_{1T}^2)}{(u_{1S}^2 - u_{20}^2 + \eta)} \right]. \qquad \ldots\ldots (10.8)$$

The velocity of first sound is obtained by taking the positive sign in (10.8), thus

$$\frac{\omega}{u_1} \simeq \frac{\omega}{u_{1S}} \left\{ 1 - \frac{(u_2^2 - \eta)(u_{1S}^2 - u_{1T}^2)}{2(u_{1S}^2 - u_2^2 + \eta) u_{1S}^2} \right\}. \qquad \ldots\ldots (10.9)$$

Since $u_{1S}^2 - u_{1T}^2 = u_{1T}^4 T\alpha^2/C_v$, the distance in which the amplitude of first sound falls to $1/e$ of its initial value is $1/I(\omega/u_1) \simeq 2\rho C_v u_1/K\omega^2 T\alpha^2$.

The velocity of second sound is obtained by taking the negative sign in (10.8), thus

$$u_2^2 = u_{20}^2 - \eta - \frac{(u_2^2 - \eta)(u_{1S}^2 - u_{1T}^2)}{(u_{1S}^2 - u_2^2 + \eta)}, \qquad \ldots\ldots (10.10)$$

in which the third term is negligible in comparison with the second. The distance in which the amplitude falls to $1/e$ of its initial value is therefore given by $2\rho C_v u_2^3/K\omega^2$.

At 1·5° K. we may insert the following values in the formulae: $\rho = 0{\cdot}145$ gm.cm^{-3}, $C_v = 0{\cdot}28$ cal.gm^{-1}, $K = 6 \times 10^{-5}$ cal.cm^{-2} deg^{-1} (the value for helium I, where the conduction is not masked by convection), $\alpha = -3 \times 10^{-3}$, $u_1 = 2{\cdot}5 \times 10^4$ cm.sec^{-1}, $u_2 = 2 \times 10^3$ cm.sec^{-1}. Then we obtain for the characteristic distance the value $3 \times 10^{17} f^{-2}$ cm. for first sound, and $2{\cdot}73 \times 10^{11} f^{-2}$ cm. for second sound, where f is the frequency in cycles per second.

The attenuation of first sound due to this cause is therefore negligible except at very high frequencies, but that of second sound will be serious near the λ-point, where $u_2 \sim 0$, and probably also near the absolute zero, where $C_v \sim 0$ with u_2 probably remaining finite.

§ 11. THE ATTENUATION OF SECOND SOUND IN A THIN TUBE DUE TO THE THERMAL CONDUCTION OF THE WALLS

The loss due to the thermal conduction of the walls of the tube may easily be estimated with the help of the impedance concept of § 4. Two impedances are involved: Z_{liq}, that of the liquid, which will give the power travelling down the tube, and Z_{sol}, the impedance of the tube walls, which will give the power flowing out sideways, the power lost by the liquid.

(i) *The impedance of the liquid.* From the work of § 4, $Z_{\text{liq}} = T'_{\text{liq}}/TH$, where H is the heat flux. Neglecting pressure and density fluctuations, $H = \rho TSV_n$, whence $H=\rho_s\rho TSV_s/\rho_n=\rho_s\rho TS^2T'/\rho_n u_2$ (by (5.8)) $)=\rho CT'u_2$ since $u_2{}^2=TS^2\rho_s/C\rho_n$. (This calculation is really unnecessary, since the result is physically obvious, $\rho CT'$ being the excess heat per unit volume and u_2 being the velocity with which it is transported (cf. Osborne 1948).) Thus

$$Z_{\text{liq}}=1/\rho TCu_2. \qquad \ldots\ldots(11.1)$$

The flux of energy travelling down the tube is therefore

$$\tfrac{1}{2}(T'_{\text{max}})^2/Z_{\text{liq}}=\tfrac{1}{2}\rho TCu_2A(T'_{\text{max}})^2, \qquad \ldots\ldots(11.2)$$

where A is the cross-sectional area of the tube.

(ii) *The impedance of the walls of the tube.* The equation of heat conduction

$$\frac{dT''}{dt}=\frac{K_{\text{sol}}}{\rho_{\text{sol}}C_{\text{sol}}}\nabla^2T'' \qquad \ldots\ldots(11.3)$$

has the solution

$$T''=T''_{\text{max}}\exp[-z(1+i)\{\omega\rho_{\text{sol}}C_{\text{sol}}/2K_{\text{sol}}\}^{\frac{1}{2}}]. \qquad \ldots\ldots(11.4)$$

Here we have neglected the curvature of the walls of the tube. The heat flux H is given by the relation $H=-K_{\text{sol}}(\partial T''/\partial z)_{z=0}=\beta T''_{\text{max}}(1+i)$, where $\beta=(\tfrac{1}{2}\omega\rho_{\text{sol}}C_{\text{sol}}K_{\text{sol}})^{\frac{1}{2}}$. Hence

$$Z_{\text{sol}}=T''/TH=1/\beta T(1+i). \qquad \ldots\ldots(11.5)$$

Taking P as the perimeter of the tube, the energy flux into the walls is, per unit length,

$$\tfrac{1}{2}(T''_{\text{max}})^2P/Z_{\text{sol}}=\tfrac{1}{2}\beta T(1+i)(T''_{\text{max}})^2P.$$

The flux of energy lost to the walls is given by the real part of this expression, i.e. by $\tfrac{1}{2}\beta TP(T''_{\text{max}})^2$. $\qquad \ldots\ldots(11.6)$

(iii) *The attenuation.* By (11.2) and (11.6),

$$\frac{\text{Loss of energy per unit length}}{\text{Energy travelling down tube}}=\frac{\beta}{\rho Cu_2}\frac{P}{A}\left(\frac{T''_{\text{max}}}{T'_{\text{max}}}\right)^2. \qquad \ldots\ldots(11.7)^*$$

Here $T''_{\text{max}}/T'_{\text{max}}$ is the ratio of the maximum temperature fluctuation in the liquid in the neighbourhood of the walls of the tube to that in the bulk liquid. Peshkov (1948) has assumed that these temperatures are the same. This simple assumption is probably false, as it neglects the effects of viscous forces, which will cause the amplitude of second sound vibrations to die out near the walls—the flow of heat in second sound is proportional to V_n, the velocity of the normal fluid, and this must vanish at a surface if there is a true viscosity. It is possible, however, that 'slip' between the liquid and the walls may not be negligible; in this case the value of $(T''_{\text{max}}/T'_{\text{max}})$ will lie between zero and unity.

§ 12. THE ATTENUATION IN A THIN TUBE DUE TO THE COMBINED EFFECT OF VISCOUS AND CONDUCTION LOSSES IN THE LIQUID

In the last section we have shown that the temperature fluctuations of second sound die away near the walls of the tube, since V_n falls off in magnitude owing to viscous effects. This coupling between the thermal and viscous effects gives

---

[*] The distance in which the amplitude falls to $1/e$ of its initial value is given by twice the reciprocal of (11.7).

rise to a loss additional to that calculated in § 6 on the basis of viscous losses only. The fundamental boundary condition is that $V_n=0$ at the surface, and the thermal losses result from the fact that the excess temperature T' is related to V_n. From (5.3) we obtain the approximate relationship

$$\frac{\partial T}{\partial t}+\frac{TS}{C}\frac{\partial V_n}{\partial x}=0.$$

By (6.1)

$$V_n=V_n^0[1-\exp\{-x(1+i)(\omega\rho_n/2\mu)^{\frac{1}{2}}\}].$$

Hence

$$T'=\frac{ST}{\omega C}V_n^0(1-i)(\omega\rho_n/2\mu)^{\frac{1}{2}}[1-\exp\{-x(1+i)(\omega\rho_n/2\mu)^{\frac{1}{2}}\}]. \quad \ldots\ldots(12.1)$$

Thus the heat flow per unit time in the boundary layer is, per unit length,

$$-K_1(\partial T'/\partial x)_{x=0}=PV_n^0TS\rho_nK_1/\mu C. \quad \ldots\ldots(12.2)$$

By I, § 6, the fraction of this heat lost to the walls is $2Z_1/(Z_s+Z_1)$. (12.1) and (12.2) give $Z_1=T'/HT=1/(1+i)TK_1(\omega\rho_n/2\mu)^{\frac{1}{2}}$, and Z_s is given by (11.5). Hence the transmission coefficient is approximately $(2/K_1)(\mu K_sC_s\rho_s/\rho_n)^{\frac{1}{2}}$, and the rate of heat loss per unit volume of liquid is BTV_n^0, where $B=(2P/A)(S/C)(K_sC_s\rho_s\rho_n/\mu)^{\frac{1}{2}}$. The equation of entropy conservation is now

$$\partial(\rho S)/\partial t+\rho S\nabla.V_n+BV_n=0 \quad \ldots\ldots(12.3)$$

and the hydrodynamical equations become

$$\begin{aligned} V_n(\rho_n-\epsilon'\rho)+\rho_sV_s-p'/u&=0,\\ u\rho'-\rho_nV_n-\rho_sV_s&=0,\\ u(\rho'S+\rho S')-V_n(\rho S+iBu/\omega)&=0,\\ uV_s+ST'-p'/\rho&=0. \end{aligned}$$

Eliminating V_n and V_s, we obtain

$$u_1^2=(\partial p/\partial\rho)(1-\epsilon')^{-1} \quad \ldots\ldots(12.4)$$

and

$$u_2^2=(TS^2/C)(\rho_n/\rho_s-\delta)^{-1}, \quad \ldots\ldots(12.5)$$

where

$$\frac{\rho_s\delta}{\rho_n}=\frac{1}{\rho}\frac{P}{A}\frac{\rho_s}{\rho_n}\left(\frac{\rho_n\mu}{2\omega}\right)^{\frac{1}{2}}(i-1)+\frac{2iu}{\omega\rho}\frac{P}{A}\cdot\frac{1}{C_1}(K_sC_s\rho_s\rho_n)^{\frac{1}{2}}. \quad \ldots\ldots(12.6)$$

For second sound, the distance in which the amplitude is reduced to $1/e$ of its initial value is thus

$$1/I(\omega/u_2)=\rho u_2\left(\frac{A}{P}\right)\left\{\rho_s\left(\frac{\mu\omega}{2\rho_n}\right)^{\frac{1}{2}}+\frac{2u_2}{C_1}\left(\frac{K_sC_s\rho_s\rho_n}{\mu}\right)^{\frac{1}{2}}\right\}^{-1} \quad \ldots\ldots(12.7)$$

whilst the corresponding distance for first sound is, to this degree of approximation, unaffected by the thermal conductivity.

The attenuation due to this cause is very important for second sound propagation. With the values given in §§ 5 and 10, and taking $K_s\sim10^{-4}$ cal.cm^{-2}deg^{-1} and $C_s\sim2\times10^{-6}$ cal.gm^{-1} for glass, $(2u_2/C_1)(K_sC_s\rho_s\rho_n/\mu)^{\frac{1}{2}}\sim3$ at 1·5° K.; this is to be compared with $\rho_s(\mu\omega/2\rho_n)^{\frac{1}{2}} \sim 5\times10^{-3}f^{\frac{1}{2}}$ at the same temperature. Thus at all but the highest frequencies the conduction effect associated with that due to viscosity is far more important than the direct effect of the viscous force. This result is hardly surprising when we recall that second sound is primarily a thermal effect.

§ 13. THE REFLECTION OF SOUND

In this section we shall examine the problem of the reflection and transmission of a wave of sound incident normally of a plate of width d. Throughout, we shall use the concept of impedance introduced in § 4. The results obtained may be applied to such problems as that of determining the disturbance of first and second sound propagation due to a thermometer or to the reflection of the waves at a metal plate forming one end of a resonance chamber.

The boundary conditions at the two surfaces are given by the continuity of the 'current' I and the 'potential' ZI. Taking Z_s to be the impedance of the plate and Z_0 that of the surrounding liquid, we obtain for the ratio of reflected to incident current

$$\frac{I_r}{I_i}=\frac{(Z_0{}^2-Z_s{}^2)(1-m^2)}{(Z_0{}^2+Z_s{}^2)(1-m^2)+2Z_0Z_s(1+m^2)} \qquad \ldots\ldots (13.1)$$

and for the transmission coefficient

$$\frac{I_t}{I_i}=\frac{4mZ_0Z_s}{(Z_0{}^2+Z_s{}^2)(1-m^2)+2Z_0Z_s(1+m^2)}, \qquad \ldots\ldots (13.2)$$

where m is the factor (in general complex) by which the amplitude of a *single* wave is reduced on passing across the plate.

(i) *Application to reflection of first sound.* We take the velocity of motion as the 'current', and the fluctuation in pressure as the product of impedance and current. The impedance of the liquid is $Z_0=p/V=\rho_0u_0$ where ρ_0 and u_0 are respectively the density of the liquid and the velocity of first sound in it. Similarly for the plate, $Z_s=\rho_su_s$. Since the current of first sound undergoes only a change of phase in passing through the plate, $m=\exp(-i\omega\, d/u_s)$.

(ii) *Application to reflection of second sound.* Here, as in § 4, we take the flow of heat as the 'current', and the fluctuation in temperature divided by the mean temperature as the 'potential'. By (11.1), the impedance of the liquid is $Z_0=1/\rho TCu_2$, and by (11.5) that of the solid is $Z_s=1/\beta T(1+i)$, where $\beta=(\frac{1}{2}\omega\rho_{\text{sol}}C_{\text{sol}}K_{\text{sol}})^{\frac{1}{2}}$. The heat current in the solid is attenuated; by (11.4), $m=\exp[-d(1+i)(\frac{1}{2}\omega\rho_{\text{sol}}C_{\text{sol}}K_{\text{sol}})^{\frac{1}{2}}]$.

REFERENCES

Dingle, R. B., 1948, *Proc. Phys. Soc.*, **61,** 9; 1949, *Proc. Phys. Soc.* A, **62,** 648.
Gorter, C. J., and Mellink, J. H., 1949, *Physica*, **15,** 285.
Groenewold, H. J., 1939, *Physica*, **6,** 323.
Landau, L., 1941, *J. Phys. USSR*, **5,** 71; 1944, *Ibid.*, **8,** 1.
Lifshitz, E., 1944, *J. Phys. USSR*, **8,** 110.
London, F., and Zilsel, P. R., 1948, *Phys. Rev.*, **74,** 1148.
Meyer, L., and Band, W., 1947, *Phys. Rev.*, **71,** 828; 1948, *Ibid.*, **73,** 226, **74,** 386, 394.
Osborne, D. V., 1948, *Nature, Lond.*, **162,** 213.
Peshkov, V. P., 1948, *J. Exp. Theor. Phys., USSR*, **18,** 857.
Rayleigh, Lord, 1896, *The Theory of Sound*, 2nd edn. (London: Macmillan), Vol. II, § 247.

APPENDIX

THE JUSTIFICATION OF THE SOLUTIONS GIVEN IN §5 AND §6

In §5, we obtained our solutions by ignoring some coupling terms in (5.9) and (5.10). We shall now demonstrate that this procedure was justifiable. A similar justification may be given for the work of §6.

The values of u are given by the condition that (5.9) and (5.10) are consistent. We are at liberty to take any pair of the variables p', ρ', S' and T' as independent. Taking

$$\rho' = \left(\frac{\partial\rho}{\partial T}\right)_p T' + \left(\frac{\partial\rho}{\partial p}\right)_T p'$$

and

$$S' = \left(\frac{\partial\rho}{\partial T}\right)_p T' + \left(\frac{\partial S}{\partial p}\right)_T p',$$

we obtain from (5.9)

$$\left[u^2(1-\epsilon)\frac{\partial\rho}{\partial p} - 1 - \frac{u^2\epsilon\rho}{S}\frac{\partial S}{\partial p}\right]p' + \left[u^2(1-\epsilon)\frac{\partial\rho}{\partial T} - \frac{\epsilon\rho u^2}{S}\frac{\partial S}{\partial T}\right]T' = 0 \quad \ldots\ldots(\text{A1})$$

and from (5.10),

$$\left[u^2\left(\frac{\rho_n}{\rho_s} - \epsilon\right)\frac{\partial S}{\partial p} - \frac{u^2\epsilon S}{\rho}\frac{\partial\rho}{\partial p}\right]p' + \left[u^2\left(\frac{\rho_n}{\rho_s} - \epsilon\right)\frac{\partial S}{\partial T} - S^2 - \frac{u^2\epsilon S}{\rho}\frac{\partial\rho}{\partial T}\right]T' = 0. \quad \ldots\ldots(\text{A2})$$

These equations will be consistent if the determinant formed by the coefficients of p' and T' is identically zero. Putting $V = \epsilon u^2 = 4i\mu\omega/3\rho$, neglecting terms in V^2, and then making some thermodynamical transformations, we obtain

$$u^4 - u^2\left[\frac{\rho_s}{\rho_n}\frac{TS^2}{C_v} + \left(\frac{\partial p}{\partial\rho}\right)_S + \frac{V\rho}{\rho_n}\right] + \frac{TS^2}{C_v}\frac{\rho_s}{\rho_n}\left(\frac{\partial p}{\partial\rho}\right)_T$$
$$+ \frac{V\rho_s}{\rho_n}\left[\frac{TS^2}{C_v} + \left(\frac{\partial p}{\partial\rho}\right)_S - \rho S\left(\frac{\partial T}{\partial\rho}\right)_S - \frac{S}{\rho}\left(\frac{\partial p}{\partial S}\right)_\rho\right] = 0. \quad \ldots\ldots(\text{A3})$$

The last two terms in (A3) and the difference between the adiabatic and isothermal compressibilities are proportional to the coefficient of thermal expansion, and may be neglected in determining the attenuation due to viscosity. Hence

$$2u^2 = (u_1^0)^2 + (u_2^0)^2 + V\rho/\rho_n \pm [(u_1^0)^2 - (u_2^0)^2 + V(\rho_n - \rho_s)/\rho_n], \quad \ldots\ldots(\text{A4})$$

where $u_1^0 = (\partial p/\partial\rho)^{\frac{1}{2}}$ and $u_2^0 = (TS^2\rho_s/C\rho_n)^{\frac{1}{2}}$. The two solutions are those given by (5.13) and (5.14).

The Angular Distribution of Synchrotron Target Radiation: A Preliminary Experimental Study

J. D. LAWSON
Atomic Energy Research Establishment, Malvern

Communicated by D. W. Fry; MS. received 20th October 1949, and in amended form 25th January 1950

ABSTRACT. The angular distribution of radiation from a synchrotron has been measured with an ionization chamber for a number of different target materials and thicknesses, and the results have been compared with a simple theory in which the radiation from a parallel beam of electrons striking a thin plate has been calculated. Detailed comparison with theory is not possible, because the precise way in which the electrons hit the target cannot be determined, nevertheless qualitative explanations have been found for most of the effects observed. The most important of these is the relative insensitivity of forward intensity and beam width to target size and material.

---

§ 1. INTRODUCTION

In this paper the results of a preliminary study of the effect of target size and material on the radiation from a synchrotron are described. Several interesting effects have been observed, though further work would be needed to obtain a full understanding of the problem. Unfortunately the way in which the electrons hit the target is very complicated, so that a detailed comparison with theory is not possible. Nevertheless a simple idealized theory has proved to be a useful guide.

Polar diagram measurements taken with absorbers sensitive only to the higher energy quanta have been reported by other workers (for example, Allen-Williams and Appleyard 1949 a, b, Lees and Metcalfe 1950); their results are in fair agreement with those given here.

§ 2. MEASURING TECHNIQUE

The machine used in these experiments is described by Fry *et al.* (1948). It was normally run at an energy of 10 MeV., with an internal target, and electron spiral pitch at the target of $1{\cdot}6\times10^{-5}$ cm. The radiation intensity was measured with a cubical ionization chamber of side 9 cm., the front wall of which could be varied in thickness. The chamber could be moved about on a table in front of the machine, and the polar diagram measurements were taken with it 1 metre from the target. The chamber subtends an angle of 5° at the target, so that for narrow diagrams a check of the shape near the maximum was made at a distance of $2\frac{1}{2}$ metres.

The chamber simply measures ionization produced, it gives no indication at all of the quality of the radiation falling on its front wall. Some indication of this can be obtained by varying the wall thickness and examining the absorption curve produced, though such information is not usually precise enough to be of much value. It is easy to distinguish the hard gamma rays (1 to 20 MeV. say) from the softer radiation, but it is difficult to be much more precise than this.

§ 3. THEORETICAL DISCUSSION OF TARGET RADIATION

The electrons in a synchrotron give up their energy to the target partly by ionizing the atoms of which it is composed, and partly by making radiative collisions (bremsstrahlung). In addition they also undergo considerable elastic nuclear scattering. It is this elastic scattering which plays the predominant part in determining the polar diagram of the radiation.

It is instructive to consider what happens when a parallel beam of electrons falls on a thin plate of uniform thickness, although this is far simpler than the conditions which exist in a synchrotron, where the target geometry is much more complicated.

If the target thickness is expressed in 'radiation lengths' (defined as

$$A/(4\alpha NZ^2 r_0{}^2 \ln 183 Z^{-1/3}),$$

where r_0 = classical electron radius = $2{\cdot}82 \times 10^{-13}$ cm., N = Avogadro's number = $6{\cdot}02 \times 10^{23}$ and α = fine structure constant = 1/137) the angular distribution of elastically scattered electrons (for small angles of scatter) after passing through a thickness t is, as shown in the Appendix,

$$F(t, \theta) = \frac{E^2}{440\pi t} \exp(-E^2\theta^2/440t), \qquad \ldots\ldots(1)$$

where E is the electron energy (assumed large compared with the rest energy) expressed in Mev. This expression is obtained by taking a multiple convolution of the formula for single scattering, and is therefore inaccurate when t is very small or θ very large.

Now if the target is thin compared with one radiation length, the energy loss in it will be small, and particles will be equally likely to have radiative collisions at all values of t. If then $F(t, \theta)$ is integrated over t, and $\int F(t, \theta)\, dt$ is combined with the radiation polar diagram for a single collision, the result will be the overall polar diagram of the radiation from the target. Assuming intuitively that the radiation polar diagram for a single collision is a gaussian curve of r.m.s. angle $\sqrt{z}\mu/E$ (where μ is the rest energy of the electron) the resulting polar diagram, normalized to be unity at $\theta = 0$, may be written

$$P(E\theta) = [-\mathrm{Ei}\{-(E\theta)^2/440t + 2\mu^2)\} + \mathrm{Ei}\{-(E\theta)^2/2\mu^2\}]/\ln(1 + 220t/\mu^2). \qquad \ldots\ldots(2)$$

From this we see that the polar diagram width is inversely proportional to the incident electron energy, and is the same for all materials of equal thicknesses expressed in radiation lengths.* Polar diagrams for different values of t are shown in Figure 1.

The variation of forward intensity with target thickness may be readily found. It is convenient in this connection to define a quantity used in aerial theory called the 'gain' of the angular distribution; this is given by

$$G = 4\pi \Big/ \int P(E\theta) 2\pi \sin\theta \, d\theta$$

---

*This treatment is due to Schiff (1946), though in the analysis given here a simpler form is taken for the polar diagram of a single radiative collision. This simplifies the analysis and is justified by the fact that no accurate information is readily available. Recent calculations by Stearns (1949) show that the r.m.s. angle of radiation from a single collision is a slowly varying function of E/μ, the photon energy and the nuclear charge, and also that the angular distribution is not gaussian. The theory presented here must therefore be treated with reserve.

and would be equal to unity for an isotropic distribution. Now when θ is small so that $\sin\theta \simeq \theta$, it may be shown (see Appendix) that

$$G = \frac{E^2}{110t} \ln(1 + 220t/\mu^2). \qquad \ldots\ldots(3)$$

Now if σt is the proportion of the electron energy converted to radiation in a thickness t of the target, the fractional forward radiation intensity per unit solid angle is given by

$$R_{\theta=0} = \sigma Gt/4\pi. \qquad \ldots\ldots(4)$$

The quantity Gt/E^2 is plotted against target thickness t in Figure 2. The curve

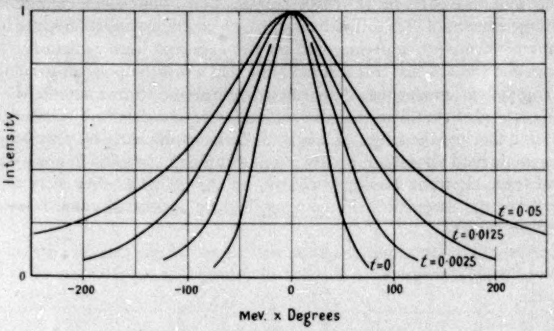

Figure 1. Theoretical polar diagrams for various thicknesses of target; horizontal scale in Mev. × degrees and vertical scale in arbitrary units of intensity.

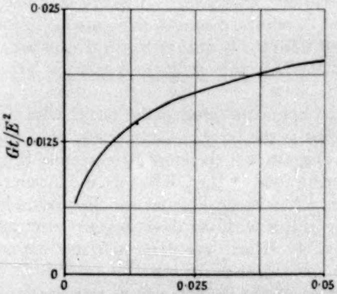

Figure 2. Theoretical curve of variation of forward intensity of radiation with target thickness. *Note*: the horizontal and vertical scales should be multiplied by 2.

rises steeply when t is small, but at larger values of t where the polar diagram width is controlled mainly by the scattering process, the forward intensity is relatively little affected by the target thickness.

The energy distribution of the radiation from a thin target will clearly be that from a single collision. For a thick target this distribution will be degraded, because some electrons will lose appreciable energy by ionization before radiating, and others will make more than one collision. The effect of the degradation from both these causes will be most marked in the radiation at large angles to the forward direction.

§ 4. EXPERIMENTAL RESULTS

(i) *Preliminary Experiments on the Nature of the Radiation*

Measurements were first made at 10 MeV. of the variation of ionization chamber reading with wall thickness. These showed that under some conditions there was a large amount of very soft radiation, which could be entirely stopped by about 1·5 gm/cm^2 of matter, superimposed on the expected hard radiation. Further investigation showed that this soft radiation had a broader polar diagram than the hard component and appeared to come from about 10 cm. outside the target. It was concluded therefore that the soft radiation consisted of electrons which had passed through the target, and been deflected sufficiently by it to escape from the magnetic field altogether, finally passing through the glass donut wall. The path of these electrons would, of course, be curved while they were under the influence of the magnetic field, causing them to appear to come from a point outside the target.

Increasing the ionization chamber wall about 1·5 gm/cm^2 did not affect the shape of the polar diagram, so that for all subsequent experiments this thickness was used.

(ii) *Polar Diagram Measurements for Different Targets*

In Figure 3 a number of polar diagrams with different targets all measured at an electron energy of 10 MeV. are shown. It will be seen that these are somewhat similar in shape to the theoretical diagrams of Figure 1. The apparent thicknesses of the targets deduced from the widths to half intensity are of the right order of magnitude, though the radiation at large angles is greater than might be expected.

The electron orbit contracts towards the target with a spiral pitch of about $1{\cdot}6 \times 10^{-5}$ cm.*, so that if the target is very thick, only its outer edge will be struck. The polar diagram will therefore be narrower than it would be if the whole target were being used. Allen-Williams and Appleyard (1949 a, b) have pointed out that this effect would account for the unsymmetrical shape of the diagram which is noticeable with the thick targets; electrons deflected inwards pass through more of the target than those deflected outwards, and thus more energy is radiated on one side than the other.

A slight broadening of the diagrams from thin targets might be expected, since as shown in § 4 (v), it is possible for electrons to pass more than once through the target. Such electrons, when they arrive at the target for the second time, would in general be moving at an angle to their original direction, so that effectively the beam striking the target would be divergent. This would broaden the polar diagram.

---

* The effective spiral pitch will however be much greater than this, since the electrons will be executing radial oscillations.

These considerations for thick and thin targets explain the fact that there is less variation in beam width from the various targets than might be expected from a direct application of the theory. The excessive radiation at large angles might be partly due to multiple radiation collisions in the target, but is probably also due to electrons which, after passing through the target, make radiative collisions in the doughnut walls.

(iii) *Effect of Changing the Electron Energy*

Diagrams from a 0·03 cm. diameter cylindrical tungsten target were measured at energies of 10 and 5 MEV., and the beam widths to half maximum amplitude were found to be 18° and 36°. $E\theta$ thus remained constant as demanded by the theory.

(iv) *Relative Forward Intensities for Different Target Materials*

The relative forward intensities from targets of different materials were measured with the aid of movable targets. The results for cylindrical targets of 0·085 cm. diameter made of tungsten, copper and aluminium, measured over the energy range 3–20 MEV. are shown in Figure 4. Although the thicknesses of the targets measured in radiation lengths are very different, the forward intensities from them are comparable. This is what would be expected from Figure 2, though the value for aluminium is too high. This is probably due to the multiple passage effect described in the next section. No accurate comparative measurements were made with tungsten targets of different diameters, though it was found that the forward intensity from a target of diameter 0·085 cm. was only about 15% higher than that from a target of diameter 0·013 cm.

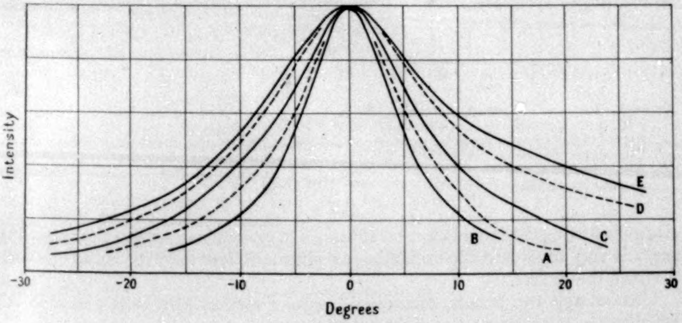

Figure 3. Polar diagrams of various targets measured at an electron energy of 10 MEV.

Curve	A	B	C	D	E
Material	Gold	Aluminium	Tungsten	Tungsten	Tungsten
Form	Foil	Wire	Wire	Wire	Wire
Thickness (cm.)	0·0013	0·085	0·013	0·05	0·2
Thickness (radiation lengths)	0·0042	0·009	0·039	0·15	0·6
Beam width to half maximum	13·5°	11°	18°	20·5°	24°
Apparent thickness (radiation lengths)	0·02	0·008	0·05	0·18	—

(v) *Experiments to Determine whether Multiple Passage through the Target Occurs*

It is suggested in § 4(ii) that electrons may pass through the target more than once. An electron might get scattered through a small angle with little loss of energy, and be refocused on the target (possibly after several revolutions) by the magnetic guide field. The scattered electrons leaving the target travelling at too wide angles or with too little energy would hit the donut walls or resonator, but those within about 3° which had not lost much energy would eventually pass through the target again. Since the period of oscillation bears no relation to the period of rotation (it will in fact be a function of the oscillation amplitude since the field index *n* varies with radius), the target might not be hit again for several revolutions, depending on its size. If now a larger target is placed at a slightly smaller radius than the original one, there will be a greater chance of electrons hitting the large target on subsequent revolutions, unless the scattering angle is very small and the oscillation amplitude is less than the radial distance between the targets.

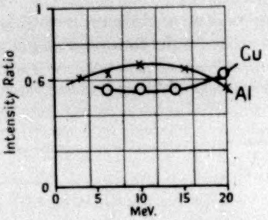

Figure 4. Ratio of forward intensity from 0·085 cm. diameter targets of aluminium and copper to that from an equal tungsten target. The target thickness in radiation lengths are: tungsten, 0·27; copper, 0·06; aluminium, 0·009.

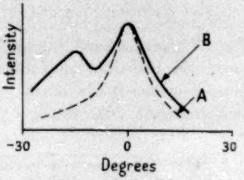

Figure 5. Curves obtained from the 'multiple passage' experiment using an aluminium target.

A. Orbit spiral 2×10^{-3} cm., outer target hit.

B. Orbit spiral $1{\cdot}6 \times 10^{-5}$ cm., both targets hit.

The relative intensities of the two curves are uncertain, but they are plotted for convenience with the same maximum value.

Accordingly two targets, each consisting of a vertical wire, were placed in the synchrotron at a very small radial separation, but an azimuthal separation of 15°; it was thus possible to see which target was being struck by measuring the output polar diagrams. An aluminium target showed considerable multiple passage when the electron spiral pitch was $1{\cdot}6 \times 10^{-5}$ cm., but very little when the spiral pitch was increased to 2×10^{-3} cm.* with the aid of pulsed contractor coils above and below the orbit. The diagrams obtained in this experiment are shown in Figure 5 and some results are tabulated below. Thicknesses are in radiation lengths.

Outer target	Thickness	Inner target	Spiral pitch	Results
0·0125 cm. W	0·038	0·05 cm. W	$1{\cdot}6 \times 10^{-5}$ cm.	No multiple passage
0·085 cm. Al	0·009	0·05 cm. W	$1{\cdot}6 \times 10^{-5}$ cm.	Multiple passage occurs
0·085 cm. Al	0·009	0·05 cm. W	2×10^{-3} cm.	Very little multiple passage

---

* Changing the spiral pitch by this amount appeared to make no difference to the output or polar diagram of the thicker targets.

The radiation from the aluminium target is in a narrower polar diagram when there is little multiple passage, as might be expected.

A second similar experiment with a gold foil target of thickness 0·0013 cm. (0·0043 radiation length) likewise showed multiple passage effects, both at spiral pitches of $1{\cdot}6 \times 10^{-5}$ cm. and 2×10^{-3} cm.

§ 5. CONCLUSION

Experiments have shown that it is not possible to exert much control over the intensity or angular distribution of synchrotron target radiation by varying the target material or geometry. Measurements on a series of targets show a variation by a factor of about two in both beam width and intensity. These results are in good general agreement with a simple theory. The theory cannot however be applied directly, because multiple passage occurs in thin targets, making them effectively thicker, whereas only the outer edge is effective in thick targets, which therefore appear thinner.

ACKNOWLEDGMENTS

The author wishes to acknowledge helpful discussions on the subject of this paper with Mr. R. K. Appleyard of the Medical Research Council, and Messrs. F. K. Goward and A. G. Ward of the Atomic Energy Research Establishment. He also wishes to thank Mr. H. E. Walford, who constructed the targets and the device for moving them while in the doughnut.

The work was carried out at Malvern in the Electronics Division of the Atomic Energy Research Establishment, and is published by permission of the Director.

REFERENCES

Allen-Williams, D. J., and Appleyard, R. K., 1949 a, *Brit. J. Radiology*, **22**, 106; 1949 b, *Proc. Camb. Phil. Soc.*, **45**, Part 2, 305.
Fry, D. W. *et al.*, 1948, *Nature, Lond.*, **161**, 504.
Lees, D. J., and Metcalfe, L. H., 1950, *Proc. Phys. Soc.* A, **63**, 661.
Rossi, B., and Greisen, K., 1941, *Rev. Mod. Phys.*, **13**, 240.
Schiff, L. I., 1946, *Phys. Rev.*, **70**, 87.
Stearns, M., 1949, *Phys. Rev.*, **76**, 836.

APPENDIX

DERIVATION OF EQUATIONS (1) AND (2)

Rossi and Greisen (1941, §23) show that the distribution of electrons after multiple scattering through a thin plate is approximately gaussian. For high energy electrons the distribution function may be written

$$F(t,\theta)=\frac{E^2}{880\pi t}\exp\left(-E^2\theta^2/880t\right), \qquad \ldots\ldots(1)$$

where E is the energy of the electrons in MeV., and t is the thickness of the plate in radiation lengths. The function has been normalized so that its integral over all angles is unity.

Now if the target is so thin that the energy loss of electrons passing through it is small, and the scattering angle is not too large, there will be an equal amount of radiation from a thickness δt of the target at all values of t. The angular distribution of the radiation from a layer of thickness δt at a depth t in the target will be a convolution of the expression in equation (1) and the expression for the radiation polar diagram for a single radiative collision. (The convolution of two two-dimensional gaussion distributions of r.m.s. angles $\sqrt{2}\theta_1$ and $\sqrt{2}\theta_2$ (written as $\exp[-\theta^2/2\theta_1^2]*\exp[-\theta^2/2\theta_2^2]$) may be shown to be

$$2\pi\frac{\theta_1^2\theta_2^2}{\theta_1^2+\theta_2^2}\exp[-\theta^2/2(\theta_1^2+\theta_2^2)]$$

when θ_1 and θ_2 are small.) The polar diagram of a radiative collision is assumed to be of the form

$$H(\theta)=\frac{E^2}{2\pi\mu^2}\exp(-\tfrac{1}{2}\theta^2E^2/\mu^2), \qquad \ldots\ldots(5)$$

where μ is the rest energy of the electron.

If now $\sigma\delta t$ is the proportion of the electron energy converted to radiation in a thickness δt of the target, the radiation per unit solid angle from such a layer will be given by

$$\begin{aligned}\delta R&=\sigma\delta t\frac{E^2}{440\pi t}\exp(-E^2\theta^2/440t)*\frac{E^2}{2\pi\mu^2}\exp(-\tfrac{1}{2}E^2\theta^2/\mu^2)\\&=\frac{E^2\sigma\delta t}{2\pi(220+\mu^2)}\exp[-\tfrac{1}{2}\theta^2E^2/(220t+\mu^2)],\end{aligned}$$

whence by proceeding to the limit and integrating from 0 to t

$$R=\frac{\sigma E^2}{440\pi}[-\mathrm{Ei}\{-\tfrac{1}{2}E^2\theta^2/(220t+\mu^2)\}+\mathrm{Ei}\{-\tfrac{1}{2}E^2\theta^2/\mu^2\}]. \qquad \ldots\ldots(6)$$

Equation (2) may be obtained by normalizing this expression to be unity when $\theta=0$.

The gain may be found by putting $\theta=0$ in equation (6); this gives

$$R_{\theta=0}=\frac{\sigma E^2}{440\pi}\ln(1+220t/\mu^2).$$

Now the fraction of energy radiated per electron is σt, so that $R_{\theta=0}=G\sigma t/4\pi$, whence

$$G=\frac{E^2}{110t}\ln(1+220t/\mu^2).$$

The function $-\mathrm{Ei}(-y)$ is defined as $\int_y^\infty y^{-1}e^{-y}\,dy$ and is tabulated in Jahnke and Emde, *Tables of Functions*, p. 6. When $\theta=0$ equation (2) is indeterminate and the asymptotic relation $-\mathrm{Ei}(-y_1)+\mathrm{Ei}(-y_2)\simeq\ln(y_2/y_1)$ must be used.

LETTERS TO THE EDITOR

Measurement of Polar Diagram of Synchrotron Gamma Radiation

In support of work by Lawson (1950), described in this issue, it was considered desirable to measure the polar diagram of the radiation from a machine similar to his by using a detector sensitive to high energy quanta only. For this purpose copper was irradiated to give the ^{62}Cu positron activity with half-life 10·5 minutes as suggested by Allen-Williams and Appleyard (1949 a, b). Baldwin and Klaiber (1948) have measured the cross section for the activation, and copper may be considered to be effectively a resonance detector at 22 Mev. A further purpose of the experiment was to use detectors smaller than those used by Lawson or Allen-Williams and Appleyard and to measure the diagram in two planes at right angles.

The machine used in the experiment was described by Fry *et al.* (1948). The electrons were allowed to shrink on to a tungsten target by turning off the radio frequency just before the peak of the magnetic field cycle, and struck the target with an energy of 24 Mev. The copper samples were about 1 cm. square and 1 mm. thick, weighing 1 gm., and the activity after irradiation was measured with a standard G.M.4 end window counter. Detectors in various positions were given a standard irradiation as measured by an ionization chamber. The results are plotted as initial induced activity against position of sample in the Figure, curve (*a*) showing the horizontal polar diagram and (*b*) the vertical diagram, the vertical diagram being measured at the peak of the horizontal one and vice versa. Two sets of results were taken at different distances from the x-ray source, the ordinates being corrected by assuming an inverse square law. The agreement may be taken as a measure of the accuracy of the experiment. It will be seen that the horizontal curve is not symmetrical; it shows the broadening due to deflection of the electrons towards the thicker parts of the target, as mentioned by Allen-Williams and Appleyard, and by Lawson. The vertical polar diagram is, however, quite symmetrical.

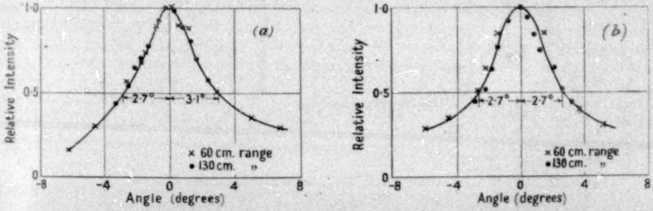

Polar diagrams of radiation from 24 Mev. synchrotron in region 11–24 Mev.

(*a*) Horizontal polar diagram. (*b*) Vertical polar diagram. Obtained with tungsten target consisting of a 0·005 in. foil bent into a cylinder of 0·36 cm. diameter. Orbital spiral pitch of the order of 10^{-5} cm.

Atomic Energy Research Establishment,
Harwell.
17th November 1949.

D. J. Lees.
L. H. Metcalfe.

Allen-Williams, D. J., and Appleyard, R. K., 1949 a, *Brit. J. Rad.*, **22,** 106; 1949 b, *Proc. Camb. Phil. Soc.*, **45** (Part 2), 305.
Baldwin, G. C., and Klaiber, G. S., 1948, *Phys. Rev.*, **73,** 1156.
Fry, D. W., Gallop, J. W., Goward, F. K., and Dain, J., 1948, *Nature, Lond.*, **161,** 504.
Lawson, J. D., 1950, *Proc. Phys. Soc.* A, **63,** 653.

Identification of Photo-Disintegration Stars in Nuclear Emulsions

Nuclear emulsions, irradiated by a continuous spectrum of gamma-rays extending to energies between 23 and 25 MeV., have been found to contain charged particle stars arising from the photo-disintegration of boron, carbon and oxygen (Goward, Titterton and Wilkins 1949, 1950, Goward, Telegdi and Wilkins 1950). In this work the criterion of 'momentum balance' was used to develop accuracy of measurement, and the present letter states the limits of resolution and identification so far achieved. This information is essential to a discussion of a new reaction in nitrogen, given in a companion letter henceforward referred to as B (Wilkins and Goward 1950). It may also be of assistance in similar nuclear emulsion work where the measurement accuracy is not explicitly determined.

If the identities of the particles of a photo-disintegration star are known, the particle energies $E_r (r=1, 2 \ldots)$ in MeV., and the momenta, p_r, in units of (MeV × mass number)$^{1/2}$, may be determined. The momentum, p_γ, of the gamma-ray is $(E_T + E_0)/43{\cdot}1$, where $E_T = \Sigma E_r$ and E_0 is the threshold of the reaction, so that, for conservation of momentum $\Delta = (\Sigma p_r) - p_\gamma = 0$. Thus $|\Delta|$ is a convenient measure of the overall accuracy.

When the reliability of an experimenter has been established by statistics on attested reactions, his ability to distinguish other reactions may be inferred. Such a test is necessary since wide variations have been found in the statistics of individuals; these variations should disappear if accuracy statistics are used to cultivate a measurement technique. Some statistics for measurements by the authors on carbon and oxygen stars in boron-loaded Ilford E1 emulsions are shown in Figures 1 (*a*) and 1 (*b*). $|\Delta|$ was found to be almost independent of E_T or E_r, unless a particle had a range less than about 2 microns. An approximate theoretical curve is fitted to Figure 1 (*a*) by assuming that the measurements give three rectangular components of Δ independently and with equal accuracy. No re-measurements were taken after $|\Delta|$ had been evaluated, so that the statistics give a realistic estimate of the accuracy expected in unknown reactions. Figure 1 (*d*) shows statistics which are considered typical of uncultivated measurements by otherwise experienced individuals. All the authors' measurements were made, using a magnification of 1400, on unselected stars; emulsion shrinkage factors were measured directly by a micrometer.

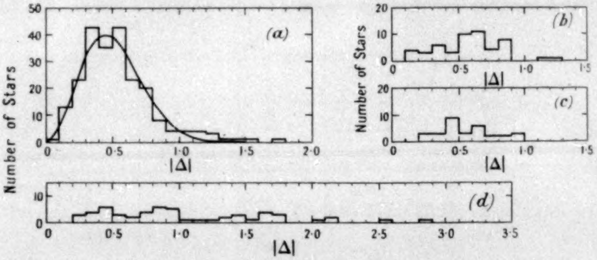

Figure 1. Statistics of $|\Delta|$ for boron loaded EI plates.

(*a*) 228 carbon star measurements by the authors. Superposed is a curve of the form $N = (K|\Delta|)^2 \exp -(K|\Delta|)^2$.

(*b*) 51 oxygen star measurements.

(*c*) Measurements on 31 stars attributable to ^{10}B(γ, D) or ^{11}B(γ, T) reactions.

(*d*) Carbon star measurements by three other experimenters, considered representative.

The allocation of stars to appropriate energetically possible reactions is conveniently accomplished by first considering that all stars consist of alpha-particle tracks only, and calculating corresponding $|\Delta|$ values. The results, for all three-particle stars in the E1 emulsions of Figure 1 are shown in Figure 2. Almost complete resolution of the carbon stars is apparent, with $|\Delta| < 1{\cdot}0$. For all stars with $|\Delta| > 0{\cdot}8$, appropriate tracks are reconsidered as ^{2}H, ^{3}H, ^{6}Li, etc., and the possibility of overlooking a fourth track is also investigated (see B); the appearance of the tracks serves to confirm the $|\Delta|$ analysis. Figure 1 (*c*) shows, for example, how a group tentatively attributable to the reactions ^{11}B(γ, T) and ^{10}B(γ, D) is resolved in this way. The ^{10}B(γ, pn) reaction gives an exceptional group of stars in which $|\Delta| \neq 0$, owing to the unobserved neutron present. Stars attributed to one or other of the boron reactions are indicated by full shading in Figure 2, but the extent to which they may be distinguished from each other, in relation to the results of the present letter, will be described in a later publication.

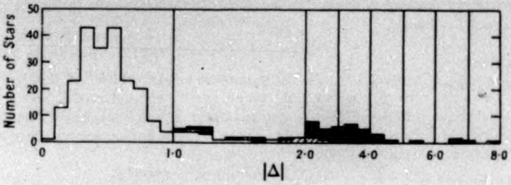

Figure 2. $|\Delta|$ values for 3-particle stars, treating all tracks as alpha particles. Unshaded rectangles indicate 228 carbon stars, fully shaded rectangles indicate 47 boron stars, and half-shaded rectangles indicate the 8 events discussed in B.

Figures 1 (*b*) and 2 represent all three- and four-particle stars observed, including those discussed in B, but excepting several stars readily identified (from appearance, energy and momentum balance considerations) as radioactive contamination stars or collisions (between, for example, protons and protons). Only 3% of the events, shown in Figure 1 (*a*) as the tail of the carbon star statistics lying outside the fitted curve, can be considered as of doubtful identity.

Atomic Energy Research Establishment,
Harwell, Didcot, Berks.
3rd February 1950.

F. K. Goward.
J. J. Wilkins.

Goward, F. K., Telegdi, V. L., and Wilkins, J. J., 1950, *Proc. Phys. Soc.* A, **63**, 402.
Goward, F. K., Titterton, E. W., and Wilkins, J. J., 1949, *Proc. Phys. Soc.* A, **62**, 460; 1950, *Ibid.*, **63**, 172.
Wilkins, J. J., and Goward, F. K., 1950, *Proc. Phys. Soc.* A, **63**, 663.

Identification of Nitrogen Photo-Disintegration Stars in Nuclear Emulsions

Of the 283 three-particle stars found in the emulsions discussed in the companion letter (Goward and Wilkins 1950), six have been attributed to the reaction

$$^{14}\text{N} + h\nu \rightarrow {}^{6}\text{Li} + 2\,{}^{4}\text{He} - 16{\cdot}1 \text{ Mev.} \qquad \ldots\ldots (1)$$

The following discussion of the certainty of this assignation provides an excellent example of the value and limitations of the identification methods described.

For the present purposes, a sufficiently accurate range–energy relation for ^{6}Li nuclei in nuclear emulsions was derived directly from that for alpha-particles (by adapting to ^{6}Li nuclei the electron capture and loss data for alpha-particles reviewed by Knipp and Teller (1941)). The momentum of a ^{6}Li nucleus of a few Mev. energy is nearly twice that of an alpha-particle of the same range. An important consequence follows, namely that the main difficulty in identifying stars from reaction (1) is to avoid confusion with the four-particle reaction

$$^{16}\text{O} + h\nu \rightarrow 4\,{}^{4}\text{He} - 14{\cdot}5 \text{ Mev.}, \qquad \ldots\ldots (2)$$

rather than (as might be expected) with the three-particle reaction

$$^{12}\mathrm{C} + h\nu \rightarrow 3\,^{4}\mathrm{He} - 7{\cdot}3\ \mathrm{MeV}. \qquad \ldots\ldots(3)$$

As shown in Figure 1, the latter differentiation is quite conclusive with the present resolution.

A reaction (2) star, however, may be mistaken for a three-particle star when the fourth track is (*a*) nearly coincident with another track or (*b*) too short to be detected. In either case, if the vector difference in momentum between the undetected particle and any other is small, satisfactory momentum balance when interpreted as a reaction (1) event is probable. Small vector differences in momentum have, in fact, proved to be common, since a ground state ^{8}Be nucleus is a frequent intermediate product in the formation of oxygen stars. If E^* is the energy released when an ^{8}Be nucleus disintegrates into two alpha-particles of energies E_A and E_B, then

$$E^* = \tfrac{1}{2}(E_A + E_B) - (E_A E_B)^{1/2} \cos\phi, \qquad \ldots\ldots(4)$$

where ϕ is the angle of separation of the alpha-particle tracks. Here E^* is only of the order of 0·1 MeV., and the resulting tracks will therefore be little separated. Two coincident tracks ($\phi = 0$) of slightly different lengths may be obtained, and have in fact been detected on close examination of appropriate stars. (Further details of the oxygen disintegrations must be left for a future publication.)

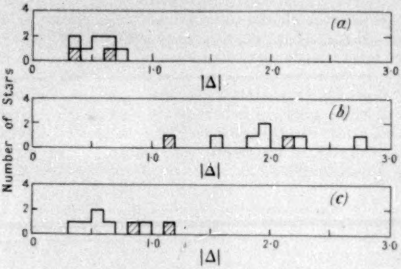

Figure 1. |Δ| values for eight suspected ^{14}N photo-disintegrations considered as
(*a*) ^{14}N disintegrations.
(*b*) ^{12}C disintegrations.
(c) ^{16}O disintegrations.

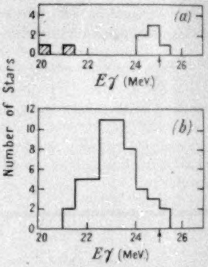

Figure 2. Variation of number of stars with energy of incident quanta.
(*a*) eight suspected ^{14}N disintegrations.
(*b*) 51 ^{16}O disintegrations.

With the above possibilities in mind, eight stars remained with no detectable fourth track, good momentum balance as nitrogen events and poor balance as carbon events, as shown in Figures 1 (*a*) and 1 (*b*). The energy and momentum of a possible undetected fourth track may be calculated from equation (4), putting $\phi \simeq 0$ and $E^* \simeq 0{\cdot}1$ MeV. The momentum unbalance data obtained on this assumption is shown in Figure 1 (*c*), and comparison with Figure 1 (*a*) gives no conclusive result. Moreover, the identity of two of the stars, indicated by shading in the Figures, at once becomes doubtful when it is observed that their possible fourth tracks would be practically undetectable (less than one micron long). The remaining six stars, if from reaction (2), should show detectable fourth tracks, 1·5 to 3 microns long (alpha-particle energies of 1·4 MeV. (4·7 microns) and 0·6 MeV. (2·4 microns) correspond to a ^{6}Li energy of 2·6 MeV.). Coincident tracks of about this length have proved to be distinguishable, as mentioned above, and on this evidence the six events may be assigned to reaction (1).

A final test is to plot the total energy of the particles of each star, E_T, plus 16·1 MeV., i.e. the incident gamma-quantum energy E_γ, as in Figure 2 (*a*). The same two events as above (which have low E_γ values) are again suspect, but the identity of the remaining six is confirmed. This is best illustrated by comparison with Figure 2 (*b*), which shows E_γ (or

$E_\gamma + 14{\cdot}5$ MEV.) for a greater number of oxygen stars. Consistency with the known peak energy of the gamma-ray spectrum, and with the relative threshold energies of the two reactions is satisfactory. On the basis of the six selected stars, reaction (1) may be assumed to occur with a cross section of the order of 10^{-28} cm^2 at around 25 MEV.

A possible alternative reaction in nitrogen is

$$^{14}\mathrm{N} + h\nu \rightarrow {}^{2}\mathrm{H} + 3\,{}^{4}\mathrm{He} - 17{\cdot}6 \text{ MEV.} \qquad \ldots\ldots (4)$$

There is no definite evidence for this reaction, although it would be possible to consider some of the shorter alpha-particle tracks in oxygen stars as deuterons without significantly altering the momentum balance.

Atomic Energy Research Establishment,
Harwell, Didcot, Berks.
6th February 1950.

J. J. WILKINS.
F. K. GOWARD.

GOWARD, F. K., and WILKINS, J. J., 1950, *Proc. Phys. Soc.* A, **63,** 662.
KNIPP, J., and TELLER, E., 1941, *Phys. Rev.*, **59,** 659.

Alpha-Particles from ^{27}Al + D

Groups of alpha-particles from the reaction ^{27}Al(d, α)^{25}Mg have been observed, using a differential ionization chamber with electron collection in argon. A thin target of aluminium, about 0·5 mm. air equivalent evaporated on brass, was bombarded with deuterons of 0·93 MEV. and the alpha-particles emitted were observed at 90° to the incident beam within a cone of semi-angle 10°. An air absorption cell of fixed length and variable pressure was mounted between target and chamber, so that particle ranges from 2·0 to 6·0 cm. could be measured.

The variation of counting rate with absorber pressure is shown in the Figure. Seven groups of particles can be distinguished. Those lettered B, C, D, E and F can be attributed to the ^{27}Al(d, α) reaction. Group A is due, mainly at least, to the ^{13}C(d, α) process in a thin layer of carbon contamination. The detector was biased so as not to record pulses from single protons or deuterons, but group G can be ascribed to protons from the ^{16}O(d, p) reaction, sufficiently intense to give multiple pulses. Similarly, the rise of counting rate at pressures below group A is caused by scattered deuterons. (By changing the bias on

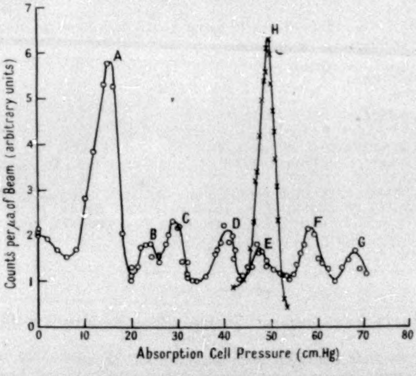

Alpha-particle groups emitted in the bombardment of aluminium by deuterons of 0·93 MEV. energy and from a ThC source.

the detector, it was always possible to distinguish alpha-particles from protons or deuterons.) Groups A and G, and also the rise of counting rate below A, were observed when a blank target was bombarded under the same conditions.

In order to convert the pressure measurements to mean ranges, the alpha-particle groups from ThC and from ^{13}C(d, α) were used. Group H (see Figure) was obtained by mounting on the target a thin source of thorium-active deposit; the position of the carbon group was established accurately during the blank run. The ranges of these groups were taken as 4·70 and 2·91 cm. respectively, the latter being based on recent measurements by Buechner *et al.* (1949), and the Cornell 1938 range–energy relation (Holloway and Livingston 1938).

The ranges, alpha-energies and *Q* values for the Al(d, α) groups are tabulated below.

Group	Absorber pressure (cm.)	Mean range (cm.)	α-energy (Mev.)	*Q* (Mev.)
B	23·8	3·34	4·83	4·75
C	29·8	3·66	5·14	5·08
D	41·0	4·24	5·64	5·68
E	47·7	4·60	5·95	6·04
F	58·8	5·18	6·43	6·62

An error of about ±0·05 Mev. is associated with any of the energies or *Q* values given in the Table.

It seems certain that group F corresponds to the transition to the ground state of ^{25}Mg; the *Q* value of 6·62 Mev. may be compared with the figure 6·46 Mev. given by Pollard *et al.* (1949), who observed four groups in all at 3 Mev. deuteron energy; in the present experiment the lowest of these would be at the position of the carbon group.

The *Q* values given in the Table indicate excited states in ^{25}Mg at 0·58, 0·94, 1·54 and 1·87 Mev. above the ground state. The first two of these agree well with the results of Allan *et al.* (1949). The energy release in the ground-state transition can be taken with the *Q* value 5·03±0·05 Mev. for the ^{24}Mg(d, p) reaction (Allan and Wilkinson 1948), to give a *Q* of 1·59±0·07 Mev. for the reaction ^{27}Al(p, α). A recent study of this reaction (Freeman, private communication) has yielded a value of 1·58±0·01 Mev., with which our result is thus consistent.

One of us (P.B.T.) is indebted to the Royal Commissioners for the Exhibition of 1851 for the award of an overseas scholarship.

Cavendish Laboratory,
Cambridge.
24th February 1950.

A. P. French.
P. B. Treacy.

Allan, H. R., and Wilkinson, C. A., 1948, *Proc. Roy. Soc.* A, **194,** 131.
Allan, H. R., Wilkinson, C. A., Burcham, W. E., and Curling, C. D., 1949, *Nature, Lond.*, **163,** 210.
Buechner, W. W., Strait, E. N., Sperduto, S., and Malm, R., 1949, *Phys. Rev.*, **76,** 1543.
Holloway, M. G., and Livingston, M. S., 1938, *Phys. Rev.*, **54,** 18.
Pollard, E. C., Sailor, V. L., and Wyly, L. D., 1949, *Phys. Rev.*, **75,** 725.

Alpha-Particles from ^{19}F Bombarded with Deuterons

It is well known that deuteron bombardment of ^{19}F causes the emission of several alpha-particle groups (Burcham and Smith 1938). These have been ascribed to the reaction ^{19}F(d, α)^{17}O, but the process ^{19}F(d, n), followed by break-up of the resulting ^{20}Ne* into ^{16}O and an alpha-particle, is also energetically possible. We have made a study of the alpha-particles to find which, if any, of the groups were due to this second process, and whether they could be related to known levels in ^{20}Ne (Bonner 1940, Powell 1943).

The method was simply to observe the dependence of particle energy on deuteron bombarding energy. In the process ^{19}F(d, n) nearly all of the bombarding energy is carried away by the neutron so that the variation of alpha-particle energy is small. In the reaction ^{19}F(d, α) on the other hand, most of the kinetic energy of the colliding nuclei is given to the alpha-particle. In our experiment alpha-particles from a thin CaF_2 target (0·5 mm. air equivalent) were observed at 90° to the incident beam, and bombarding energies of 0·63 and 0·93 MeV. respectively were used. The expected shifts of mean alpha-particle energy under these conditions are +0·22 MeV. for the direct transition and −0·005 MeV. for the two-stage process. For alpha-particle energies from ~3·5 MeV. to ~7 MeV., measurements were made with a differential ionization chamber and absorption cell; the region between 2 and 3 MeV. was studied with a magnetic analyser and scintillation counter (Burcham and Freeman 1949).

The results are shown in the Figure in the form of numbers–energy curves. No attempt has been made to link the magnetic analyser measurements with the rest. In addition measurements on the lowest peak of the curve obtained using the differential chamber were repeated, using a higher bias setting of the discriminator (full circles) to ensure that the position of the maximum was not affected by scattered deuterons. Seven peaks can be distinguished. That labelled A is due to an intense group of protons and was therefore not studied in detail. Group D arises from carbon contamination on the target, as was verified by its position and the increase of its intensity with time. The remainder can be attributed to fluorine. It will be seen that the positions of peaks B, E, F and G change noticeably with bombarding energy, whereas peak C is broadened (as one would expect), but

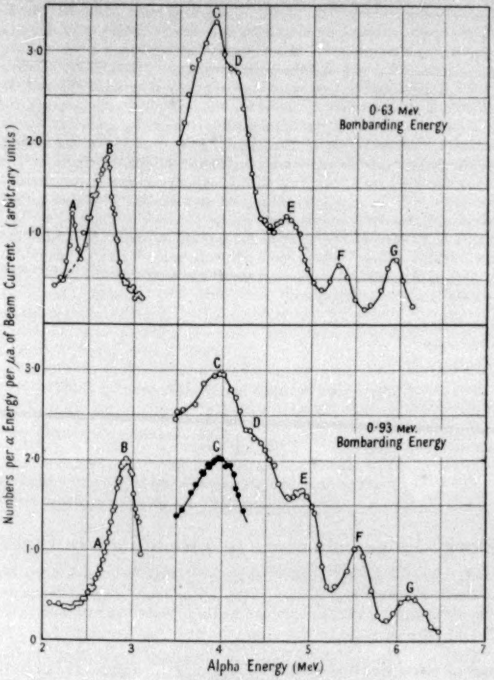

Energy distributions of alpha-particles emitted by fluorine bombarded with deuterons of 0·63 and 0·93 MeV.

only slightly shifted; From the diagram the following table can be constructed; E_b indicates bombarding energy.

Group	α-energy (Mev.)		Difference
	$E_b = 0{\cdot}63$ Mev.	$E_b = 0{\cdot}93$ Mev.	(Mev.)
B	2·70	2·93	0·23
C	3·90	3·96	0·06
E	4·71	4·91	0·20
F	5·31	5·54	0·23
G	5·93	6·16	0·23

One can conclude that groups B, E, F and G are due to the reaction ^{19}F(d, α)^{17}O, the corresponding Q values being 2·81, 5·26, 6·03, 6·79 Mev. The last three of these are consistent with values obtained by Burcham and Smith (1938), who did not study lower energies. Assuming that group C arises from the two-stage process described above, one obtains a value of 9·7 Mev. for the corresponding level in ^{20}Ne. This is not in good agreement with results obtained on neutron spectra by Bonner (1940) and Powell (1943), but it is difficult to find another mechanism which could be responsible for this group. The shift of the peak of group C, though slight, appears to be quite genuine and may point to the presence of a relatively weak unresolved ^{19}F(d, α)-group in this region. No group was found in the present experiment corresponding to the 7·8 Mev. level in ^{20}Ne reported by Powell, nor has this level been identified in experiments on scattering of alpha-particles by oxygen (Brubaker 1938, Devons 1939, Ferguson and Walker 1940), so it seems likely that alpha-emission from this level is forbidden.

Thanks are due to Miss J. M. Freeman for making available the magnetic analyser used in these experiments. This work has been made possible for two of us (P.M. and P.B.T.) by assistance from the British Council and the Royal Commissioners for the Exhibition of 1851 respectively.

Cavendish Laboratory,
Cambridge.
24th February 1950.

A. P. French.
P. Meyer.
P. B. Treacy.

Bonner, T. W., 1940, *Proc. Roy. Soc.* A, **174**, 339.
Brubaker, G., 1938, *Phys. Rev.*, **54**, 1011.
Burcham, W. E., and Freeman, J. M., 1949, *Phil. Mag.*, **40**, 807.
Burcham, W. E., and Smith, C. L., 1938, *Proc. Roy. Soc.* A, **168**, 176.
Devons, S., 1939, *Proc. Roy. Soc.* A, **172**, 127.
Ferguson, A. J., and Walker, C. R., 1940, *Phys. Rev.*, **58**, 666.
Powell, C. F., 1943, *Proc. Roy. Soc.* A, **181**, 344.

The Energy-Release in some (pα) Reactions in Light Nuclei

Q-values for the reactions ^{27}Al(pα)^{24}Mg and ^{23}Na(pα)^{20}Ne have been determined, as already described (Freeman and Baxter 1948), by measuring the differences between the ranges of the alpha-particle groups obtained in these reactions and that from the reaction ^{19}F(pα)^{16}O*; the range of alpha-particles from the latter was found absolutely by comparison with a thorium-C source. The corresponding energies were taken from the 1938 Cornell range–energy curve for alpha-particles (Holloway and Livingston 1938), and the Q-values then computed. Recent determinations, based on direct energy measurements, of the energy-release in the reaction ^{19}F(pα)^{16}O* (Burcham and Freeman 1949 a, Chao, Tollestrup, Fowler and Lauritsen 1949, Strait, Van Patter and Buechner 1950) have shown that the result obtained from the range measurement is too low, possibly because the range–energy curve is not accurate in this region. The range comparisons mentioned above can now be used to recalculate the alpha-particle energies, and hence the Q-values, for the aluminium and sodium reactions, because the ranges of the alpha-particle groups emitted in the three reactions are close together and only the slope of the range–energy curve over a limited region is required. This slope appears, from our range measurements and from other work, to be fairly reliable in the 2 Mev. region. The most accurate Q-value available for the ^{19}F(pα)^{16}O* reaction is 1·977 ± 0·008 Mev. (Chao *et al.* 1949), and with this the energy-releases in ^{27}Al(pα)^{24}Mg and ^{23}Na(pα)^{20}Ne become 1·57 ± 0·03 Mev. and 2·37 ± 0·045 Mev. respectively.

As a check on these results direct energy measurements of the alpha-particle groups have now been made with the aid of a magnetic analyser, calibrated with particles of known energy as previously described (Burcham and Freeman 1949 b), and thin targets of Al and NaCl. Corrections were made for target thickness and carbon contamination, and the energy of the alpha-particles emitted in the reaction $^{27}\text{Al}(p\alpha)^{24}\text{Mg}$ at a proton bombarding energy of 940 kev. and an angle of 135° was then found from several measurements to have the mean value 1·991 ± 0·010 Mev., giving a *Q*-value of 1·585 ± 0·015 Mev., in agreement with the previous figure, and consistent with the value 1·59 ± 0·07 Mev. (French and Treacy 1950) deduced from the reactions $^{27}\text{Al}(d\alpha)^{25}\text{Mg}$ and $^{24}\text{Mg}(dp)^{25}\text{Mg}$. For the reaction $^{23}\text{Na}(p\alpha)^{20}\text{Ne}$ the energy of alpha-particles emitted at 135° with a proton bombarding energy of 590 kev. was measured as 2·28 ± 0·03 Mev., giving a *Q*-value of 2·34 ± 0·04 Mev.; the probable error in this case was larger because of greater uncertainty in the analyser calibration in this region. The mean *Q*-value from the range and energy measurements is 2·35 ± 0·04 Mev.

Adding the new *Q*-value for $^{19}\text{F}(p\alpha)^{16}\text{O}^*$ and the energy of the gamma-radiation from the excited $^{16}\text{O}^*$ gives the energy-release in the reaction $^{19}\text{F}(p\alpha)^{16}\text{O}$ as 8·10 ± 0·03 Mev., according to Chao *et al.* (1949). The energy-release in this reaction has been determined here by comparing the range of the alpha-particle group with that from the reaction $^{7}\text{Li}(p\alpha)^{4}\text{He}$ and using for the latter the *Q*-value 17·28 ± 0·03 Mev. found by Smith (1939). Thin targets of calcium fluoride and oxidized lithium were mounted on a rotatable target head so that either target could be irradiated with a proton beam of 840 kev. energy, and the alpha-particles emitted at 90° passed through a mica window of 3·9 cm. stopping power into a shallow air-filled ionization chamber whose distance from the window could be varied. The difference in the extrapolated ranges of the two groups was found to be 2·828 ± 0·007cm. of standard air. Corrections were applied for straggling and variation in stopping power of the mica window; the range–energy relation, which is well-established in the required region, was used and a value of 7·075 ± 0·030 Mev. was deduced for the energy of the alpha-particles from the fluorine reaction. This result gives a *Q*-value of 8·06 ± 0·04 Mev., which is consistent with the value quoted above and in good agreement with the recently published value (8·068 Mev.) of Strait *et al.* (1950).

In the course of this work similar observations were made on the reactions $^{15}\text{N}(p\alpha)^{12}\text{C}$ and $^{18}\text{O}(p\alpha)^{15}\text{N}$. Thick targets of aluminium nitride and copper oxide were used, and a mica window of 2 mm. stopping power. In each case the range of the alpha-particle group was compared with that from a thorium-C source (extrapolated range assumed to be 4·796 cm.) inserted in place of the target button. The *Q*-values thereby deduced were 4·96 ± 0·05 Mev. and 3·97 ± 0·05 Mev. for the nitrogen and oxygen reactions respectively, in good agreement with the values of Burcham and Smith (1939).

The *Q*-value results presented are summarized below:

$^{27}\text{Al}(p\alpha)^{24}\text{Mg}$: $Q = 1{\cdot}585 \pm 0{\cdot}015$ Mev.
$^{23}\text{Na}(p\alpha)^{20}\text{Ne}$: $Q = 2{\cdot}35 \pm 0{\cdot}04$ Mev.
$^{19}\text{F}(p\alpha)^{16}\text{O}$: $Q = 8{\cdot}06 \pm 0{\cdot}04$ Mev.
$^{18}\text{O}(p\alpha)^{15}\text{N}$: $Q = 3{\cdot}97 \pm 0{\cdot}05$ Mev.
$^{15}\text{N}(p\alpha)^{12}\text{C}$: $Q = 4{\cdot}96 \pm 0{\cdot}05$ Mev.

Part of this work was carried out during the tenure of a Studentship awarded by the Commonwealth Scientific and Industrial Research Organization of Australia.

Cavendish Laboratory,
Cambridge.
15th March 1950.

Joan M. Freeman.

Burcham, W. E., and Freeman, J. M., 1949 a, *Phys. Rev.*, **75,** 1756; 1949 b, *Phil. Mag.*, **40,** 807.
Burcham, W. E., and Smith, C. L., 1939, *Nature, Lond.*, **143,** 795.
Chao, C. Y., Tollestrup, A. V., Fowler, W. A., and Lauritsen, C. C., 1949. *Bull. Amer. Phys. Soc.*, **24,** No. 8, 11.
Freeman, J. M., and Baxter, A. S., 1948, *Nature, Lond.*, **162,** 696.
French, A. P., and Treacy, P. B., 1950, *Proc. Phys. Soc.* A, **63,** 665.
Holloway, M. G., and Livingston, M. S., 1938, *Phys. Rev.*, **54,** 18.
Smith, N. M., 1939, *Phys. Rev.*, **56,** 548.
Strait, E. N., Van Patter, D. M., and Buechner, W. W., 1950, *Bull. Amer. Phys. Soc.*, **25,** No. 1, 33.

The L–M and K–M Discrepancies in the Rare Earths

It has long been known that for many of the heavier elements the measured values of ν/R for the M_{IV} and M_V absorption edges differ from the values calculated from the relations

$$M_{IV}=L_{II}-L\beta_1$$
$$M_{IV}=L_{III}-L\alpha_2$$
$$M_V=L_{III}-L\alpha_1$$

by amounts which appear to be greater than can be accounted for by experimental error. This ‘ discrepancy ’ can only arise from differences in the end levels of the transitions from $L_{II,\,III}$ and $M_{IV,\,V}$ induced by absorption. Where the difference Δ, given by

$$\Delta=M_{\text{meas}}-M_{\text{calc}},$$

is negative and small it seems possible that it may be accounted for by the operation of selection rules, the end levels being in the neighbourhood of the conduction bands, but in cases where it is positive (and large) Phelps (1934), McGrath (1939) and Cauchois (1942) have shown that it is necessary to assume transitions into lattice levels beyond the conduction levels. In reviewing the data available in 1934 Phelps (1934) showed that Δ is positive from ^{83}Bi to ^{73}Ta (the latter being the element of lowest atomic number for which data have hitherto been available) and predicted that it would very likely vanish for the rare earth elements below ^{71}Lu. In a later review Cauchois (1942) showed that Δ is very likely negative for ^{92}U, ^{91}Pa and ^{90}Th, positive from ^{83}Bi to ^{73}Ta (reaching a maximum of more than 40 ev. round about ^{74}W) and expressed the opinion that it would vanish probably in the neighbourhood of ^{70}Yb.

During the past two years we have been carrying out an investigation into the fine structure of the M_{IV} and M_V absorption edges of a number of the rare earth elements in the form of their oxides and have incidentally measured the wavelengths of the edges themselves. By combining these with such L data as are available we have estimated Δ for the elements ^{59}Pr, ^{60}Nd, ^{62}Sm, ^{63}Eu, ^{64}Gd and ^{66}Dy. Of these only ^{62}Sm had previously been investigated by Rule (1945), and our results for this element are in close agreement with his. The values for Δ are given in Table 1 in ν/R and in electron volts. It will be seen that in all cases Δ is negative and with one exception exceeds 5 ev. The wavelengths of the L edges and lines have been taken from the tables of Cauchois and Hulubei (1947), with the exception of those for ^{66}Dy where we have taken the more recent values of Barrère (1947).

Table 1

	M_{IV}		M_V	
	$\Delta(\nu/R)$	Δ (ev.)	$\Delta(\nu/R)$	Δ (ev.)
^{59}Pr	−0·52	$-7{\cdot}0_7$	−0·49	$-6{\cdot}6_1$
^{60}Nd	−0·66	$-8{\cdot}9_7$	−0·45	$-6{\cdot}1_2$
^{62}Sm	−0·71	$-9{\cdot}6_5$	−0·56	$-7{\cdot}6_1$
^{63}Eu	−0·53	$-7{\cdot}2_0$	−0·52	$-7{\cdot}0_7$
^{64}Gd	−0·73	$-9{\cdot}9_2$	−0·75	$-10{\cdot}2_0$
^{66}Dy	−0·49	$-6{\cdot}6_1$	−0·27	$-3{\cdot}6_7$

Obtained as they are by combining our own measurements with those of many different observers it is difficult to estimate the probable error, but we consider that it is unlikely to be much more than ±5 ev. It would appear likely therefore that from ^{59}Pr to ^{66}Dy the discrepancy though possibly small is negative. In many cases the M edges observed by us are accompanied by a ‘ white line ’ on the long wavelength side, due probably to transitions to unoccupied levels in the $N_{VI,\,VII}$ electron groups, and a correction to the measured value of the edge should be made on this account, as described by Sandström (1935); since, however, the profiles of the lines are not sufficiently well brought out on our photographs we have used the uncorrected values in our calculations of Δ. The effect of the correction would be to *increase* the wavelength by one or two parts in 10,000, which would have the effect of making the Δ's slightly more negative. To these results we may add the very doubtful case of ^{70}Yb; here the M_{IV} edge was badly obscured by that of the K-edge of the aluminium foil on which the ytterbium was deposited, while instead of the M_V edge we have been able to get only what appears to be a narrow and sharp absorption line, in agreement with an earlier observation of Lindberg (1931). Assuming the long wave edge of this line to be the M_V edge we find the corresponding Δ to be $-9{\cdot}92$ ev.

For three of the elements studied by us, namely Pr, Nd, and Sm, estimates of the M_{IV} and M_V levels based on K emission data have been given by Rouault (1939). The discrepancies between these values and our measured values are given in Table 2. It will be seen that they are all negative and differ from the L–M discrepancies by amounts probably of the order of magnitude of the experimental error, three of them being greater than and three less than the L–M discrepancy. It would certainly seem unwise at this stage to attach significance to the fact that individual values do show differences.

Table 2

	M		M_V	
	$\Delta(\nu/R)$	Δ (ev.)	$\Delta(\nu/R)$	Δ (ev.)
^{59}Pr	$-1{\cdot}05$	$-14{\cdot}2_7$	$-0{\cdot}96$	$-13{\cdot}0_5$
^{60}Nd	$-0{\cdot}45$	$-6{\cdot}1_2$	$-0{\cdot}36$	$-4{\cdot}8_9$
^{62}Sm	$-0{\cdot}93$	$-12{\cdot}6_4$	$-0{\cdot}56$	$-7{\cdot}6_1$

The accompanying diagram shows a plot of the L–M_V discrepancy against Z taken from Cauchois' table (1942) with our own results added. A similar plot for the M_{IV} discrepancy resembles this closely. With such uncertain and limited data any generalization is necessarily unsafe, but the diagram does suggest that the 'normal' condition is for the end level in $M_{IV,V}$ absorption to be a few electron volts below that for $L_{II,III}$ absorption but that for elements 72 to 83 exceptional circumstances mask the negative discrepancy and convert it into a large positive one. In view of the difficulties likely to be encountered in filling the gap between ^{90}Th and ^{83}Bi, the elements ^{72}Hf and ^{71}Lu promise to be of particular interest and it is hoped shortly to investigate these substances.

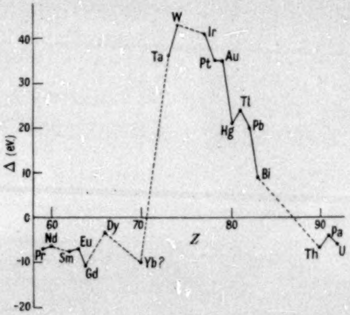

Physics Department,
Leicester University College.
22nd February 1950.

E. A. Stewardson.
H. F. Zandy *

---

* Now at the University of Teheran.

Barrère, G., 1947, *J. Phys. Radium*, **8,** 72.
Cauchois, Y., 1942, *C. R. Acad. Sci., Paris*, **214,** 68.
Cauchois, Y., and Hulubei, —, 1947, *Constantes selectionées: Longueurs d'onde des émissions* x *etc.* (Paris : Hermann et Cie).
Lindberg, E., 1931, *Nova Acta Reg. Soc. Sci. Upsal.*, Ser. iv, **7,** no. 7, 68.
McGrath, J. W., 1939, *Phys. Rev.*, **56,** 137, 765.
Phelps, W. D., 1934, *Phys. Rev.*, **46,** 357.
Rouault, S., 1939, *C. R. Acad. Sci., Paris*, **209,** 434.
Rule, K. C., 1945, *Phys. Rev.*, **68,** 246.
Sandström, A., 1935, *Nova Acta Reg. Soc. Sci. Upsal.*, Ser. iv, **9,** no. 11, 55.

Inhomogeneity of Deformation in Metal Single Crystals

The presence of strain hardening, and the occurrence of asterism in X-ray Laue photographs shows that plastic deformation of metal crystals by slip is not merely a simple geometrical translation of parts of the crystal along the slip plane. The process is accompanied by local changes of orientation which do not, as the phenomenon of asterism itself indicates, amount to a random fragmentation. In some cases asterism has been shown to be due to a macroscopic bending of the slip lamellae, but no such evidence has been obtained for cubic metals. The question arises whether there is a connection between asterism and the phenomenon of deformation bands (Barrett 1939) or kinking (Orowan 1942) which leads to local changes of orientation. An obvious method of studying this question is the X-ray technique developed by Berg (1934) and later used for metallurgical investigations by Barrett (1945). In what follows the results of an investigation of local orientation changes in deformed aluminium crystals by means of a modification of the Berg method will be given.

The principle of the method is shown in Figure 1. An X-ray beam from a line focus falls on a crystal which is rotated till a Bragg reflection occurs. The reflection represents a point for point image of the crystal surface, and changes in orientation, e.g. local rotations or bending, are revealed as striations in the image. The most satisfactory results are obtained on large crystals with flat faces which have been electropolished. The image is detected on a fluorescent screen which is then replaced by a Kodak Maximum Resolution Plate placed close to the crystal, but shielded from the direct beam. The resolution of the method is such that the image can be usefully enlarged 50–100 times, and so microscopic features of the deformation can be observed.

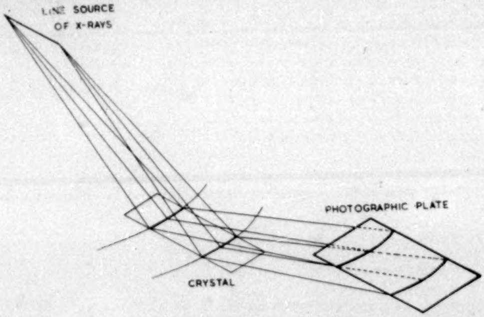

Figure 1.

Large aluminium crystals (99·5% pure) lightly deformed in tension (1–10% elongation) were examined in this way, and in all cases fine networks of bands were observed in the images. Figure 2 shows an image enlarged to 50 diameters from a crystal after 4% elongation. The plane on which the bands form can be determined by examination of two surfaces at right angles. The fact that this plane is usually a (110) shows that the bands are not slip bands. They are practically invisible in the optical microscope up to elongations of about 5% but can be detected after heavier deformation as very narrow deformation or kink bands in which the lattice is sharply bent. In the crystals examined they were usually about 0·05 mm. apart while their width was about 0·005 mm. Careful adjustment of the single crystal enables also the slip lines to be detected (Figure 3) and thus their relation to the deformation bands can be studied. Fine deformation bands have been observed in all aluminium single crystals so far examined, and are present after as little as 1% elongation in tension. They become broader and more clearly visible in the microscope in regions where the deformation is less homogeneous, e.g. at the shoulders of the specimen and in the vicinity of small included grains, while in polycrystalline specimens, the familiar macroscopic deformation bands are often observed.

It seems that there is a connection between the occurrence of fine deformation bands and the existence of asterisms in X-ray Laue photographs. The author has found that asterisms occur in aluminium single crystals after as little as 1% extension, and that in all cases the asterism possesses a fine structure which is not due to absorption edges of the crystal or of the film. In the continuous smear of the asterism, intensity maxima can be detected; the number increases as the size of the beam is made larger. It has been shown that this occurs immediately after the deformation and is not due to a recovery process such as polygonization, which is only observed in deformed aluminium crystals on annealing at 300° c. or higher (Cahn 1949). In the light of the above experiments, this phenomenon can be explained if it is assumed that, as a result of the deformation, the crystal breaks up into small blocks or layers varying slightly in orientation, which produce the dark spots in the Laue asterisms. The blocks are joined by narrow bent regions which give rise to the continuous background of the asterisms. It seems clear that these regions provide the visible curvatures as distinct from the hypothetical 'local curvatures' postulated by Yamaguchi, Taylor and Burgers as the cause of X-ray asterisms. It is perhaps relevant to mention that the author has found that with cadmium single crystals of suitable orientation extended by 100% in tension, the Laue spots can remain practically free from asterism. Cadmium crystals deformed in tension when examined by the above X-ray method show no deformation bands.

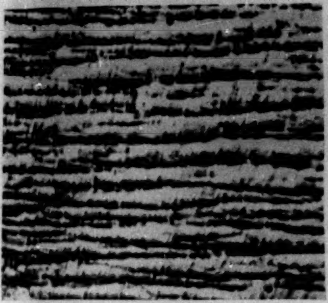

Figure 2. Aluminium crystal—4% elongation in tension. X-ray photograph (× 37·5). (Cu radiation).

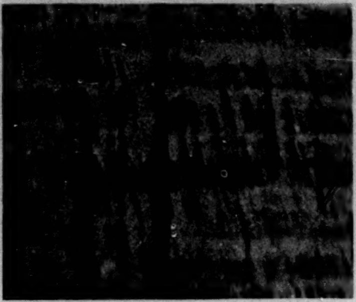

Figure 3. Aluminium crystal—4% elongation in tension. X-ray photograph (× 37·5). (Cu radiation).

It is well established that deformation bands or kinking plays an important part in the deformation of polycrystals. The above results show that this mode of deformation is significant also in the tensile deformation of single crystals, and thus even in these circumstances, the plastic deformation is often far from homogeneous.

The author wishes to thank Dr. E. Orowan, for helpful advice and criticism, and acknowledges an I.C.I. Fellowship during the tenure of which this work was begun, and a Fellowship from the Armourers and Braziers' Company which is enabling its continuation.

Cavendish Laboratory,
Cambridge.
28th February 1950.

R. W. K. HONEYCOMBE.

BARRETT, C. S., 1939, *Trans. Amer. Inst. Min. Met. Engrs.*, **135**, 296; 1945, *Ibid.*, **161**, 15.
BERG, W., 1934, *Z. Kristallogr.*, **89**, 286.
CAHN, R. W., 1949, *J. Inst. Metals.* **76**, 121,
OROWAN, E., 1942, *Nature, Lond.*, **149**, 643.

Singlet System B of ZrO

In a previous communication (Afaf 1949) the author drew attention to the discovery of a $^1\Sigma$–$^1\Sigma$ system, since designated as A, in the spectrum of ZrO. This system is in the ultra-violet region, with the (0, 0) band head at λ 3682. The vibrational constants in the lower $a^1\Sigma$ and the upper $b^1\Sigma$ states were evaluated from the data of nineteen band heads. The constants in the $b^1\Sigma$ state were $\omega_e' = 843{\cdot}75\ \mathrm{cm}^{-1}$ and $x_e'\omega_e' = 3{\cdot}15\ \mathrm{cm}^{-1}$, and those in $a^1\Sigma$ state were found to be 978·07 and 5·04 cm^{-1} respectively. Further details are given in a later article (Afaf 1950). It has been shown that the $a^1\Sigma$ state lies somewhere about 1,300 cm^{-1} above the $x^3\Pi_0$ ground state. The $b^1\Sigma$ state should therefore be about 28,451 cm^{-1} above the $x^3\Pi_0$ state. Further efforts have now been made to assign the remaining unclassified bands. The most prominent heads of these are at λλ 4460·4 (2), 4736·9 (12), 5185·0 (7), 5553·1 (10), 5610·1 (10), 5629·5 (14).

The author has now established the identity of another singlet system for ZrO, of which the λ 5185 band head is the (0, 0) band. This system has been designated as system B. In all only nine band heads were observed for this system. The record of the various band heads as measured by the author in the region of the bands of system B, along with the analysis offered, is presented below. It will be noted that a few more bands have been recorded for triplet system α of ZrO, extending the system to the longer wavelength.

λ_{air}	I	ν_{vac}	Classification
4736·91	(6)	21105·0*	Several band heads of system α (λλ 4730–4900), given elsewhere (Lowater 1932), are omitted here.
4769·41	(1)	20961·0*	
4798·91	(0)	20832·3*	B (3, 1)
4863·09	(3)	20557·3*	
4895·31	(1)	20422·0	
4969·82	(2)	20115·9	B (1, 0)
4996·28	(2)	20009·3	B (2, 1)
5022·95	(1)	19902·9	B (3, 2)
5052·95	(1)	19785·6	α (0, 2) R_a
5073·94	(1)	19703·1	α (0, 2) R_b
5077·60	(1)	19688·9	α (0, 2) R_c
5102·28	(0)	19593·6 ?	α (1, 3) R_b ?
5103·77	(0)	19587·9*	α (1, 3) R_c
5128·80	(0)	19492·3	α (2, 4) R_b
5131·67	(0)	19481·4	α (2, 4) R_c
5155·39	(0)	19391·8	α (3, 5) R_b
5156·28	(1)	19388·4*	
5158·64	(0)	19379·6	α (3, 5) R_c
5185·04	(6)	19280·9*	B (0, 0)
5205·65	(0)	19208·3	
5212·17	(1)	19180·5*	B (1, 1)
5240·17	(0)	19078·1	B (2, 2)
5436·87	(3)	18387·8*	β (3, 2) X_a
5438·23	(2)	18383·2	
5439·47	(3)	18379·0*	γ (5, 2) R_a ?
5448·88	(1)	18347·3	B (0, 1)
5456·56	(6)	18321·5*	β (1, 0) R_c
5461·55	(4)	18304·7*	β (1, 0) X_c
5465·38	(2)	18291·9*	β (4, 3) X_b
5478·39	(0)	18248·5	B (1, 2)
5485·74	(7)	18224·0*	β (2, 1) R_c

The bands marked with an asterisk (*) were also recorded by Miss Lowater (1932).

The Deslandres Table of system B is given below.

v' \ v''	0	Δ″1/2	1	Δ″3/2	2	
0	19280·9	*(933·6)*	18347·3			
Δ′1/2	*(835·0)*		*(833·2)*			*(834·1)*
1	20115·9	*(935·4)*	19180·5	*(932·0)*	18248·5	
Δ′3/2			*(828·8)*		*(829·6)*	*(829·2)*
2			20009·3	*(931·2)*	19078·1	
Δ′5/2			*(823·0)*		*(824·8)*	*(823·9)*
3			20832·3	*(929·4)*	19902·9	
		(934·5)		*(930·9)*		

The vibrational differences $\Delta'(v'+\frac{1}{2})$ in the upper state of system B, viz. 834·1, 829·2 and 823·9 cm^{-1}, agree very closely with those in the upper state $b^1\Sigma$ of system A, viz. 836·6, 830·1 and 823·9 cm^{-1}. This shows that the upper state of system B is $b^1\Sigma$. Since the band heads of system B are definitely single and no trace of *Q* branches can be found, it follows that the lower state of system B should also be $^1\Sigma$, and is henceforth termed $c^1\Sigma$. The state $c^1\Sigma$ $(v''=0)$ should lie about 9,170 (28,451–19,281) cm^{-1} above the $x^3\Pi_0$ ground state.

System A and system B involve respectively the following transitions : $b^1\Sigma \rightarrow a^1\Sigma$ and $b^1\Sigma \rightarrow c^1\Sigma$. The possible intercombination system, viz. $c^1\Sigma \rightarrow a^1\Sigma$, will lie in the infra-red region near about 13,000 A., and should be observed with some difficulty because of the somewhat weak intensity in the bands.

A further point of interest is the fact that, while at a temperature of 2400 A. enough molecules might be maintained in the $a^1\Sigma$ state (1,300 cm^{-1} above $x^3\Pi_0$) to cause absorption to take place in the Late Type Stars in the bands of system A, such an absorption is extremely unlikely to take place in the bands of system B on account of the greater excitation of the lower level (9,170 cm^{-1} above $x^3\Pi_0$). Absence of absorption in the spectra of Late Type Stars in bands of system B would be consistent with the present analysis.

The formula relating band heads of system B is

$$\nu_h^{v',v''}=19330{\cdot}5+\{839{\cdot}2(v'+\tfrac{1}{2})-2{\cdot}56(v'+\tfrac{1}{2})^2\}-\{938{\cdot}1(v''+\tfrac{1}{2})-1{\cdot}80(v''+\tfrac{1}{2})^2\}.$$

The investigation is being continued.

The author expresses his gratitude to Assistant Professor R. W. B. Pearse for valuable guidance throughout this work.

Department of Physics,
Imperial College of Science and Technology,
London, S.W.7.
27th March 1950.

M. Afaf.

Afaf, M., 1949, *Nature, Lond.*, **164,** 752; 1950, *Proc. Phys. Soc.* A, **63,** in the press.
Lowater, F., 1932, *Proc. Phys. Soc.*, **44,** 51.

REVIEWS OF BOOKS

Theory of Atomic Nucleus and Nuclear Energy-Sources, by G. Gamow and C. L. Critchfield. Pp. vi+344. 3rd Edition of *Structure of Atomic Nucleus and Nuclear Transformations.* International Series of Monographs in Physics. (Oxford : Clarendon Press, 1949.) 30*s*.

This book is presented as the third edition of Gamow's pioneer treatise of 1931 on the structure of the atomic nucleus. *Quantum mutatus ab illo* ! It was then possible in a slender volume to give an exhaustive account of our knowledge of nuclear properties. Now, with its size doubled, the book brings only a selection of the most important topics of nuclear physics in a much condensed form. The senior author, moreover, felt the need of calling a collaborator to the rescue, and, as in the second edition, the treatment has more the sedate character of a textbook than had that survey of a strange and novel world which the first edition presented. However, the spirit of adventure, which gave this early attempt its special charm, has not entirely disappeared : the cosmogonical chapter, which forms one of the most valuable additions of the present issue, is as Gamovian as one could wish.

The difficult task of selecting and arranging the subject-matter, and of reducing the account of the various aspects presented to their most essential features, has on the whole been successfully accomplished by the authors ; they have produced a readable, well-balanced and authoritative survey of the many-sided subject. There are, however, some weaknesses in the composition of the book and in the presentation of some questions. For instance, chapters III and VIII, which deal with nuclear forces and with nuclear collisions, are rather sketchy and confused, and the way in which the all-important concept of the compound nucleus in nuclear reactions is introduced, is very unsatisfactory. When discussing the proton and neutron as elementary nuclear constituents, the mistaken impression is conveyed to the unwary reader that the conception of these particles as distinct species is somehow essentially different from their description as two states of the ' nucleon ' species. Apart from such minor criticisms, one can but praise the clever selection of the illustrative examples from the experimental material, and the reliability of the information given. In fact, it is so difficult to catch the authors dozing that I can only point to a single wrong statement, viz. that the symmetrical meson theory would not be consistent with the saturation properties of the nuclear forces.

On the other hand, I must violently object to the first pages of the book, purporting to be an ' historical ' introduction. It is hardly conceivable that scientists (our authors are not the only sinners in this respect) loath to put down a single technical statement without carefully checking its accuracy, can allow themselves to be so lax when dealing with historical matters. The result of this attitude in the present case has been to produce a startling hotch-potch of Democritean atoms and Aristotelian elements, and an unfortunate confusion between the French chemist Proust and the British physician Prout.

From another point of view, it is a matter for regret that the authors should uphold the illogical nomenclature electron–positron, instead of adopting the correct usage of the word electron for any sign of the charge, and the words negaton–positon to distinguish between these signs. This terminology has been lately recommended by the Cosmic-ray Commission of the International Union of Physics, and it is a bad example indeed to show so little regard for the efforts, however modest, made by scientists to put their own house in order.

L. ROSENFELD.

Introduction to Atomic Physics, by S. TOLANSKY. Pp. xi + 371. 3rd Edition. (London: Longmans, Green and Co., 1949.) 15*s*.

The third revised and enlarged edition of this popular textbook for undergraduate students is welcome. Two new chapters have been added, one on the neutron and the second on nuclear fission and atomic energy. There are new sections dealing with the radioactive estimation of the age of the earth, K-capture and isotope separation. The chapter on cosmic rays has been revised, with sections on the photographic plate technique and mesons.

In a book of manageable size and such wide scope, dealing equally with the electronic and nuclear properties of the atom, each section must necessarily be sketchy and brief. The whole book integrates the present knowledge and outlook and gives a perspective of this field which makes it an excellent introductory text.

W. I. B. SMITH.

Higher Physics, by E. NIGHTINGALE. Pp. xvi+808. (London: G. Bell and Sons Ltd., 1948.) 27*s*. 6*d*. Also in separate parts: Pt. I. *Mechanics and Properties of Matter*, 7*s*. 6*d*.; Pt. II. *Heat*, 7*s*. 6*d*.; Pt. III. *Light and Sound*, 10*s*.; Pt. IV. *Electricity*, 12*s*. 6*d*.

The clarity of style which has characterized Mr. Nightingale's many school texts in the past is in evidence in his latest effort. This book is of intermediate standard and is primarily intended for sixth form scholars.

The wide field of subject-matter which is covered within the confines of this single volume has necessitated considerable ' condensing ' in certain sections, but on the whole this process has been carried out quite efficiently. However, it is inevitable that some subdivisions become unduly compressed when room is found for such topics as the theory of flight, the quantum theory of spectra, etc.

An undesirable effect of the lag, so prevalent in the post-war era, between the preparation of an MS. and its publication is exemplified in the present instance by the author's failure to record the recent official acceptance (October 1946) of the absolute system of electrical units as the practical system, to the exclusion of the International Scale. Also no mention is made, rather surprisingly, of the M.K.S. system of units.

The author makes frequent use of the methods of dimensions in the various sections of the book and the use of graphs in exhibiting experimental results is also stressed in the text.

The errors noted are remarkably few, but one which should be noted is the mention, on page 633, of the use of an iron former for the suspended coil of a galvanometer.

Line diagrams which are capable of reproduction by the student are freely employed thoughout the text, and another feature which commends the book as one to be treasured by the scholarship candidate is the large selection of examination questions at the end of each chapter.

R. W. B. S.

A Textbook on Heat, by J. H. AWBERY. Pp. x+302. 1st Edition. (London, New York and Toronto: Longmans, Green and Co., 1949.) 15*s*.

This is a book which has been written because the author, who is a specialist in the subject, has a conviction that heat is one of the fundamental parts of physics and therefore all physicists will find something of value in a fresh study of its principles.

The first seven chapters give an excellent account of the definition and measurement of temperature and of modern calorimetric practice which is based upon first-hand knowledge. The author then turns to the more theoretical topics, introducing the chapters on thermodynamics with a clear explanation of the meaning of partial differentiation which ensures that the mathematics which follows does not obscure the physics of the problems. Unfortunately in some of the later chapters this clarity is lost. In Chapter XVI, which deals with the conduction of heat, the author includes a large number of special mathematical methods of solving certain problems of heat flow. In some cases the account is too brief, for instance, half a page scarcely gives much idea of the method of the Fourier transform. In others there is a tendency to lead the reader half-way through a lengthy piece of analysis and there to leave him.

Throughout the book the mathematics is seldom set out in such a way as to be easily read, being too closely interwoven with the text. There is also a shortage of diagrams, and the choice of these at times appears a little strange; in the first three chapters there is only one, and that is of a maximum and minimum thermometer, while further on, on p. 84, a graph taken from some published paper illustrates, not very clearly, a small point in the text. These are probably matters of economy which may be remedied in a second edition.

On the whole this is a book of an original character which will make a useful supplement to the existing textbooks. It would, in particular, make refreshing reading for students at the end of a degree course, but there is something in it for readers at all stages.

E. M. WILLIAMSON.

Die Methoden zur angenäherten Lösung von Eigenwertproblemen in der Elastokinetik, by K. HOHENEMSER. Pp. 89. 2nd Edition. (Berlin: Springer-Verlag, 1943; New York: Chelsea Publishing Company, 1949.) No price.

In the classical theory of elasticity, the eigenvalue problem arises when a function y (representing, for example, displacement or stress or strain) is determined by a linear, homogeneous differential equation involving variables $x_1, x_2, \ldots . x_n$, the coefficients of y and its derivatives being given as functions of the variables x_r and of certain parameters $\lambda_1, \lambda_2, \ldots . \lambda_n$. In addition, a number of boundary conditions for y and its derivatives are given, and the eigenvalue problem consists in finding the values of the parameters λ_r which satisfy both the differential equation and the boundary conditions. In practice, it is convenient to subdivide problems of this type into two categories: (*a*) statical problems in which the variables do not include time, e.g. Euler's treatment of the buckling of a thin rod, and (*b*) dynamical or vibration problems, in which time enters, e.g. Bernoulli's solution of the transverse vibration of a stretched string. In the former case, the parameters λ_r are usually associated with critical loads or stresses at the onset of instability, and, in the latter, with the frequencies of free vibrations of the system.

The aim of Professor Hohenemser's monograph is to survey the modern mathematical techniques available for the solution of the dynamical problems, and the scope of the work may be judged from the specific cases which are treated as examples of the general methods: torsional and transverse vibrations of bars of various forms of cross section, the critical speeds of rotation of shafts, the vibrations of simple types of frame-structures, and the transverse vibrations of plates.

The first part of the book is devoted to a review of the general methods: the integral equations of the vibrations of elastic bodies, including induction (or influence or Green's) functions; iteration processes and the methods of extreme values for the calculation of eigenvalues; differential equations methods; replacement of continuous elastic system by a system with concentrated inertia and restoring forces; the solution of frequency determinants. This section is illustrated by treating the specific examples mentioned already.

The book is exceedingly well written and the treatment throughout is very general in character; it has the usual advantages and disadvantages of this approach. On the one hand, the general framework of the subject is clearly shown and it forms an admirable introduction for readers who are mathematically inclined; on the other hand, it is apt to prove disappointing to a practising Physicist or Engineer who requires information relating to the solution of a particular problem. A very valuable feature of the book is the extensive bibliography of the subject, although it is rather surprising to find that *Rayleigh's Principle*, by G. Temple and W. G. Bickley (Oxford University Press 1933), is not mentioned; the value of the bibliography would have been increased had an author index been included.

R. M. D.

PUBLICATION RECEIVED

High Vacuum Technology, by A. S. D. Barrett.

Abridged version of the 23rd Anniversary Address given to the King's College Engineering Society at the Institution of Mechanical Engineers on 10th March 1949. (London: W. Edwards & Co. Ltd.)

CONTENTS FOR SECTION B

PAGE

Dr. K. D. Froome. The Behaviour of the Cathode Spot on an Undisturbed Liquid Surface of Low Work Function 377

Dr. Mary B. Hesse. The Calculation of Magnetic Lens Fields by Relaxation Methods 386

Dr. D. J. Malan and Dr. B. F. J. Schonland. An Electrostatic Fluxmeter of Short Response-time for use in Studies of Transient Field-changes . . . 402

Dr. G. G. Macfarlane and Mr. H. G. Hay. Wave Propagation in a Slipping Stream of Electrons: Small Amplitude Theory 409

Dr. J. A. Gledhill and Dr. M. E. Szendrei. Theory of the Production of an Ionized Layer in a Non-Isothermal Atmosphere Neglecting the Earth's Curvature, and its Application to Experimental Results 427

Mr. J. E. H. Braybon. A New Method of Measurement of the Variation with Wavelength of the Refractive Index and Absolute Stress Optical Coefficients of Amorphous Solids 446

Dr. Mary D. Waller. Vibrations of Free Elliptical Plates 451

Letters to the Editor:

- Dr. D. K. C. MacDonald and Mr. J. E. Stanworth. Preparation of Alkali Metals in Glass 455
- Mr. W. H. Shortt. The Dissipation of Energy by a Pendulum Oscillating in Air at Low Pressures 456

Reviews of Books 458

Contents for Section A 461

Abstracts for Section A 462

ABSTRACTS FOR SECTION B

The Behaviour of the Cathode Spot on an Undisturbed Liquid Surface of Low Work Function, by K. D. FROOME.

ABSTRACT. The cathode spot of transient arcs using the liquid sodium–potassium alloy for cathode has been studied by means of the Kerr cell apparatus capable of taking a sequence of photographs. It is found that for a given current the spot takes, as in the case of mercury, the form of a line or broken line of total length roughly proportional to the current. This is also true for a spot in a magnetic field. Again as for mercury, if the current rises slowly the length of line increases proportionally to the current. If the rate of growth of current is greater than a value lying approximately between 10^8 and 2×10^8 amp/sec., then fresh spots form and spread out radially from the point of formation into thin semicircular or circular lines moving with a maximum radial velocity of about 10^4 cm/sec. The apparent current density of emission lies between 2·5 and 5×10^6 amp/cm^2, and consequently is higher than for mercury.

The Calculation of Magnetic Lens Fields by Relaxation Methods, by MARY B. HESSE.

ABSTRACT. The field and lens constants are calculated for two typical magnetic lenses as used in electron microscopes, using the relaxation method developed by Southwell for the solution of potential problems. The results are compared with those based on simple analytic approximations to the field distribution in the work of Glaser and Ramberg, and are shown to agree closely as regards those characteristics on which the discussion of the performance of the lens is based.

An Electrostatic Fluxmeter of Short Response-time for use in Studies of Transient Field-changes, by D. J. MALAN and B. F. J. SCHONLAND.

ABSTRACT. The fluxmeter consists of a conducting system of small capacity which is alternately exposed to and screened from the electric field by the movement of a rapidly rotating metal shield, thus producing an alternating E.M.F. of period 0·83 millisecond. The output, after amplification, is displayed on the screen of a cathode-ray oscillograph and the record carries an automatic indication of the sense of the field every 7·5 milliseconds.

At the maximum sensitivity employed the device gives a deflection of one centimetre in a field of 20 volts/metre, with a background noise-level of 0·15 cm. (3 volts/metre).

The response-time of the instrument is one half-cycle (0·42 millisecond).

The fluxmeter has been developed to give the rapid response and high sensitivity required for studies of the electric fields of thunderstorms in the intervals between the separate strokes of a lightning discharge.

Wave Propagation in a Slipping Stream of Electrons: Small Amplitude Theory, by G. G. MACFARLANE and H. G. HAY.

ABSTRACT. A theoretical study is presented of the TM-waves that can travel along a slipping stream of electrons. A slipping stream is defined as one in which the electrons move in parallel paths with velocity which varies with distance transverse to the motion. It is found that amplifying waves can travel along a slipping stream for all frequencies. It is also found that the slipping-stream tube has the remarkable property of combining the characteristics of a two-beam tube and a travelling-wave tube. This is due to the occurrence in the stream under suitable conditions of resonance layers, which act as highly reactive impedance sheets and can guide TM-waves of slow phase velocity in the same way as the spiral or corrugated surface in a travelling-wave tube.

The slipping-stream tube behaves differently according to the fractional velocity range of the electrons. If the velocity varies linearly from V_a to V_{-a} across the stream and $\alpha=(V_a-V_{-a})/(V_a+V_{-a})<0{\cdot}42$ it behaves primarily as a two-beam tube with plasma resonance frequency $\omega_0/2$, and therefore having a cut-off frequency $\omega_1=\omega_0/\alpha\sqrt{2}$ and maximum gain $2{\cdot}1\omega_0/V_0$ decibels per unit length, where ω_0 is the plasma resonance frequency of the slipping stream; in addition it has a low gain for $\omega > \omega_1$. However, if $\alpha > 0{\cdot}42$ it behaves primarily like a travelling-wave tube and the rate of gain is about $0{\cdot}53\omega_0/V_{-a}$ decibels per unit length at all frequencies above the plasma resonance frequency. This rate of gain is low compared with the gain possible with a travelling-wave tube in which the electron velocity is V_{-a} but it is achieved without the need for any external slow-wave waveguide.

Wave propagation along a slipping stream inside a waveguide, which in the absence of the electrons can guide a TM-wave of slow phase velocity, is also discussed. It is shown that this slipping stream travelling-wave tube has very much the same characteristics as a travelling-wave tube with a uniform electron beam. Maximum gain occurs when the phase velocity v_0 of the wave in the empty guide is about equal to the velocity of the electrons nearest to the reactive impedance sheet of the guide—in the example considered this is the fastest electron velocity V_a. A parametric set of curves is given relating the complex propagation constant to the frequency for different ratios v_0/V_a.

Theory of the Production of an Ionized Layer in a Non-Isothermal Atmosphere Neglecting the Earth's Curvature, and its Application to Experimental Results,

by J. A. GLEDHILL AND M. E. SZENDREI.

ABSTRACT. A new theory of ionospheric layer formation is developed, in which the temperature is assumed to vary linearly with height. The equations are compared at each step with those obtained by Chapman in his theory of layer formation in an isothermal atmosphere. The equations for the maximum of electron density and its height are also given. The effect of the parameters on the shape of the layer is shown in graphical form.

The equations are somewhat complex in form, but an ingenious graphical method has been devised suitable for the application of the theory to results given in the form of a Booker and Seaton parabolic distribution of electronic density with height. By application of the theory to mean hourly values for four summer months in South Africa, values are obtained for the temperature gradient, the temperature at 200 km., and its variation over the middle part of the day. The results obtained are in accordance with previous estimates and offer numerical confirmation of the theory that the atmosphere expands bodily upwards during the middle part of a summer day.

A New Method of Measurement of the Variation with Wavelength of the Refractive Index and Absolute Stress Optical Coefficients of Amorphous Solids, by

J. E. H. BRAYBON.

ABSTRACT. White light is passed through a Michelson interferometer in one of whose arms a thin lamina of the substance in the shape of a tension member is supported by a loading frame. The emergent beam, examined by a spectrometer, shows a continuous spectrum crossed by interference fringes. For the unstressed lamina the position of the fringes gives the variation of refractive index with wavelength. For the stressed lamina the behaviour of the fringes gives the stress optical coefficients. No modification of the interferometer, and only three sets of observations on the fringes, are required. For the calculation of absolute values of the refractive index the values of two wavelengths must be known.

Full details of the method are given, and photographs of tests on Columbia Resin 39 are included. These show that CR39 becomes positively birefringent under tension.

Vibrations of Free Elliptical Plates, by MARY D. WALLER.

ABSTRACT. The systematic observations which have been made on the normal vibrations of free elliptical plates confirm Chladni's results. The nodal systems may be divided into the same four classes of symmetry as those of rectangular plates.

The correspondence which exists between the vibrations of elliptical, rectangular and circular plates is traced. Combined modes of vibration do not occur on elliptical plates as they occasionally do on rectangular plates.